Scara5 as a Cell Fate Determinant of Osteoblasts and Adipocytes

UNIVERSITY OF OXFORD

Miss Yi-Hsuan Lee

Wadham College

University of Oxford

Nuffield Department of Orthopaedics, Rheumatology and Musculoskeletal Sciences (NDORMS)

DPhil Molecular and Cellular Medicine, Michaelmas 2021

Supervisors: Prof Nicole Horwood,

Dr Nicholas Platt & Associate Prof Afsie Sabokbar

Table of Contents

Table of Figures

Table of Tables

Acknowledgments

My sincere gratitude goes to my supervisors, Prof Nicole Horwood, Dr Nicholas Platt, and Associate Prof Afsie Sabokbar for their tremendous help and support. Special thanks go to Dr Linda Troeberg for her help and advice in developing and troubleshooting ELISA, Mr Pengjun Xi for FACS and analysis, Dr Tracey Swingler for her help in fat tissue section and histology, Dr Adel Ersek for her kind guidance and advice, and Miss Caterina Suelzu for handling and preparing experimental animals. I especially appreciate the invaluable advice from my thesis committee and confirmation assessors, Prof Katja Simon, Associate Prof Sarah Snelling, and Dr Emma Morris. I am thankful for the warm and generous support from previous lab members and others who I had work with during my study, Dr Lynett Danks, Associate Prof James Edwards, and Dr Houfu Leng. This work was partially funded by Taiwan Ministry of Education.

Abbreviations

2T3	Murine osteoblast-like ‘BMP-2 T-Ag-3’ cell line
ALP	Alkaline phosphatase
ATF4	Activating transcription factor 4
BAT	Brown adipose tissue
BMA	Bone marrow adiposity
BMAds	Bone marrow adipocytes
BMAT	Bone marrow adipose tissue
BMPs	Bone morphogenetic proteins
BMSCs	Bone marrow stromal cells
BSA	Bovine serum albumin
BSP2	Bone sialoprotein 2
C/EBPs	CCAAT/enhancer-binding proteins
CNS	Central nervous system
COL1A1	Collagen type I alpha 1 chain
CSF1	Colony stimulating factor 1, also known as macrophage colony-stimulating factor (M-CSF)
DMEM	Dulbecco’s modified eagle medium
DPP4	Dipeptidyl-peptidase 4
FBS	foetal bovine serum
FGF21	Fibroblast growth factor 21
FGFs	Fibroblast growth factors
FOXO1	Forkhead Box O 1
FOXP1	Forkhead box P1
GCs	Glucocorticoids
GH	Growth hormone
GLP1	Glucagon-like peptide 1
GSK-3β	Glycogen synthase kinase-3β
H&E	Haematoxylin and eosin staining
Hh	Hedgehogs
IGF1	Insulin-like growth factors 1
LEF1	Lymphoid enhancer-binding factor 1

LRP5	Low-density lipoprotein receptor-related protein 5
M-CSF	Macrophage colony stimulating
MCP1	Monocyte chemoattractant protein 1
OCN	Osteocalcin
OPN	Osteopontin
PD	Paget's disease
PGC1α	Peroxisome proliferator-activated receptor-gamma coactivator 1 alpha
PTH	Parathyroid hormone
RANK	Receptor activator of nuclear factor kappa-B
RANKL	Receptor activator of nuclear factor kappa-B ligand
RUNX2	Runt-related transcription factor 2
SCARA5	Scavenger receptor class A member 5
Scara5$^{-/-}$	*Scara5*-deficient
SHP1	SH2-domain-containing phosphatase 1
SIRT1	Sirtuin 1
SOST	Sclerostin
SR-A	Class A scavenger receptor 1, the prototypic scavenger receptor
SRs	Scavenger receptors
SSCs	Skeletal stem cells
SVF	Stromal vascular fraction
TAZ	Transcriptional co-activator with PDZ-binding motif
TGF-β	Transforming growth factor-beta
TH	Thyroid hormones
Thy1	Thymus cell antigen 1
TNFα	Tumour necrosis factor alpha
TRAP	Tartrate-resistant acid phosphatase
WAT	White adipose tissue
WNT	Wingless-type MMTV integration site

Abstract

Bone loss disorders associated with an imbalance in osteoblast and adipocyte differentiation, such as osteoporosis, are fast-growing health challenges in our aging populations. Cell fate differentiation shifts towards fat-storing adipocytes at the expense of bone-forming osteoblasts resulting in bone loss and increased fat mass. There is published evidence that murine models lacking specific scavenger receptors show alterations in bone and metabolic phenotypes. Herein, mice lacking scavenger receptor class A member 5 (*Scara5*) exhibited significantly greater bone mass and markedly reduced bone marrow adipose tissue than control WT animals. This was consistent with *in vitro* differentiation of *Scara5*-deficient (*Scara5*$^{-/-}$) bone marrow stromal cells (BMSCs), showing a reduction in adipocyte differentiation and an increase in osteoblast bone nodule formation. The underlying mechanism was investigated using recombinant SCARA5 and bone-related ligands, including ferritin, HMGB1, and WNT-related proteins. These *in vivo* and *in vitro* findings underscore the crucial role of *Scara5* in BMSC lineage allocation and demonstrate that *Scara5* is a negative regulator of bone mass and osteogenesis. Additionally, *Scara5*$^{-/-}$ animals carried leaner body mass and a smaller percentage of subcutaneous inguinal fat than the age and sex-matched

controls. This project proposes *Scara5* as an important modulator of bone and adipocyte formation, which could be reciprocally manipulated as a potential therapeutic target for body fat and bone formation.

Chapter 1 Introduction

1.1 Bone as a dynamic tissue

Under a rigid and inert façade, bone is in fact an intricate and highly active connective tissue that supports more than just body weight, movement and protection for vital organs [1]. The structural strength of skeletal bones comes from the compact cortical bone and cancellous trabecular bone structures. The cortical bone is dense and tough and laid down the outer bone surface, whereas trabecular bone is formed by interconnecting bone plates and bars inside the bone marrow that are less dense than the cortical bone [2]. Other important functions of bones include the reservoir of essential minerals and ions, the production of blood cells (haematopoiesis) inside the bone marrow, as well as more recent evidence of bone contribution to endocrine activities [3, 4]. These functional capacities are largely contributed by multiple cell types in the bone marrow environment, including bone cells, bone marrow adipocytes, and haematopoietic cells to maintain healthy bone turnover and renewal [1].

The maintenance of healthy skeletons throughout life requires constant bone remodelling by the coordinated activities of osteoblasts, osteoclasts, and osteocytes (Figure 1.1). Bone remodelling is an important metabolic process that renews and replaces the old and dead bone tissue,

repairs damages, and maintains structural integrity and mineral homeostasis [2]. During bone remodelling, osteoblasts produce organic bone matrix and aid mineralization with inorganic materials together via calcium and phosphate ions nucleation to form hydroxyapatite crystals for new bone formation [1]. Meanwhile, osteoclasts resorb bone mineral and break down extracellular matrix proteins, and osteocytes transmit mechanical as well as biochemical signals connecting bone cells, matrix and bone surface [5].

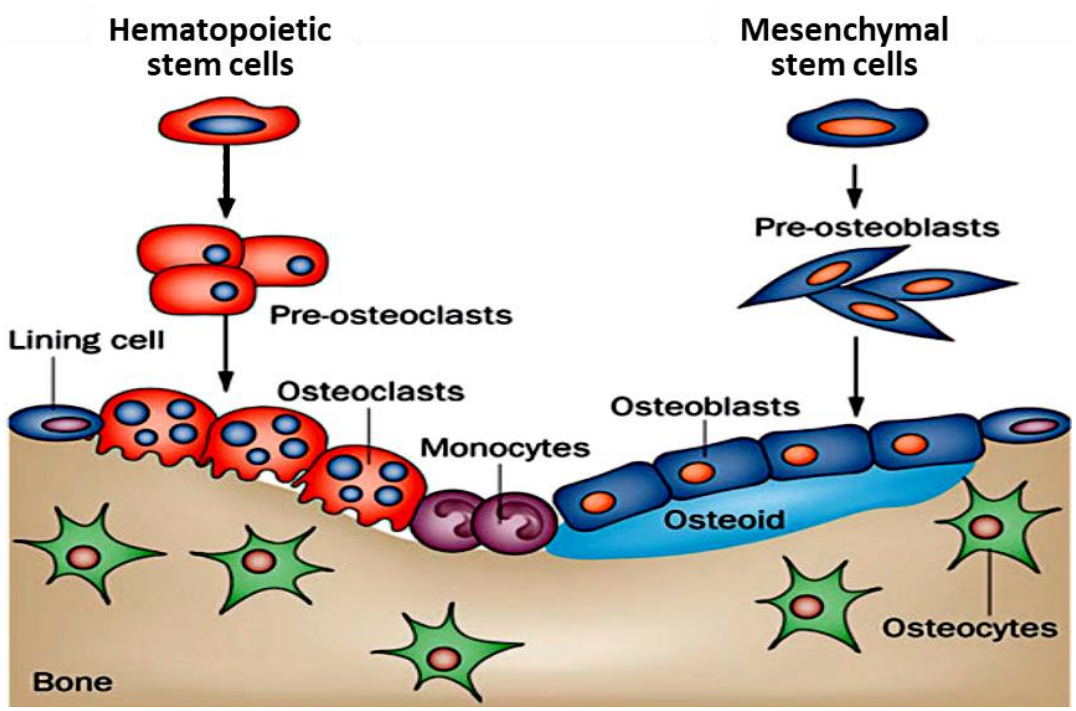

Figure 1.1 Schematic of primary bone cells and their precursors (adapted from [6]). The major bone cells are osteoblasts, osteoclasts, osteocytes, and bone lining cells. Osteoblasts derive from bone marrow mesenchymal stem cells and can further differentiate into either osteocytes or bone lining cells. Haematopoietic stem cells can give rise to osteoclasts via myeloid lineage precursors.

In contrast, haematopoietic stem cells residing in the bone marrow give rise to red and white blood cells for oxygenation and the immune system, while marrow adipocytes fill the marrow void to provide structural support and potentially regulate local energy and systemic metabolism [4]. Together, these cellular components and their collaborative functions within the dynamic bone marrow environment provide skeletal integrity and homeostasis. Therefore, skeletal bones have functional importance beyond their rigid mechanical roles. The following literature review will focus on the differentiation and regulation of bone cells, the remodelling process, and bone homeostasis in skeletal disorders.

1.1.1 The function, differentiation and regulation of bone cells

Osteoblasts, derived from bone marrow mesenchymal/stromal cells (BMSCs) and periosteum [7], are the only cell type responsible for bone formation. The two types of bone formation are known as endochondral and intramembranous ossification, where the former produces long bones, such as femur and tibia, and the latter forms flat bones like skull and clavicle [8]. To generate bone tissue, osteoblasts first synthesize and secrete organic matrix that is made up of the unmineralized layer of osteoid, which consists of mainly

type I collagen and a minimal of proteoglycans, fibronectin and bone specific proteins [5]. Subsequently, the bone matrix mineralization occurs through the release of phosphate by phosphatases and the nucleation of phosphate and calcium ions resulting in the formation and spread of hydroxyapatite crystals in the surrounding bone matrix [1, 9]. Mature osteoblasts possess the abilities of bone formation and mineralization and can further differentiate into osteocytes or bone lining cells. Although osteocytes and bone lining cells lose their bone forming ability, they play important roles in skeletal development and homeostasis. Osteocytes function to sense mechanical stimuli, transmit biochemical signals and produce sclerostin to inhibit bone formation, while bone lining cells are proposed to form temporary anatomical structures called basic multicellular units and compartmentalize the bone remodelling site [9].

Osteoblast lineage differentiation from BMSCs to preosteoblasts then to mature osteoblasts is temporally orchestrated by signalling pathways and transcription factors that act at specific stages (Figure 1.2). The master regulators, RUNX2 and its downstream Osterix transcription factor, are crucial in the commitment of BMSCs towards osteoblast precursors. These osteoblast precursors subsequently proliferate and differentiate into Osterix-positive preosteoblasts which mature into bone forming osteoblasts that secrete bone

matrix proteins (e.g. collagen type I, osteocalcin and bone sialoprotein) [10]. In addition, RUNX2 is involved in several signalling pathways that critically regulate osteogenic differentiation, including canonical WNT (i.e. WNT/β-catenin), transforming growth factor-β (TGF-β) and bone morphogenetic proteins (BMPs) signalling pathways. These pathways form a network with other signalling pathways, such as Hedgehog (Hh), fibroblast growth factor (FGF), and Notch dependent activities, to coordinate osteoblast differentiation, bone growth, remodelling, and overall skeletal homeostasis [10-12].

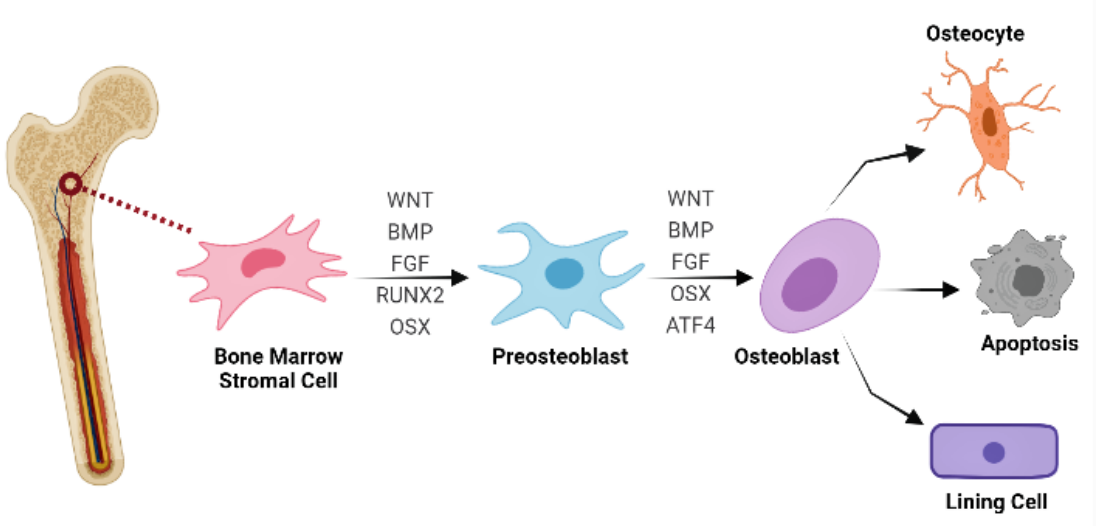

Figure 1.2 Key molecular signals in osteoblast differentiation. Bone marrow stromal cells are regulated by multiple factors and stimuli in the bone marrow and can commit to the osteoblast lineage and differentiate into preosteoblasts and osteoblasts under the correct molecular signals. Key molecular signals include, but are not limited to, WNT, BMP, and FGF dependent activities and the transcription factors RUNX2, OSX and ATF4. Osteoblasts can further differentiate to become osteocytes, bone lining cells, or can undergo apoptosis. Abbreviations: WNT, wingless-type MMTV integration site family; BMP, bone morphogenetic protein; FGF, fibroblast growth factor;

RUNX2, runt-related transcription factor 2; OSX, osterix; ATF4, activating transcription factor 4. Created with Biorender.com.

Supported by gain- and loss-of-function studies in mice models, Hh signalling is essential for appropriate bone formation, which induce RUNX2 that initiate mesenchymal cells into osteoblast precursors [10]. WNT signalling is critical to multiple stages of osteogenesis and is required during osteoblast maturation [13, 14]. WNT signaling in bone formation is associated with several WNT proteins (e.g. WNT1, WNT3 and WNT5A), receptors (e.g. Frizzled and LRP5), and inhibitors (e.g. SOST and SFRP4) reported by gene mutation studies in mouse and human bone disorders [13, 15, 16]. Clinical evidence has confirmed that mutations in the WNT protein co-receptor low-density lipoprotein receptor-related protein 5 (LRP5) presents either a high or low bone density phenotype among other abnormalities [5, 10]. Both TGF-β and BMPs belong to the structurally diverse TGF-β superfamily and they function extensively throughout the skeletogenic process [11]. For example, Camurati–Engelmann and Brachydactyly type A2 bone diseases result from *TGFB1* and *BMP2* gene mutations [11]. In addition, the dysregulation of TGF-β/BMP signalling is frequently associated with osteoarthritis in both human and mouse models [17, 18]. The induction of FGF signalling through regulating FGF receptors by

RUNX2 is necessary, at least in part, for osteoblast proliferation and can promote osteoblast differentiation synergistically with BMP signals [11, 12].

As a consequence of being the only bone forming cell that resides in the bone marrow, osteoblasts have pivotal roles in skeletal development and homeostasis.

Osteoclasts, originated from mononuclear progenitor cells of haematopoietic lineage, are multinucleated cells formed by the fusion of mononuclear osteoclast precursors [1, 8]. The primary function of osteoclasts is to resorb bone matrix during bone remodelling. Activated osteoclasts polarise and develop specialized membrane domains which are sealing zone, ruffled border, functional secretory and basolateral domains [19]. The polarisation of bone-resorbing osteoclasts involves rearrangement of the actin cytoskeleton that forms an F-actin ring that consists of highly dynamic podosomes in a dense continuous zone, where a membrane area is subsequently isolated and developed into a ruffled border [1]. The maintenance of the ruffled border, formed to enable the trafficking of lysosomes and endosomes carrying bone resorptive proteins, plays an indispensable part in the bone degradation activity of osteoclasts. The degraded products of bone matrix and mineral (e.g. collagen fragments, calcium and phosphate) are endocytosed by osteoclasts,

and are then proteolyzed by Cathepsin K and Tartrate-resistant acid phosphatase (TRAP) before being released at functional secretory domains via transcytosis [5].

Osteoclast differentiation, the process by which haematopoietic stem cells differentiate to mononuclear osteoclast precursors and finally to multinucleated osteoclasts, mainly depends upon two factors, macrophage colony-stimulating factor (M-CSF) and receptor activator of nuclear factor kappa-B ligand (RANKL) [1, 20]. M-CSF secreted by osteoblasts and stromal cells is essential to the proliferation and survival of mononuclear precursor cells via signalling through the receptor c-fms. Similarly, RANKL, the osteoclast differentiation factor, binds to RANK on the cell surface of mononuclear osteoclast precursors and commits them to osteoclast differentiation and formation [21]. In contrast, osteoprotegerin (OPG) secreted by osteoblasts, osteocytes and osteogenic stromal cells is a decoy receptor of RANKL and serves to limit excessive bone resorption by osteoclasts [22, 23]. Synergic stimulation of M-CSF and RANKL promotes preosteoclast fusion and continued c-fms and RANK-dependent signalling is necessary for the survival of mature osteoclasts [5, 9]. The RANKL pathway, together with the co-stimulatory immunoreceptor tyrosine-based activation motif pathway activates

calcium/NFATc1 signalling that regulates gene expression of TRAP, Cathepsin K and matrix metalloproteinase 9, which are essential for the formation and functions of multinucleated osteoclasts [19].

Importantly, osteoclasts and osteoblasts reciprocally regulate the activities of each other through secreting factors, direct cell-cell interactions, and the release of bone matrix-derived factors during resorption [19]. Taken together, osteoclasts, which are derived from haematopoietic stem cells and differentiate as a result of exposure to M-CSF and RANKL degrade bone matrix and absorb minerals via the secretion of osteolytic enzymes.

Osteocytes, derived from osteoblast terminal differentiation, are the most abundant (about 90-95% of total bone cells) and long-lived bone cells and are in charge of sensing mechanical loading and compression [1]. During osteocyte differentiation from osteoblasts, osteocytes go through profound morphologic changes to a final stellar shape with an increased nucleus to cytoplasm ratio, which is accompanied by a huge reduction (~70%) in cell organelles that includes rough endoplasmic reticulum and Golgi apparatus and cytoplasmic volume, which corresponds to decreased protein synthesis and secretion [5, 24]. Osteocytes are incorporated into mineralized bone matrix at maturation and develop long filopodial extensions (osteocyte processes) that

are rich in actin cytoskeletons that form connections to bone lining cells and osteoblasts on the bone surface, as well as to neighbouring osteocytes via gap junctions at the tips of osteocyte processes [19, 25].

The unique connection network allows osteocytes to not only process and transmit mechanical signals but also communicate with other bone cells, which facilitates osteoblast and osteoclast regulation during bone development and remodelling [23, 24]. Osteocytes integrate and convert mechanical stimuli into biological signals, such as ATP, nitric oxide, and prostaglandins, thereby facilitating adaptation to mechanical forces and structural maintenance of bone [26]. Moreover, sclerostin (SOST) produced by mature osteocytes impairs the bone formation activity of osteoblasts through inhibition of WNT/β-catenin signalling [27]. In addition, osteocytes can also secrete molecules, such as osteoprotegerin (OPG), RANKL, and M-CSF, that regulate osteoclast differentiation and activity [23, 28]. Therefore, although the primary function of osteocytes is mechanosensing, they also produce factors that have important effects on osteoblasts and osteoclasts.

1.1.2 Bone remodelling and homeostasis

Adult bones undergo continuous metabolic processing, termed

remodelling, that achieves their constant renewal and repair throughout life. Bone remodelling is vital to the maintenance of bone strength, structural integrity, and homeostasis as well as the systemic mineral balance [29]. There are five sequential phases (Figure 1.3) involved in bone remodelling: initiation/ activation, resorption, reversal, formation and termination/quiescence [30]. This highly coordinated and controlled process requires several local and systemic factors that regulate the coupling of the activities of two major bone cell types: bone formation by osteoblasts and bone resorption by osteoclasts [31, 32].

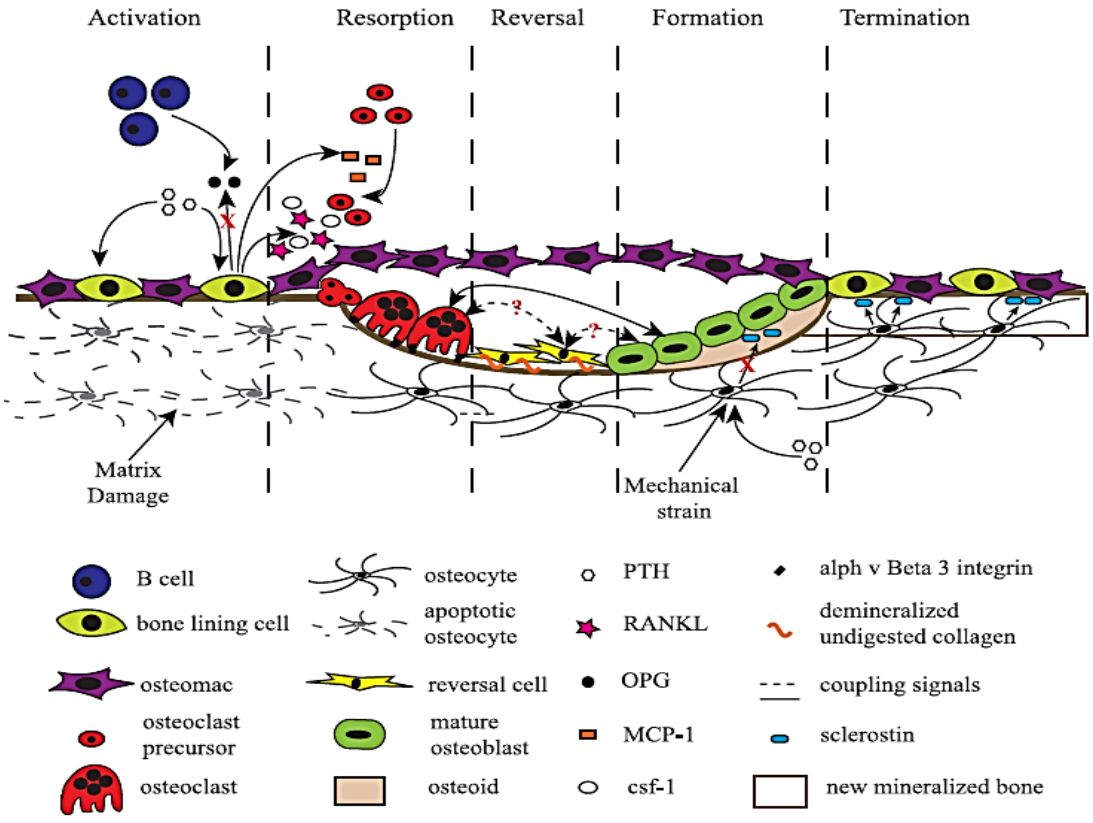

Figure 1.3 The bone remodelling process [29]. The different phases of bone remodelling shown are, from left to right; activation, resorption, reversal, bone formation, and termination. Bone remodelling involves the coordination of various cell types, cytokines, matrix proteins, as well as the proper coupling of

signals between these cells. Abbreviation: CSF1, colony stimulating factor 1, also known as macrophage colony-stimulating factor (M-CSF); MCP-1, monocyte chemoattractant protein-1.

Initiation of bone remodelling requires activation signals, for example, microdamage resulting in osteocyte apoptosis, adaptation to mechanical loading and strain, or hormonal stimulation by calcitonin, parathyroid hormone (PTH), or oestrogen [29, 31]. Apoptotic osteocytes then recruit osteoclast precursors to the remodelling sites by transmitting signals or releasing factors, such as RANKL, that promote osteoclast differentiation and activation [33]. In addition, reduced TGF-β secretion by osteocytes due to apoptosis and/or bone matrix damages attenuates inhibitory signals, thereby enhancing osteoclast formation [34]. By contrast, PTH signalling through its receptors on osteoblasts and stromal cells stimulates M-CSF and RANKL expression that promotes osteoclast precursor differentiation, whereas oestrogen signalling via Fas and Fas ligand induces osteoclast apoptosis [29, 35].

During the resorption phase, recruited osteoclast precursors proliferate and differentiate into mature multinucleated osteoclasts. Meanwhile, bone lining osteoblasts secrete matrix metalloproteinases and degrade osteoid collagen matrix lining the bone surface to expose RGD adhesion sites within

mineralized bone and as a result facilitate osteoclast attachment [36]. Once attached to mineralized bone surface, osteoclasts develop specialized membrane structures and create an isolated microenvironment to resorb and degrade bone matrix with proteolytic enzymes under acidic conditions maintained by the release of hydrogen and chloride ions [29, 30]. Following osteoclast resorption activity, the exposed collagen fibrils and demineralized matrix debris remain at the remodelling surface. The mononuclear reversal cells, recently confirmed to be of osteoblast lineage, remove these digested matrix remnants and prepare the bone surface for transition to subsequent bone formation step [29, 37]. A recent study suggested that the bone formation phase is initiated when the osteoprogenitor cell density reaches above a certain threshold that switches activity from bone resorption to formation [38].

At the bone formation stage, a variety of coupling signals are strictly coordinated and consequently contributed to bone formation and mineralization, including the matrix-bound growth factors released upon bone resorption, such as BMPs, TGFβ and insulin-like growth factors, membrane and soluble molecules from osteoclasts and signals from osteocytes [38, 39]. As osteoblasts deposit new matrix proteins and bone mineralization progresses, they also differentiation into osteocytes, bone lining cells or undergo apoptosis.

Besides bone formation, OPG secreted by osteoblasts, a decoy receptor for RANKL that suppresses osteoclast formation, help prevents excessive bone remodelling activity [30]. Finally, the bone remodelling cycle is terminated when the amount of bone resorbed is replaced by an equivalent volume of new bone formed by osteoblasts [39]. Although not completely understood, the return of sclerostin expression by osteocytes may act as a termination signal that inhibits further bone forming activity [29, 30]. In brief, constant and normal bone remodelling, involving balanced and controlled coupling activities between bone resorption and bone formation, ensure the maintenance of healthy bone mass, structural strength and integrity, and skeletal homeostasis.

1.1.3 Bone disorders with aberrant bone remodelling

The delicate equilibrium of the bone remodelling process is disturbed in several bone disorders. Osteoporosis, as a well-known and common bone disorder, is characterized by the significant loss of bone mass and density leading to greater risk and susceptibility to fragility fractures [40]. Clinically, postmenopausal and aging-associated causes are classified as primary osteoporosis, whilst secondary osteoporosis involves skeletal complications of other medical conditions and the consequences of therapeutic interventions to

treat other diseases [19]. In postmenopausal osteoporosis, estrogen deficiency enhances the secretion of cytokines interleukin-1 and tumour necrosis factor alpha (TNFα), thereby stimulating RANKL expression by osteoblasts and stromal cells, which together acts to promote osteoclast differentiation and activities in favour of bone resorption [40, 41]. In comparison to postmenopausal osteoporosis in females, age-related osteoporosis affects both genders and the pathogenesis results from the decline of sex hormone levels and aging responses of the whole organism [40]. Although the decrease in bone formation due to changes in the levels of PTH and insulin-like growth factor 1 are shown as predominant factors causing age-related osteoporosis in men, it is now appreciated that the reduction of bioavailable sex steroids also play a role in increased bone resorption [42].

Complications of bone loss and fractures are commonly seen in multiple inflammatory and autoimmune diseases, where the consequence of persistent inflammation, compounded with treatments like glucocorticoids (GCs), exacerbate bone degradation. Pharmacological concentration of GCs alters the balance of bone remodelling and detrimentally affects multiple bone cell types both directly and indirectly; for example, by inhibiting osteoblast differentiation and functions, inducing osteocyte apoptosis, and promoting

osteoclast formation and survival [40]. However, most treatments and clinical management of osteoporosis struggle to reverse microstructural alterations and enhance structural integrity, despite the improvement in bone density formation, and remodelling with lower bone resorption rates [19, 43].

Paget's disease (PD) of bone is a remodelling disorder prevalent with increasing age. In the affected bone region of PD, the abnormal increase in osteoclast activity exacerbates bone degradation, which consequently induces a rapid but disorganized bone formation response. Clinical presentation varies according to the severity and the location of the affected bone in PD patients [40]. Treatments of PD of bone usually include pain relief or anti-resorptive drugs, whilst surgery may be required for the case of severe bone deformities [44]. On the other hand, osteopetrosis is characterized by unusually elevated bone density resulting from decreased bone resorption due to defects in osteoclast differentiation, formation and/or functions. This is a heterogenous group of rare heritable bone disorders caused by several separate gene mutations with different severity, symptoms and age of onset [45]. The key mutations of osteopetrosis involve genes regulating carbonic anhydrase II, proton pump, chloride channel, and RANK [40]. The treatments of osteopetrosis rely on management of disease complications or in severe cases bone marrow

transplant may prolong survival [46].

In conclusion, an imbalance in or aberrant bone remodelling process can contribute to but not limit to the skeletal disorders discussed here, since the intimate crosstalk between osteoblasts and osteoclasts along with tightly coordinated activities of multiple cell types within bone are required. Recently, the importance of the skeleton at the systemic and metabolic level is being increasingly appreciated because of its association with diverse clinical conditions such as diabetes and cancer metastasis. This recognition may help reveal novel disease mechanisms and drive new therapeutic interventions.

1.2 Bone marrow adipocytes as a distinct fat depot

The past two decades have seen a significant in investigations in the area of bone marrow adiposity (BMA) and related topics. From the initial notion of being simply a space filler in BM, bone marrow adipocytes (BMAds) have now been identified as a distinct and important fat depot with understanding of its physiology and pathogenesis constantly evolving [47].

Two distinct subpopulations of bone marrow adipose tissue (BMAT), constitutive BMAT (cBMAT) and regulated BMAT (rBMAT), have been described (Figure 1.4) [48]. Several differences between cBMAT and rBMAT have been identified: cBMAT adipocytes, situated in the distal part of long bones, phalanges and caudal vertebrae in rodents, are larger in size, contain more unsaturated lipids, express elevated levels of the adipogenic transcription factors *Cebpa* and *Cebpb*, and are resistant to external or pathophysiological changes, whereas rBMAT adipocytes are smaller in size, interspersed within haematopoietic red marrow, contain higher lipid saturation, express lower *Cebpa* and *Cebpb*, and are sensitive to environmental or pathophysiological stimuli [48].

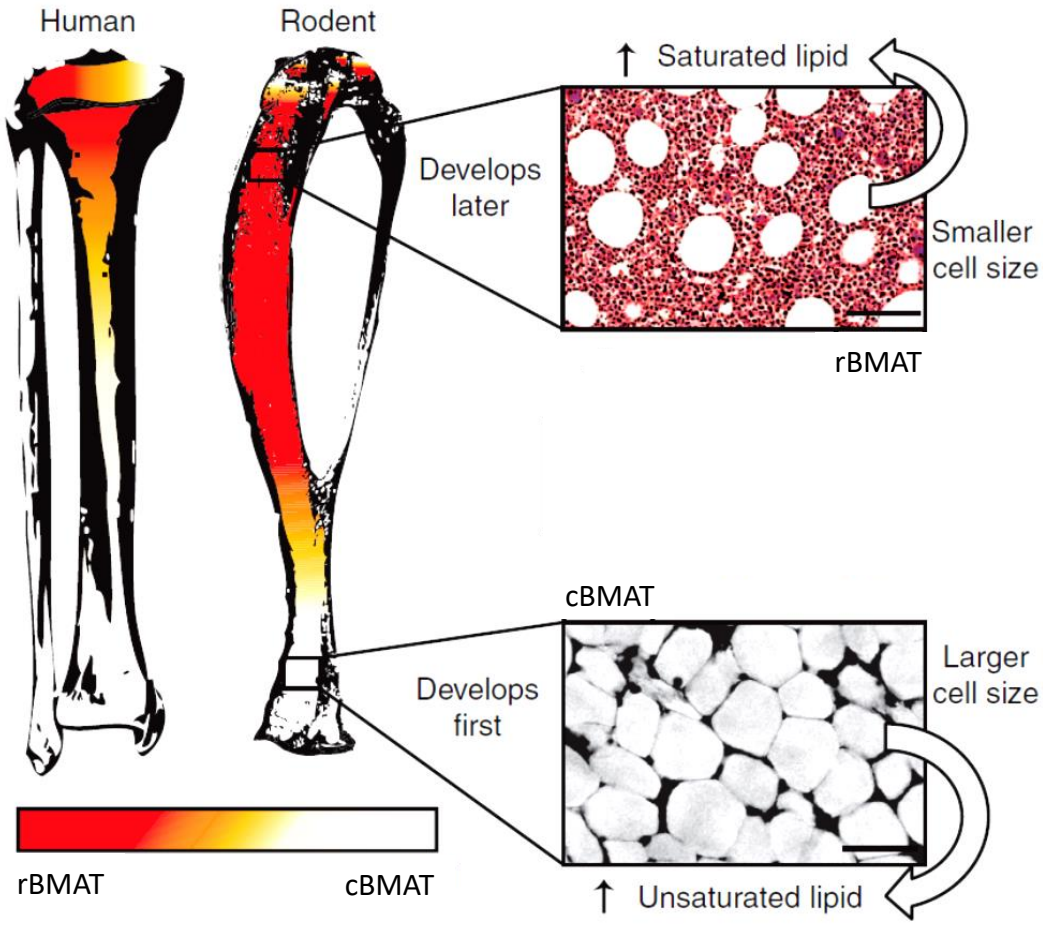

Figure 1.4 Schematic of constitutive BMAT (cBMAT) and regulated BMAT (rBMAT) (Adapted from [48]). rBMAT adipocytes are located within the red marrow, whereas cBMAT are present in the distal section of the bone in human and mouse tibia. In some instances, the histological features corresponding to rBMAT and cBMAT adipocytes may be present in the same region, especially in larger species like humans; bone areas coloured in orange suggest this possibility. cBMAT adipocytes form shortly after birth and appear as confluent adipocytes with increased level of unsaturated fatty acids, that are relatively larger in size and devoid of haematopoiesis. rBMAT develops throughout life interspersed within areas of active haematopoiesis. In comparison to cBMAT, the lipid saturation profile of isolated rBMAT adipocytes is similar to that of WAT adipocytes which are smaller in size and more saturated.

It has been established that marrow adipocytes are distinct from white and brown adipose tissue in many aspects, such as their cellular origin, functional and metabolic characteristics [49, 50]. Although BMAT histologically resembles white adipose tissue (WAT), it is counterintuitive when considering the increase of BMAT in both high-fat diet and caloric restriction murine models [51, 52]. Moreover, the amount of BMAT is generally not correlated with typical indicators of adiposity measurements, such as waist-to-hip ratio, body mass index, and visceral or subcutaneous fat ratio [53, 54]. Conversely, BMAT has been shown to respond to temperature and exhibit brown adipose tissue (BAT) markers (Prdm16, Dio2, FoxC2, and PGC1a, but not UCP1), yet the thermogenic ability of BMAT is not known [55, 56]. Importantly, changes in BMAT, such as its volume and functions, may be affected by ageing, gender, and clinical conditions, but it is not fully understood [57].

Since the recognition of BMAT as a distinct and unique fat depot, the field of research has stimulated interests in exploring BMAT-related topics ranging from skeletal, cancer, and stem cell studies, as well as its contributions to haematopoiesis and metabolism. Below, the development, cellular identity and functional aspects of BMAT are described in more detail, followed by the association of BMAT with pathological conditions.

1.2.1 The development, cellular origin, and identity of bone marrow adipocytes

Unlike WAT that can seemingly expand without limit, BMAT is confined within the spatial boundaries of the skeleton. In the unique skeletal anatomy where BMAT resides, the development of BMAT in human and mammals such as rodents generally follows a centripetal pattern, starting from the distal skeletal regions such as phalanges and tail (in rodents), followed by the appendicular skeleton (from the diaphysis of the long bones towards the distal and proximal ends), and finally reaching the axial skeleton [54, 58]. During development, cBMAT forms early in the distal skeleton, for example hands, feet, and distal tibia where haematopoietic activity is relatively devoid, and it normally persists over a lifetime after reaching its peak volume. rBMAT develops later in the haematopoiesis active bone regions, including metaphasis of tibia and femur and lumbar vertebrae, and increases gradually with age and slowly occupies BM cavity throughout life [48, 58].

It is commonly thought that all adipocytes, independent of type (white, brown, or marrow adipocytes), originate from the mesenchymal lineage and precursors of their specific depots. Studies have shown some similar cellular and functional profiles of BMAT to those of WAT and BAT adipocytes, such as

unilocular morphology and sensitivity to high-fat diet, as well as BAT adipocytes' gene expression patterns and temperature responsiveness [48, 51]. Nevertheless, contradictory results found in caloric restriction and anorexia nervosa, where WAT decreases but BMAT increases, suggests that marrow adipocytes may arise from a separate progenitor population [59]. In addition, BMAds have characteristics distinct from WAT and BAT, including cell size, free fatty acid content, glucose metabolism, along with cytokine, adipokine, and stem cell marker expression [50, 59, 60]. Furthermore, the distinct biochemical and physiological properties of rBMAT and cBMAT adipocytes are likely be influenced by the unique microenvironments they reside within the bone marrow region [60]. Therefore, it is hypothesized, but remains unproven, that separate progenitor populations exist for the generation of rBMAT and cBMAT. Recent studies using murine genetic lineage tracing models have revealed BMAds originate from a non-haematopoietic, non-endothelial and mesenchymal progenitor pool [59, 61].

A number of reports generally support that osteoblasts and marrow adipocytes derived from a common multipotent stromal cell population in the bone marrow and that their cell fates are determined by distinct genetic and epigenetic factors [62-64]. It has been shown that *Myf5*$^{-}$*/Pax7*$^{-}$ progenitor cells

give rise to WAT, whereas BAT adipocytes are *Myf5*$^{+}$*/Pax7*$^{+}$, suggesting distinct WAT and BAT adipocyte lineages [65, 66]. In addition to the morphologic difference in unilocular BMAds and multilocular BAT adipocytes, BMAds are *Myf5* negative in the *Myf5-cre:mT/mG* mice, indicating BMAds are morphologically and developmentally different from BAT adipocytes [61]. On the other hand, BMAds are traced in the tibia and femur by *Prx1* expression (expressed by osteoprogenitors in periosteum and limb bud mesenchyme during development) in *Prx1-Cre:mT/mG* mice, however, *Prx1* is untraced in most BAT or any visceral WAT with variable *Prx1* expression in subcutaneous WAT [67-69]. Surprisingly, *Osx1* expression, once thought to be osteoblast specific, was positively traced in marrow adipocytes of *Osx1-Cre:mT/mG* mice, while all WAT and BAT depots were *Osx1* negative [70-72]. These murine lineage tracing results indicate that BMAds arise from a mesenchymal-osteogenic precursor population that is distinct from both WAT and BAT.

Other studies showed positive leptin receptor (LepR) expression in most marrow adipocytes and osteoblast populations and accounts for 94% of colony-forming unit fibroblasts in adult but not developing BM; these LepR^{+} cells also largely overlap with Nestin^{+}-traced BM population [73, 74]. In contrast, Gremlin1 expressing marrow cells represent a more lineage-restricted

precursor population than the Nestin^{+}/LepR^{+} progenitors, which are unable to differentiate into adipocytes, but are capable of self-renewal and giving rise to marrow stromal cells, osteoblasts and chondrocytes [75]. Expression of specific cell surface molecules has been used to identify and distinguish marrow progenitor populations with distinct differentiation potential. BM progenitors with high adipogenic, but limited osteochondrogenic differentiation potential *in vitro* are CD45^{-} CD31^{-} PDGFRα^{+} Sca1^{+} cell population. Further separation of this progenitor population by CD24 showed that only the CD45^{-} CD31^{-} PDGFRα^{+} Sca1^{+} CD24^{-} population could differentiate into adipocytes, whereas CD45^{-} CD31^{-} PDGFRα^{+} Sca1^{+} CD24^{+} progenitors can give rise to not only osteoblasts and chondrocytes but also to adipocytes [64]. On the contrary, none of the cells shared WAT adipocyte progenitor markers (Lin^{-} CD29^{+} CD34^{+} Sca1^{+} PDGFRα^{+}), indicating again that BMAds derive from a distinct precursor population [72]. Taken together, the consensus is that bone marrow adipocytes are derived from BM-resident mesenchymal progenitors with a cell lineage origin different from WAT and BAT adipocytes.

1.2.2 Functional aspects of bone marrow adipocytes

Like WAT adipocytes with large unilocular lipid droplets, BMAT's

appearance of unilocular adipocytes reflects their ability to store lipids and indicates a role as an energy reservoir of functional importance in energy metabolism [76]. The metabolic processes whereby adipocytes store and breakdown lipids are regulated by the insulin and β-adrenergic signalling pathways, respectively [77]. Nevertheless, opposite and varied BMAT responsiveness have been reported in conditions such as caloric restriction, anorexia nervosa and starvation [52, 78, 79]. Supporting information linking BMAT to energy metabolism includes insulin receptor expression by marrow adipocytes and increased BMAT volume in response to high-fat diet, obesity, and rosiglitazone and other anti-diabetic thiazolidinediones (PPARγ-agonists with potent insulin-sensitizing effects that improve systemic glucose homeostasis) [51, 56, 80]. Additionally, an approximate 50% decrease in BMAT volume due to reduced adipocyte size was observed in the distal tibia of *Adipoq-Cre* mice that lack insulin receptor expression specifically in BMAds [81]. These studies demonstrate that BMAds are responsive to and rely, at least partly, upon insulin signalling for lipid storage. It is also suggested that the presence of lipids and fatty acids in BM sera can be utilized to generate energy by bone cells, favouring BMAT as a BM energy depot [76, 82, 83].

Although rBMAT is more susceptible compared to cBMAT in this

instance, lipolysis and fatty acid metabolism induced by β-adrenergic signals were found to occur in BMAT to facilitate hydrolysis of triglycerides into glycerol and fatty acids [77]. It is worth noting that although BMAT presents a degree of similarity to WAT, the adrenergic response of BMAT *in vivo* and *ex vivo* is less significant compared to peripheral WAT regardless of skeletal site and particularly in cBMAT region [77]. Recent technical advancements have permitted the large-scale study of metabolites (i.e., metabolomics) [84]. Metabolomic studies using mass spectrometry of subcutaneous adipocytes [85] and nuclear magnetic resonance spectroscopy of serum [86], have been found. The former study identified cyclic adenosine monophosphate (cAMP) - regulated transcriptional coactivator 3 played a regulatory role in lipid metabolism in porcine subcutaneous adipocytes [85], and the latter showed that metabolomic alterations with higher lipoprotein concentration were associated with higher adipocyte volumes that linked to cardiometabolic diseases [86]. To date, there has no published study on BMAT metabolomics [49]. Thus, research into the metabolomic profile of BMAT is highly warranted.

Only recently has BMAT been identified as an endocrine and secretory-active organ that can produce adipokines, cytokines, and other factors to exert systemic effects and local influences within bone [87].

Adiponectin, previously discovered in WAT as a secreted hormone, is an important adipokine that defines the endocrine function of BMAT [88]. Adiponectin is expressed by BMSC-derived adipocytes in vitro and by primary BMAds isolated from mouse and human long bones, as well as by the intact BMAT depots of mouse caudal vertebrae and tibial of rabbits and humans [89-93]. Circulating adiponectin concentrations negatively correlates with WAT mass as hypo-adiponectinaemia is closely related to obesity and insulin-resistance, whereas elevated circulating adiponectin levels along with BMAT expansion occurs in patients with anorexia nervosa and in humans and animals during caloric restriction [79, 94, 95]. Moreover, it was demonstrated that adiponectin in the circulation required BMAT expansion to increase fully, however, the systemic effects of adiponectin from BMAT are yet to be elucidated [93]. Leptin, recognized for its role in whole-body energy metabolism, is expressed by marrow adipocytes [87, 96, 97]. Leptin inhibits MSC adipogenesis and diminishes marrow adiposity in calorie-restricted, type I diabetic, and leptin-deficient *ob/ob* mice [98-100]. However, a separate investigation suggested that leptin increased adipogenic differentiation of MSCs in *Prx1-Cre LepR* deficient mice [101]. Other secretory factors, such as tumour necrosis factor-α (TNF-α), interleukins (ILs) and RANKL, are also

expressed by BM adipocytes [102-104]. The expression of adiponectin and leptin underscores the endocrine potential of BMAT and the secretion of other factors are indicative of paracrine functions within the BM microenvironment.

It is highly speculated that BMAds functionally participate in bone metabolism and remodelling because of their anatomical location and proximity to a unique BM niche environment rich in osteogenic and haematopoietic activities. Several clinical and animal studies have found that BMAT is reciprocally associated with bone mass, skeletal integrity, and haematopoiesis [105, 106]. In healthy populations, a strong inverse correlation between bone mineral density (BMD) and marrow adiposity is demonstrated across the age spectrum with different racial backgrounds, even though BMAT accumulates and increases during bone growth and peak bone acquisition in long bones [53, 107-109]. The positive association of BMAT with bone loss and fracture risk is further observed in postmenopausal women with low bone density and prevalent osteoporotic fractures, together with an increase in BMAT saturated lipid content [110, 111]. This reciprocal relationship may possibly be due to the skewing of cell fate of BM mesenchymal progenitors between BMAds and osteoblasts. Alternatively, BMAds may secrete factors, such as dipeptidyl peptidase-4, RANKL, and factors mentioned earlier, that perturb osteoblast and

osteoclast functions in bone remodelling [87].

BMAT is generally considered to be a negative regulator of haematopoiesis. Clinical evidence showed that BMAT volume increases after radiation treatment for BM transplantation and in aplastic anaemia patients, and that BMAT expansion subsides after haematopoietic cell recovery and in response to increased erythropoiesis need [87, 112]. In animal studies, haematopoietic regeneration was reduced when haematopoietic stem cells (HSCs) were implanted together with adipogenic progenitors or preadipocytes, whereas improved recovery and haematopoietic reconstitution was improved when BMAds were depleted using either genetic or pharmacological methods [64, 113]. However, other work has suggested that BMAds support the regeneration and function of HSCs. It is shown that stem cell factor (SCF) secreted by marrow adipocytes is required for the maintenance of haematopoietic cells in caudal vertebrae and its absence impairs the reconstitution capacity of HSCs after irradiation leading to a lower survival rate in mice with SCF knockout in adiponectin-Cre expressing cells [114]. Similarly, post-irradiation treatment in mice with leukaemia, BM adipogenesis induced by PPARγ-agonist treatment improved the haematopoietic maturation and reconstitution through regeneration of healthy erythroid progenitors and

granulocytes while suppressing leukemic cell growth [115]. However, the inverse relationship between BMAT and bone mass or haematopoiesis is apparently not absolutely, probably because interactions between BMAds, bone and haematopoietic cells within the BM niche environment are complex and highly context dependent.

1.2.3 Bone marrow adipocytes in metabolic and bone disorders

Osteoporosis, currently the most common and rapidly rising metabolic bone disorder in today's advancing age population, is characterized by low bone density, typically with a marked infiltration of marrow adipocytes and positively correlates to the prevalent risk of fragility fractures [116, 117]. Although multiple factors are known to predispose to the onset of osteoporosis and bone loss, BMAds likely contribute to the disruption of bone homeostasis and remodelling through the secretion of adipokines, paracrine mediators, and fatty acids that affect the differentiation, survival or functions of osteoblasts and osteoclasts and/or through affecting BMSC lineages towards adipogenesis [116, 118]. Various factors, including hormones (adiponectin and leptin), cytokines (IL-6 and TNFα), chemokines (CXCL1 and CXCL2), and lipid products, are reported to be expressed by marrow adipocytes *in vitro*, suggesting a role of

BMAds in bone remodelling, yet *in vivo* mechanistic studies are still insufficient [87, 118]. Alternatively, a clonal shift of BMSCs from osteogenesis to adipogenesis, due to aging, hormonal deficiency, glucocorticoid use, or other genetic or metabolic determinants, can result in decreased osteoblast differentiation, thereby causing bone loss due to reduced bone formation (Figure 1. 5) [119-121]. Moreover, not only is the volume of BMAT an independent risk factor but the lipid composition of BMAT is recently viewed as an important contributor to fracture risk in osteoporosis and other disorders, such as obesity, diabetes and anorexia nervosa, in which increased BM fat saturation is associated with low bone density [105, 111, 122].

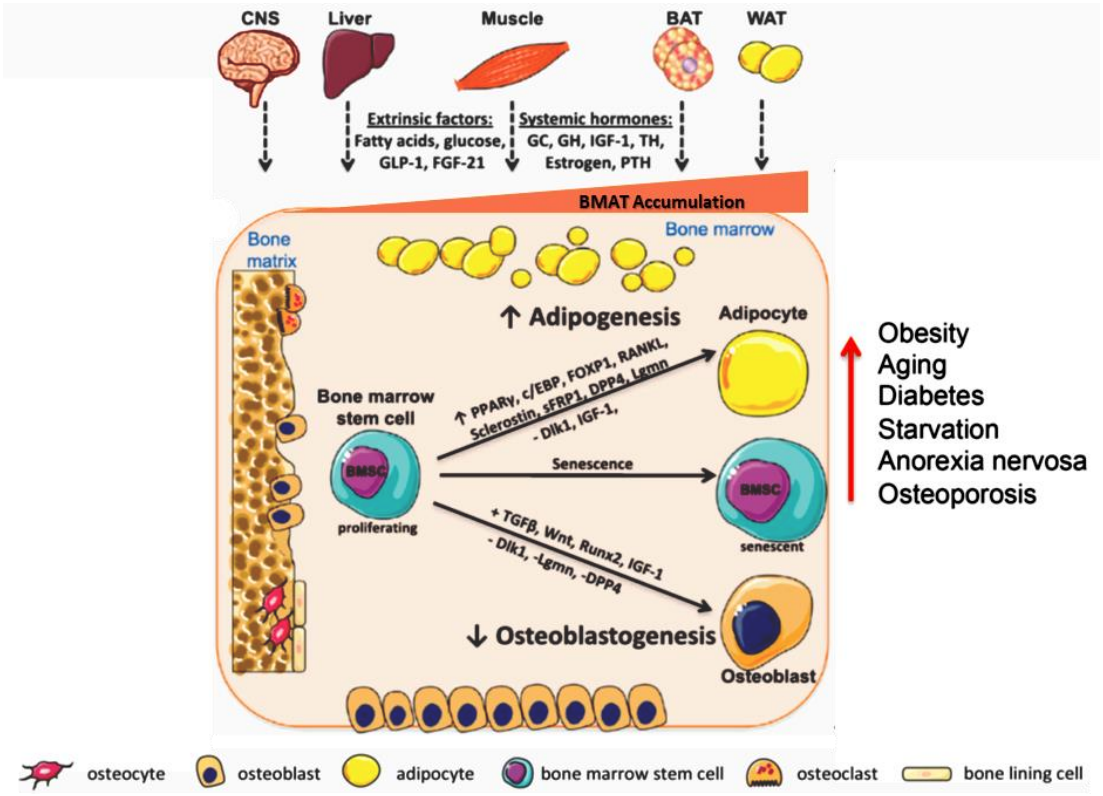

Figure 1.5 Factors and conditions that influence BMSC differentiation favouring adipogenesis over osteoblast formation. Adapted from [123, 124]. BMSCs differentiation into osteoblasts or adipocytes is regulated via multiple transcription factors and secreted molecules, that are either locally produced or released by peripheral tissues such as liver, WAT, BAT, CNS or skeletal muscle, and circulate to the bone marrow niche. This crosstalk between peripheral tissues and bone plays an important role in bone homeostasis and energy metabolism. Imbalance and/or stimulation under conditions such as osteoporosis, diabetes, anorexia nervosa can result in differentiation shift towards an increase in adipocyte formation. *Abbreviations:* CNS, central nervous system; BAT, brown adipose tissue; WAT, white adipose tissue; GH, growth hormone; GLP-1, glucagon-like-peptide-1; FGF21, fibroblast growth factor-21; IGF-1, insulin-like growth factors-1; GC, glucocorticoid; TH, thyroid hormones; PTH, parathyroid hormone; Lgmn, legumain; DPP4, dipeptidyl-peptidase-4; FOXP1, forkhead box P1; DLK1, protein delta homolog 1; TGFβ, transforming growth factor-beta.

In energy imbalance and metabolic disorders, for example anorexia nervosa, obesity and diabetes, marrow adiposity is a potential contributing factor to the increased risk of fragility fracture [118, 125]. Type 1 diabetic subjects have a significantly higher fracture risk than the non-diabetic population, with altered bone microstructure accompanied by an elevated BMAT volume [106, 125]. Animal studies of type 1 diabetes mellitus (T1DM) in streptozotocin-induced and non-obese diabetic mice showed similar results to those reported in human and have low bone volume and BMD and increased marrow adipocytes [126, 127]. However, recent investigations reported no

difference in marrow adiposity between T1DM patients and healthy controls, whilst marrow adiposity was positively correlated to serum lipid levels [128, 129]. Similarly, conflicting results of BMAT volume have been reported in type 2 diabetes mellitus (T2DM), where patients suffer from increased fractures risk but usually exhibit only average or slightly higher BMD [125]. Nonetheless, clinical presentations of T2DM, besides insulin resistance, generally correspond with disturbed metabolic profiles, adipose tissue inflammation, and excess weight or obesity [118]. Although the amount of marrow fat is not different between overweight individuals with and without T2DM, a positive correlation between marrow adiposity and HbA1c level of glycaemic control has been shown in T2DM patients [130]. Additionally, studies have observed a negative association of lipid unsaturation level in BMAT with diabetes and fracture; clearly the relationship between BMAT and T2DM deserves further investigation [111, 118, 130]. It is worth noting that inhibition of the BMAT accumulation does not prevent bone loss in T1DM or post-ovariectomy, indicating that effects of bone strength and microstructure depend on additional mechanisms [131, 132].

A significant increase of marrow fat is observed in obese individuals, as well as an increased fracture risk at specific bone sites due to altered skeletal

quality and microstructure has been reported in several clinical and epidemiologic studies [133-135]. Indeed, high body fat is positively correlated with high marrow fat in obese subjects as compared to healthy and normal-weight controls [136, 137]. Moreover, studies show that increased marrow adiposity is associated with bone loss and skeletal fragility due to a decrease in bone formation as observed histologically [118, 138]. Comparable to humans, high-fat diet induced obesity increases bone marrow fat in multiple mouse models [51, 139].

At the other end of weight spectrum, patients with anorexia nervosa are characterized by self-restrictive eating and starvation resulting in extreme weight loss [122]. Clinical observations show that despite the profound depletion of visceral and subcutaneous fat, anorexic patients have a much greater marrow adiposity along with bone loss and frequent fracture incidence [118, 140]. In human and animal models of anorexia nervosa, an inverse correlation between marrow adiposity and BMD is consistently observed, though no difference was found in the BMAT fatty acid composition when comparing anorectic patients with control subjects [106, 122]. Conversely, individuals who have recovered from anorexia have vertebral marrow fat and BMD comparable to healthy controls [140, 141].

In summary, these studies provided controversial yet intriguing results regarding the status of bone marrow adiposity in skeletal and metabolic disorders, including but not limited to those described here. Although the association and mechanism require further elucidation, the research clearly indicates that BMAT may serve different purposes and have distinct functional capacity dependent on the individual's physical state, including age and nutritional, metabolic and hormonal status [105, 118, 142].

1.3 Bone marrow stromal cells as common progenitor cells of osteoblasts and adipocytes

Bone marrow stromal cells (BMSCs), also known as skeletal or mesenchymal stem cells, are a heterogeneous population of multipotent cells residing in bone marrow (BM) stroma, that give rise to osteoblasts, chondrocytes, and adipocytes, under appropriate stimuli and physiological demands (Figure 1.6) [143]. Technology advancements and research efforts over many years have delineated sub-populations of heterogeneous BMSCs with regard to their lineage differentiation capacities through the use of cell surface markers, gene and transcriptome expression, single-cell analysis, and murine lineage tracing models [64, 73, 75, 144].

Osterix expression specifies distinct stromal progenitor populations in BM development during foetal, neonatal, and adult phases, that respectively are transient stromal and nascent bone cells, long-lived marrow stroma and osteolineage cells, and progenitors restricted to osteolineage [63]. In contrast, BM stromal progenitors that express leptin receptor (LepR) develop postnatally and comprise most bone cells and marrow adipocytes in adult mouse BM [73].

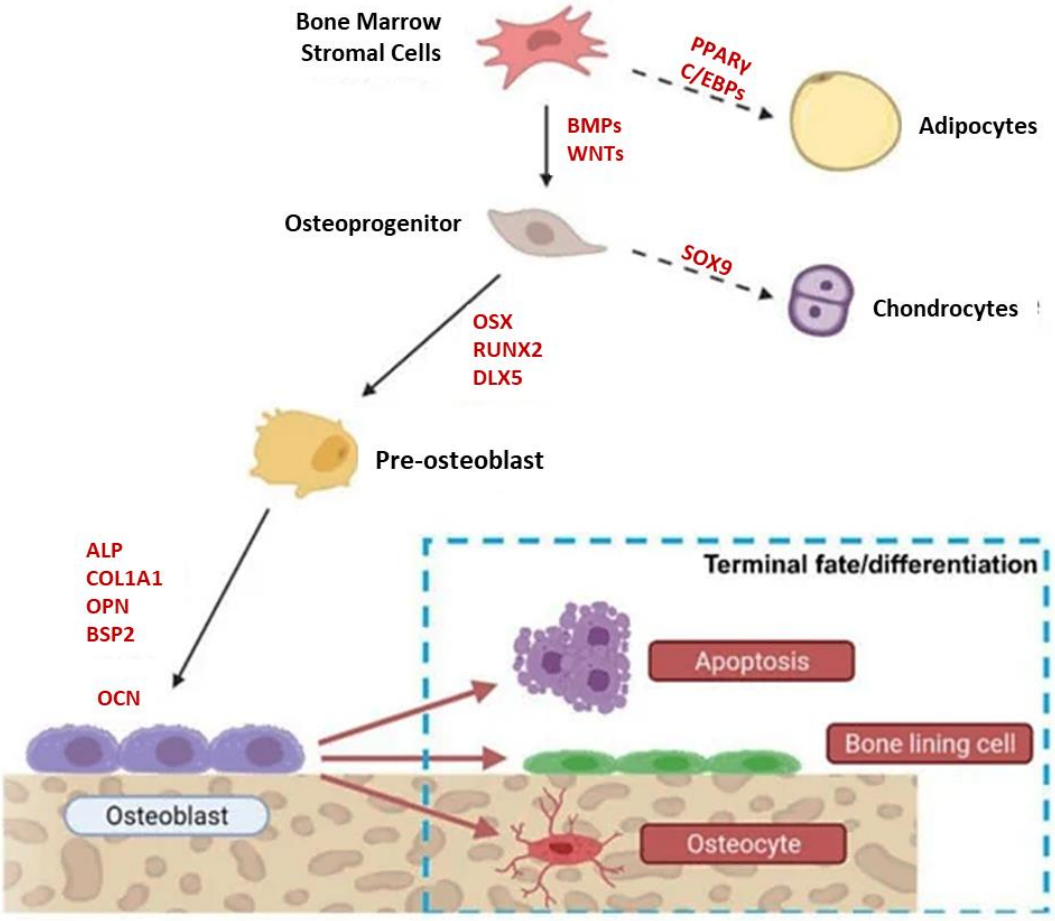

Figure 1. 6 Schematic illustration of the possible cell fate differentiation of bone marrow stromal cells (adapted from [145]). BMSCs can differentiate into osteoblasts, adipocytes, or chondrocytes depending on, but not limited to, specific factors and signalling pathway such as BMP and WNT pathway or master transcription factors like RUNX2, PPARγ, and SOX9. Osteoblast differentiation begins with commitment toward a common osteoprogenitor cell,

that is subsequently committed to pre-osteoblast following the activation of osteogenic transcriptional factors, such as RUNX2 and OSX. This committed pre-osteoblast then transcribes early osteogenic genes, such as *ALP* and *COL1A1*, and develops into osteoblasts with expression of common osteoblast markers, such as *BSP II* and *OCN*. Mature osteoblasts have three possible fates, which are (1) apoptosis; (2) becoming bone lining cells or (3) osteocytes.

Skeletal stem cells (SSCs) that are able to generate osteoblasts, chondrocytes, and BM stroma, but not BM adipocytes, are distinguished by expression of an array of cell markers or BMP antagonist gremlin 1 in the mouse postnatal skeleton [75, 144]. Two separate studies from Longaker's lab have identified $CD45^{-}Ter\text{-}119^{-}Tie2^{-}AlphaV^{+}Thy^{-}6C3^{-}CD105^{-}CD200^{+}$ mouse SSCs and $PDPN^{+}CD146^{-}CD73^{+}CD164^{+}$ human SSCs with lineage-restricted capability to generate bone, cartilage, and marrow stroma [144, 146]. The cell state hierarchy and differentiation trajectories of BMSCs to stromal, osteoblast, chondrocyte, and adipocyte lineages have recently been mapped and validated via a combination of single-cell RNA sequencing, cell fate-marked reporter mouse strains, and gene knockdowns and differentiation assays [147]. Together, these studies demonstrate the heterogeneity of BMSC populations and support the concept of BM-resident multipotent cells as the source for bone, fat and stroma cell types that provide for skeletal development, repair, and homeostasis.

A regulated and balanced allocation of BMSC lineage cells is

important since BMSCs give rise to all the major cell types that constitute the BM and skeleton. Master regulators and key signalling mechanisms have been shown to regulate the commitment and differentiation of BMSC to osteoblasts and adipocytes; the transcription factors RUNX2 and Osterix (OSX/Sp7) for osteogenic differentiation and peroxisome proliferator-activated receptor γ (PPARγ) and CCAAT/enhancer-binding protein alpha (C/EBPα) for adipogenesis, and WNT and BMP dependent signalling are involved in lineage differentiation [124, 148]. In addition, other factors, such as hormones, cytokines, mechanical stimuli, and aging, also contribute to cell fate decision of BMSCs [148]. A number of bone disorders are caused by the disturbance and dysfunction of BMSC differentiation and regulatory mechanisms, that leads to altered skeletal remodelling and repair, resulting in bone fragility and abnormal changes [124, 149]. Therefore, synergistic and tight coordination between cellular and systemic regulation, and adaption to external factors are crucial to maintain healthy and balanced cell fate differentiation of BMSCs. In the following sections, key transcription factors, signalling regulators, and bone diseases involved in lineage determination of BMSC cell fate are described.

1.3.1 Key transcriptional regulators of BMSC lineage differentiation into osteoblasts and adipocytes

The cell fate decision of BMSCs is strictly orchestrated by master transcriptional regulators; RUNX2 and OSX/Sp7 are essential for osteoblast differentiation whilst PPARγ and C/EBPs are indispensable for adipogenesis (Figure 1.7) [150, 151]. These four transcription factors are recognized for their central roles in lineage determination of BMSCs and interestingly RUNX2 and PPARγ are able to reciprocally suppress each other [152].

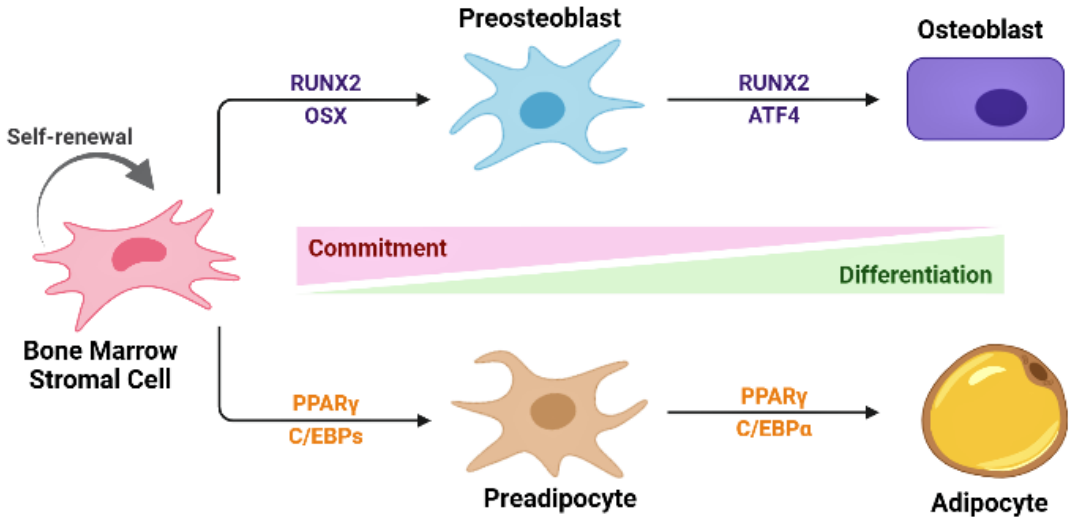

Figure 1.7 Transcriptional regulators of osteoblastic and adipocytic differentiation of bone marrow stromal cell. BMSCs have the potential to self-renewal and differentiate towards osteoblast and adipocyte lineages dependent upon multiple transcriptional factors and specific signals. The key transcriptional regulators RUNX2, ATF4 (activating transcription factor 4) and OSX (osterix) control osteoblast lineage differentiation. The master transcription factors, PPARγ and C/EBPs regulate adipocyte lineage differentiation. Created with biorender.com.

During osteoblast differentiation, *Runx2* is expressed weakly in uncommitted BMSCs, and is then gradually upregulated in osteochondrogenic progenitors following commitment to osteoblast lineage. *Runx2* reaches its highest expression level in immature osteoblasts before it is down-regulated in mature osteoblasts that are embedded in the bone matrix [153]. Importantly, not only does RUNX2 have a crucial role in early osteoblast differentiation, but it is also involved in key signalling pathways regulating the osteogenic process [12]. The proliferation of osteoblast progenitors is regulated via RUNX2 induction of FGFR2 and FGFR3 signalling. The inhibitory regulation of *Runx2* expression in osteoblast lineage cells was shown in studies of *Runx2* knockout animals and siRNA knockdown cells, in which *Runx2* expression declined with increased osteoblast maturation, [154, 155].

OSX/Sp7, regulated by upstream RUNX2, is another essential transcription factor for activating osteoblast specific genes during osteoblast differentiation [63, 156]. While *Runx2* expression segregates osteochondrogenic progenitors to osteoblast precursors, OSX/Sp7 induces the continued differentiation of preosteoblasts into mature and bone matrix-producing osteoblasts [156]. It has been shown that both $Sp7^{-/-}$ and $Runx2^{-/-}$ mice exhibit cartilaginous skeletons that lack mineralized bone formation,

because osteoblasts fail to differentiate in *Sp7*$^{-/-}$ mice and *Runx2*$^{-/-}$ mice lack *Sp7* expression observed in the skeleton [12, 157, 158]. Putative response elements in addition to *Runx2*, such as *Sox9*, *VDRE*, *Dlx5* and *Sp1*, are also presented upstream of the *OSX/Sp7* promoter region [159]. Studies showed that BMP signalling induced *OSX/Sp7* expression by upregulating *Dlx5* that interacts with the *OSX/Sp7* promoter and can synergistically increase *OSX/Sp7* expression with insulin-like growth factor signalling via MAPK and protein kinase D pathways [160, 161]. These results demonstrate that signalling mechanisms apart from RUNX2, may also be critical to OSX regulation during osteoblast differentiational progression.

In contrast, PPARγ, a nuclear receptor highly expressed in adipocytes, is a master regulator of adipogenesis [162]. Activation of PPARγ can modulate BMSC cell fate into adipocyte terminal differentiation and maintain the differentiated state of adipocytes [163], while also acting in concert with C/EBPα to establish the mature adipocyte phenotype in adult stages [164]. Functional expression of PPARγ is essential for embryonic development and adipogenesis *in vivo* and *in vitro*, as systemic PPARγ deletion is embryonic lethal in mice [165]. Depletion of PPARγ that is limited to adipose cells results in extensive loss of adipose tissue, severe insulin resistance and diabetes, fatty liver, and

multiple abnormalities in bone, skin, and mammary glands [166, 167]. Conditional PPARγ deficiency demonstrated that the survival of mature adipocytes requires PPARγ expression [163]. Nevertheless, PPARγ cooperates with C/EBPα, as they mutually induce the expression of each other during adipogenesis. However, the activity of C/EBPs are dependent upon PPARγ expression to be functionally efficient [167].

During adipocyte commitment and differentiation, C/EBPs collaborate closely with PPARγ and initiate a transcriptional cascade, as C/EBPβ and C/EBPδ are upregulated promptly in the early adipogenesis stage and activate the expression of C/EBPα and PPARγ [168, 169]. Mice lacking C/EBPβ and C/EBPδ (*Cebpb*$^{-/-}$ *Cebpd*$^{-/-}$), which have normal expression levels of C/EBPα and PPARγ, display significantly reduced epididymal fat mass and are defective in lipid droplet accumulation in brown adipose tissue [170]. Adipocyte-specific and inducible knockout of C/EBPα in mice confirmed it is essential for white adipocyte development in adult but not embryonic stages [171]. In contrast, C/EBPα was unable to promote adipogenesis in the absence of PPARγ [172]. Although PPARγ and C/EBPα are central to adipogenic commitment, other transcription factors (e.g. Zfp423, KLFs, and C/EBPβ), epigenetic mechanisms (e.g. gene acetylation or methylation), and several signalling pathways (e.g.

WNT, TGFs, and Hh pathways) contribute at different stages of differentiation [173, 174].

1.3.2 Major signalling pathways of BMSC lineage differentiation

Lineage commitment and differentiation of BMSCs towards either an osteogenic or adipogenic cell fates is highly regulated process that involves the activities of distinct transcriptional factors. Induction of specific signalling pathways is also important [148]. It is discussed below that whilst some signalling cascades are identified as pro-osteogenic, others are context dependent and can affect both osteogenesis and adipogenesis [175]. Relevant signalling pathways include, but not limited to, wingless-type MMTV integration site (WNT) signalling, TGFβ/BMP signalling, Hedgehogs (Hh), and fibroblast growth factors (FGFs) [148, 175].

The WNT family of proteins comprises of multiple secreted glycoproteins that share highly conserved cysteine residues and depending on intracellular responses [176]. WNT signalling is classified into the β-catenin dependent canonical WNT (WNT/β-catenin) pathway and the non-canonical WNT pathway involving jun N-terminal kinases and protein kinase C. Although the contribution of WNT signalling to osteogenic differentiation is contentious,

with reports of both stimulatory and inhibitory effects, canonical WNT/β-catenin pathway activation, in general, facilitates osteogenesis and inversely inhibits adipogenic differentiation [14, 176, 177]. Canonical WNT signal transduction initiates via extracellular WNT ligands binding to transmembrane frizzled receptors, which induces the formation of ternary complex with the co-receptor low-density lipoprotein receptor-related protein 5/6 (LRP5/6) and activates intracellular Dishevelled proteins (Figure 1. 8) [14]. This signalling cascade results in accumulation and nuclear translocation of unphosphorylated β-catenin that heterodimerizes with lymphoid enhancer-binding factor / T-cell-specific transcription factor to promote gene transcriptional activity and thereby influence the cell fate of BMSCs [178].

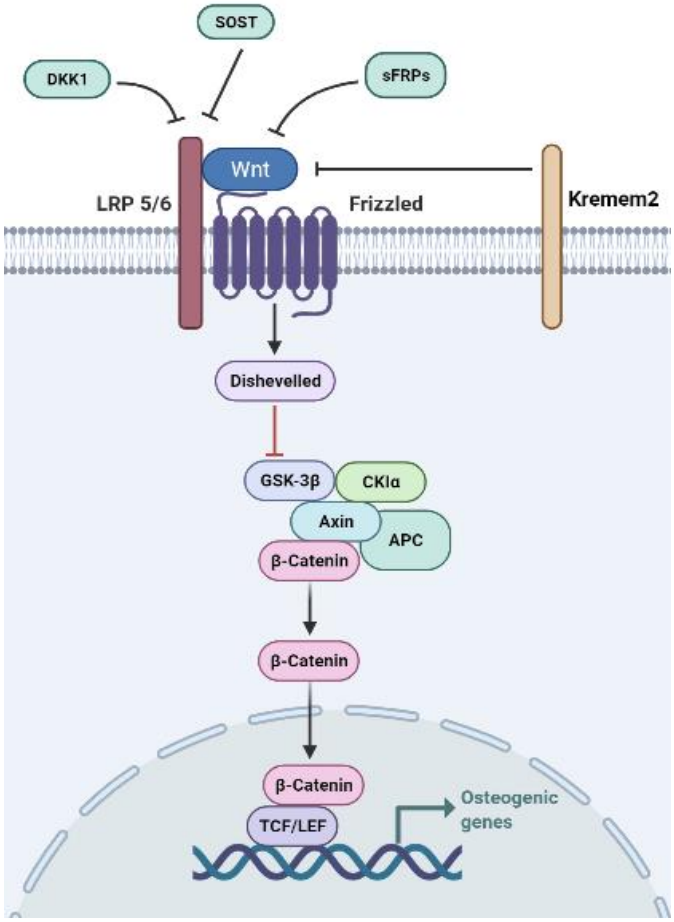

Figure 1.8 WNT/β-catenin signalling pathway. WNT/β-catenin signalling is activated via binding of WNTs to frizzled receptors and phosphorylation of LRP5/6 co-receptor by CK1, which recruits Dishevelled proteins to the plasma membrane and suppresses GSK-3β (glycogen synthase kinase-3β) activity in the β-catenin complex with Axin. This allows β-catenin to accumulate in cytosol and translocate into nucleus and complex with TCF/LEF to activate target genes. Created with biorender.com.

The importance of WNT/β-catenin pathway to bone formation and differentiation has been demonstrated in humans and animal models. The link between WNT/β-catenin signalling and bone biology was identified through the mutational studies of *Lrp5* [13, 175], where the loss-of-function mutations of *Lrp5* resulted in low bone mass and frequent bone fracture, conversely, *Lrp5* gain-of-function mutations result in high bone density phenotype [179, 180]. In contrast, *Lrp5*-deficient mice exhibited a reduction in bone mass [181] and mice lacking β-catenin in osteoblast lineage cells displayed severe osteopenia with

significantly greater numbers of osteoclasts [177]. In addition, WNT3a signalling, mediated by co-receptor LRP5/6, promoted key regulators of osteoblast differentiation expression, such as BMPs, FGFs, and WNT proteins [182]. In separate studies, WNT3a improved bone remodelling and angiogenesis in postmenopausal mice under mechanical loading [183] and localized WNT3a treatment of large osseous defects restored bone formation after osteomyelitis debridement surgery [184]. Moreover, various studies have implicated the functional importance of WNT3a in osteoblast metabolism (e.g. glycolysis), and the osteogenic transcription factors (e.g. LEF and TAZ) and signalling (e.g. FGF-2 and LRP5/6) to osteoblast differentiation [182, 185-187].

WNTs have been shown to suppress adipogenesis. For example, WNT10b maintained the undifferentiated state of preadipocytes by inhibiting the master adipogenic transcription factors PPARγ and C/EBPα [188-190]. Additionally, significantly less adipose tissue accumulated in transgenic mice overexpressing WNT10b under the control of the FABP4 adipocyte-specific promoter when maintained on normal chow diet and under diet-induced obesity conditions [191]. Overall, these studies demonstrate that WNT/β-catenin pathway activation generally exerts a positive regulatory role in osteogenic differentiation and negatively impacts adipogenesis.

The BMP signal transduction pathway is a crucial pathway involved in the regulation of osteogenic differentiation and of bone formation. BMP and WNT signalling pathways have extensive interactions in coordinating osteogenic and adipogenic lineage differentiation [192], where WNT-induced osteogenic differentiation can be either enhanced or antagonized by different BMPs [193] and at the same time, osteogenesis induced by BMPs relies on functional WNT signalling pathways [194]. For instance, canonical WNT signalling downregulation was shown to be modulated by BMPs via expression of the WNT antagonists sclerostin and Dkk-1 leading to decreased bone mass, whereas decreased levels of sclerostin and Dkk-1 in mice lacking BMP receptor type 1 in osteoblasts increase bone mass [195]. Moreover, whilst β-catenin downregulation suppressed postnatal osteogenesis in mice, BMP-2 induced expression of multiple WNT receptors and their ligands and increased the levels of osteogenic differentiation markers, suggesting that WNT/β-catenin signalling is highly activated during BMP-2-mediated osteoblast differentiation [196]. Alternatively, BMP-induced adipogenesis involved the activation of Smad and MAPK downstream of BMP signalling pathway [197]. Jin *et al.* [198] showed that in support of adipocyte differentiation, upon BMP-2 stimulation, Schnurri-2 entered the nucleus and directly interacted with both Smad1/4 and C/EBPα to

activate PPARγ2. Interestingly, a significant increase in BMP-4 expression was confirmed during early adipogenesis to preadipocyte development [199] and the overexpression of BMP-4 in preadipocytes was sufficient to induce mesenchymal progenitor cells (C3H10T1/2) commitment to adipocyte lineage differentiation [200].

In summary, WNT and BMP signalling pathways interact in a complex and dynamic network. However, not all signalling pathways involved in osteogenic and adipogenic differentiation are discussed here. The balance and reciprocal relationship between adipocyte and osteoblast differentiation have become a topic of interest in pathophysiologic conditions, such as aging, osteopetrosis, and osteoporosis, in which there is an inverse correlation between bone and fat formation.

1.3.3 The inverse correlation between adipogenesis and osteogenesis

Chronic metabolic diseases, such as diabetes and osteoporosis, are major public health concerns with an increased fracture risk as a common complication leading to considerable morbidity and mortality rates [106]. Human cross-sectional studies [201, 202] have established an inverse correlation between bone mass and bone marrow fat particularly in skeletal

ageing and osteoporosis, when high marrow adiposity is closely linked to reduced bone integrity, thereby resulting in high risk of bone fracture [106]. An extensive investigation of different murine osteoporotic models, induced by aging, sex hormone deficiency and glucocorticoids, supports an association between increased BMAT with bone loss [149]. In agreement with the reciprocal relationship between marrow adiposity and bone mass reported in diseases, cellular commitment between the two lineages is considered contradictory [106]. As the prevalence of these disorders increases, greater understanding of the inverse association between bone and BMAT should provide insights into disease mechanisms and importantly, identify targets for novel treatments to ameliorate bone loss.

BMSC differentiation toward osteogenic and adipogenic lineages is tightly orchestrated by the cascade of molecular cues and transcriptional regulators in the bone marrow microenvironment [148]. Studies indicated that tradeoffs occurred between osteoblast and adipocyte cell fate during lineage differentiation of BMSCs [106, 148]. A robust study identified a specific subset of BMSCs that differentiate unilaterally into committed osteogenic or adipogenic precursors and further indicated detrimental effects of marrow adipocytic cells on hematopoiesis and fracture repair (Figure 1.9) [64, 203]. Furthermore, an

adverse relationship, where an increase of BMAT occurs at the expense of bone formation, has been demonstrated [204, 205]. Yu *et al.* [205] showed that deleting peroxisome proliferator-activated receptor-gamma coactivator-1alpha (*Pgc1α*) in mesenchymal cells enhanced bone loss and BMAT accumulation, whilst enhancing *Pgc1α* diminished BMAT and improved bone formation in a murine osteoporosis model. In contrast, SOST impaired bone formation and increased marrow adiposity, whilst conditional deletion of SOST in osteoprogenitors dramatically increased bone mass [206]. Fan *et al.* [204] showed that wild type mice exposed to intermittent PTH exhibited significantly reduced BMAT volume comparable to male osteoporotic patients. This study confirmed that the mechanism underlying the benefit of a PTH therapy was its ability to direct BMSC cell fate.

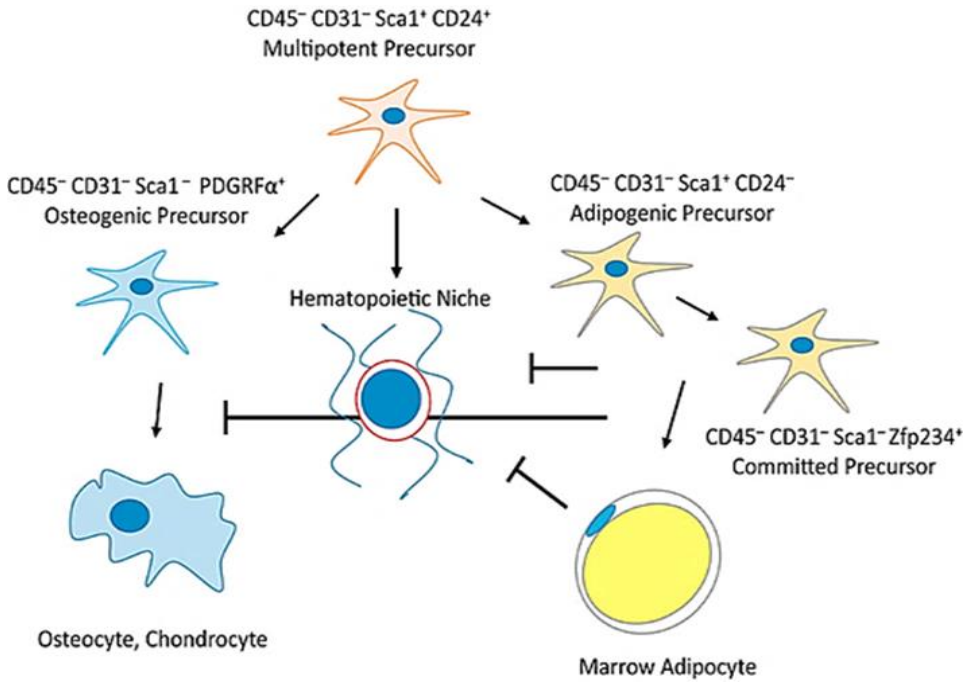

Figure 1.9 Precursor hierarchy in bone marrow (adapted from [203]). Lineage-tracing efforts by Ambrosi *et al.* [64] identified a shared population of BMSCs ($CD45^-$, $CD31^-$, $Sca1^+$, $CD24^+$ multipotent precursor cells) that can give rise to both osteogenic precursors ($CD45^-$, $CD31^-$, $Sca1^+$, $PDGFR\alpha^+$) and adipogenic precursors ($CD45^-$, $CD31^-$, $Sca1^+$, $CD24^-$). Both precursor types are further committed to osteoblast and adipocyte lineages and later develop into mature osteocytes and adipocytes. The inhibitory effects of adipocytic cells on osteogenesis and hematopoiesis are also emphasized here.

The well-known paradigm of bone loss results from an imbalance between bone resorption by osteoclasts and bone formation by osteoblasts. Current drug treatments to prevent bone loss include multiple lines of drugs that target osteoclastic bone resorptive function (anti-resorptive drugs) to slow down the destruction of bones [207]. Although anti-resorptive agents allow longer time for bone formation, they do not improve bone accruement function by osteoblasts and may have side effects, such as affecting the metabolism of old and damaged bone during bone remodelling, thereby causing unwanted complications such as atypical fracture [208]. There is increasing evidence that pathogenic mechanisms involve aberrant osteogenic and adipogenic lineage allocation of BMSCs [106, 148]. Imbalanced lineage distribution of BMSCs can lead to bone disorders, including osteopenia, osteoporosis and osteopetrosis, since the osteogenic differentiation of BMSCs is coordinately inhibited during adipogenic differentiation [148, 209]. The switch of BMSC fate exposes a

crucial mechanism that is altered in skeletal aging and related diseases.

Drugs that are used to treat osteoporosis are broadly either anti-resorptive drugs that reduce bone resorption or anabolic agents that promote bone formation. Current pharmacologic treatments includes a majority of anti-resorptive agents, with bisphosphonates and denosumab as the most commonly prescribed therapeutics [210]. In contrast, there are currently just three anabolic agents (teriparatide, abaloparatide and romosozumab) and of which only teriparatide is currently clinically approved worldwide [207]. Bisphosphonates produce good outcomes by lowering the fracture risk and improving bone marrow density (BMD) with initial short-term (3-4 years) treatment but fail to demonstrate a long-term clinical benefit with no further increase in hip BMD and high risk of atypical fracture [210]. In contrast, the bone anabolic drugs teriparatide and abaloparatide can rapidly increase bone formation when use intermittently, but the bone resorption rate increases with their sustained used [211]. The latest anabolic drug romosozumab has shown great promise owing to its dual effects of stimulating bone formation whilst inhibiting bone resorption. However, within 6 months, the increase of bone formation levels off despite continuous administration [212]. Therefore, bone-anabolic and dual-action treatments reduce fracture risk and increase BMD in

the short term, but do not currently offer sustained benefit and anti-resorptive treatments should be followed [210]. In light of these limitations, the search for new pharmacologic agents that offer better therapeutic management is ongoing.

1.4 Scavenger receptor class A number 5 (SCARA5/SR-A5) as a molecular switch between bone and fat formation

Scavenger receptors (SRs) constitute a large group of membrane-bound pattern recognition receptors that are structurally diverse and recognize a wide range of ligands, including both host-derived endogenous molecules and pathogen-associated ones [213]. SRs are known to be involved in a broad range of biological processes not only due to the largely diverse receptors in SR family but also due to their association with various signalling pathways and receptors, making their functions extremely versatile [214]. Currently, mammalian SRs have been classified into 11 distinct classes (A-L) as illustrated in Figure 1.10 [213]. Although SRs were initially identified on macrophages due to their ability to bind and internalize modified low-density lipoproteins, thereby contributing to atherosclerosis, increasing research efforts have revealed their multiple biological roles, particularly within innate immunity [215]. More relevantly, several recent studies on SRs have started to explore their activities in bone formation and BMSC differentiation, suggesting a potential role in bone biology [216-220].

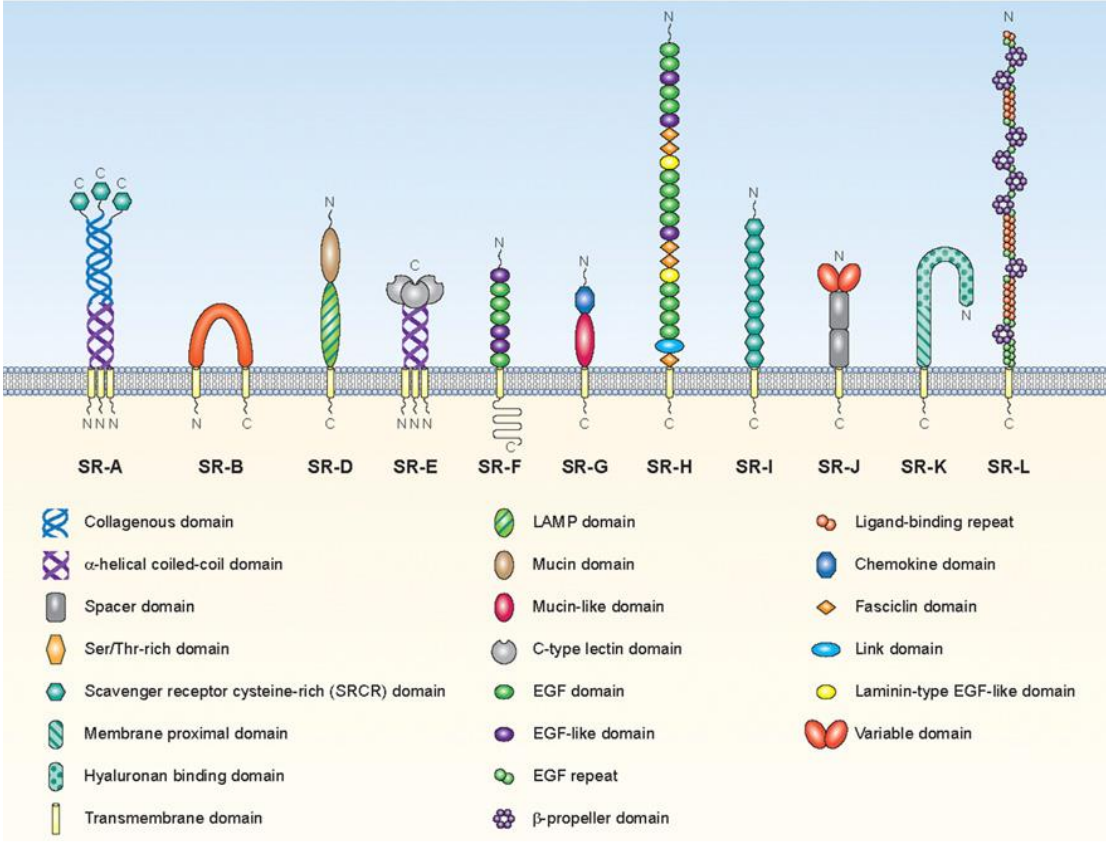

Figure 1.10 Schematic representation of scavenger receptors categorised into different classes [213]. A total of 11 classes of mammalian scavenger receptors are shown. The various protein or carbohydrate receptor domains are identified in the figure key. As Class C is found only in Drosophila melanogaster, it is not shown here.

Class A scavenger receptor was originally identified in macrophages for their function to take up modified low-density lipoprotein (LDL) and the scavenger receptors class A number 1 (also known as SR-A1/SCARA1/MSR1) was the first scavenger receptor cloned by Kodama *et al.* [221, 222]. A workshop in 2017 attempted to agree upon and standardise the nomenclature of scavenger receptors as shown in Figure 1.10 [213]; however, a lack of

consistency of the use of names in the published literature remains. For example, the receptor originally referred to as MSR1 is also known as SR-A SR-A1 , or SCARA1; whilst SCARA5 (the subject of this thesis) is also known as SR-A5 or TESR. To minimize confusion and to maintain consistency in this thesis, the name used will be that from the publication that is being cited.

Class A scavenger receptors (SR-As) are Type II membrane proteins, with unique collagenous domain form a homotrimers on cell membrane [215]. SR-As share structural similarity based upon protein domains and comprise a cytoplasmic N-terminal tail, a transmembrane and spacer regions, α-helical coiled-coil and collagenous domains, and a scavenger receptor cysteine-rich C-terminal domain (Figure 1.10) [213]. SR-A1 and SR-A6 are expressed primarily in macrophages, whereas SR-A3, SR-A4, and SR-A5 are ubiquitously expressed by multiple tissues and cell types [213]. Although investigations of SR-A1 originally focused on the uptake of modified LDL, interest in the biology of SR-As has diversified beyond roles in atherosclerosis and vascular diseases. Studies have implicated SR-As in innate immunity, inflammation, and cancer progression [223]. Meanwhile, several other studies have revealed activities related to osteoclast biology, adipocyte and osteogenic differentiation, and BMSC fate determination [217, 219, 224, 225], thereby linking their roles to

bone metabolism. Here, a few of the studies that have associated SRs with bone biology will be described.

1.4.1 Scavenger receptors in the skeletal realm

Due to structural and functional diversity with a large repertoire of ligands and expression on multiple cell types, studies on SRs are dispersed into different research fields. However, it is exciting to find a handful of recent investigations that begin exploring functional aspects of SRs in bone cells, bone formation and differentiation.

Since SRs were initially discovered on macrophages capable of internalizing modified low-density lipoproteins (LDLs) [213], some studies looked further into its derivative cell, osteoclasts, for their specific cellular roles and functions. It was found that *SR-A* deletion led to an increase in bone volume, trabecular bone density and thickness, that correlated with a dramatic decrease in osteoclast number compared to control wild-type (WT) mice [216]. The authors also demonstrated that exogenous stimulation with soluble SR-A extracellular domain significantly promoted osteoclast differentiation of RAW264.7 cells in the absence of RANKL. Later, Takemura *et al.* [218] again confirmed the effect of *SR-A1* deficiency on osteoclast number and

differentiation, and further revealed that *SR-A*$^{-/-}$ osteoclasts expressed significantly lower RANK and RANK-related osteoclast differentiation molecules compared to WT controls. A study by Guo *et al.* [226] identified that the significant decrease in *SR-A*$^{-/-}$ osteoclasts was resulted from the downregulation of extracellular signal-regulated kinase (ERK) and c-Jun N-terminal protein kinase (JNK) signalling pathways. Moreover, it was shown that inhibitory function of oxidised-LDL on osteoclastogenesis was mediated through SR-A, as blocking SR-A restored the inhibition of oxidised-LDL on osteoclastogenesis [225]. These studies suggested a crucial role of SR-A in osteoclast formation and activity.

Several studies explored the roles of different SRs in bone due to their expression on osteoblasts [227, 228] and the links of lipoprotein metabolism to bone mass with SRs being lipoprotein receptors [229]. CD36, a class B scavenger receptor (SR-B2) that is present on multiple cells, including platelets, monocytes/macrophages, endothelial cells, adipocytes, and bone cells, was found to influence bone formation [220]. A phenotype of low bone volume and trabecular density was observed in *CD36*-deficient mice compared to WT controls (1-6 months), which correlated with plasma markers and histochemistry analyses showing reduced levels of bone formation markers,

mineral apposition, and bone formation rate [220]. Similarly, a decrease in bone volume and trabecular thickness was reported in *Scarb1*$^{-/-}$ mice at 16 weeks but not at 8 weeks [230]. Additionally, analysis of specific osteoblast and osteoclast-related mRNAs showed a significant decrease in *Scarb1*$^{-/-}$ bone cells, and *in vitro* differentiation assays demonstrated reduced osteoblast and osteoclast formation in the absence of SCARB1 [230]. These data indicated that the lack of *Scarb1* and *CD36* expression diminished bone formation and negatively affected bone volume in mice.

One study reported upon the role of MSR1 (SR-A1) in macrophages in bone fracture healing and how MSR1 affected BMSC differentiation in co-culture [224]. The authors demonstrated that *MSR1* knockout (KO) mice had impaired intramembranous bone healing as compared to WT mice in a tibial defect model. The underlying mechanism was downregulation of the PI3K/AKT/GSK3β/β-catenin pathway that promoted BMSC osteogenic differentiation under *MSR1* depletion [224]. Recently, a connection between SCARA3 and BMSC differentiation was revealed by Chen *et al.* [219]. They showed that *Scara3* overexpression enhanced osteogenesis and suppressed adipogenesis and that increasing SCARA3 expression through intra-bone marrow injection mitigated bone loss and reduced marrow fat in ovariectomized

and aged mice [219]. *Scara3* overexpression increased FOXO1, an autophagy inducer and positive regulator of bone formation [231, 232], indicating that SCARA3 modulated BMSC cell fate switch via autophagy flux and FOXO1 [219].

To sum up, SRs are involved in bone biology via their associations with the macrophage-osteoclast lineage link, their expression on osteoblasts, and because they are lipoprotein receptors. To date there are no published studies into the role(s) of SCARA5 in bone formation and, in particular, there is a lack of *in vivo* studies. The following sections document previous studies on SR-A5 and evidence for its potential association with bone formation.

1.4.2 The similar dissimilarities of scavenger receptor class A member 5

SCARA5 was first identified and characterized by Jiang and colleagues as a receptor with a structure typical of the class A scavenger receptors [233]. The molecule consists of a N-terminal intracellular, transmembrane, collagenous, and C-terminal cysteine rich domains. The characterization of SCARA5 presented a unique tissue distribution pattern that was similar, but not identical, to other scavenger receptor class A family members [233]. *Scara5* transcripts was first found in populations of epithelial cells and later histology and immunostaining analyses revealed its primary

expression by fibroblast subpopulations in the interstitial stroma of various mouse tissues, with strong expression in testis, liver, and heart and weaker detection in lung, skeletal muscle, kidney, spleen, and brain [234]. In addition, the inability of SCARA5 to endocytose acetylated or oxidized LDLs distinguished it from other SR-As [233]. To date, SCARA5 has been implicated in ferritin transport, tumour progression, and adipocyte differentiation [235-238].

Ferritin, composed of 24 subunits of heavy (H) and light (L) chains and with a large cavity for iron deposition in a mineral form (ferrihydrite), is required for iron storage and detoxification of free radicals [239, 240]. Both heavy and light chain ferritins can incorporate iron independently, with the light chain nucleates iron and the heavy chain possesses ferroxidase activity [240]. Investigation by Li *et al.* discovered that SCARA5 was an important ferritin receptor in murine embryonic kidney that bound and endocytosed ferritin for iron delivery [241]. The authors found that SCARA5 was significantly upregulated, as a result of depletion of transferrin receptor. Another separate study also demonstrated SCARA5 to be a ferritin light chain (L-ferritin) receptor specifically expressed in murine endothelial and smooth muscle cells of the retinal vasculature [235]. It was shown that SCARA5 bound and facilitated ferritin across the blood retinal barrier and that its expression dramatically

decreased during induced retinopathy, suggesting SCARA5 as a potential therapeutic target [235].

SCARA5 has been implicated in the progression of several tumours, such as osteosarcoma, liver, and lung cancers. Huang *et al.* found that *SCARA5* downregulation due to allelic loss and epigenetic DNA hypermethylation was associated with human hepatocellular carcinoma (HCC) vascular invasion [236]. The authors demonstrated that downregulation of *SCARA5* enhanced tumorigenesis and metastasis of HCC-derived cell lines in mice. Additionally, SCARA5 was found physically interacting with focal adhesion kinase (FAK) and inhibited tyrosine phosphorylation and activation of the FAK-Src-Cas signalling pathway [236], a key regulator of cancer proliferation, migration, and invasion [242]. The intimate association of SCARA5 with FAK has been corroborated in other studies of lung and bone cancers. It was reported in both lung adenocarcinoma and osteosarcoma cancer studies that *SCARA5* overexpression inhibited FAK signal activation and thereby suppressed tumour growth and metastasis [237, 243]. Taken together, these results suggest that SCARA5 is a tumour suppressor via FAK signalling inhibition.

A recent study by Lee *et al.* found that SCARA5 is a crucial regulator

in adipocyte lineage commitment of MSCs [217]. *Scara5* was highly expressed in the stromal vascular fraction of white adipose tissue, with a higher level in preadipocytes as compared to mature adipocytes and uncommitted MSCs. It was shown that *Scara5* expression increased during expansion and early adipogenesis of A33 preadipocytes, but rapidly decreased under adipocyte differentiation within 48 hours [217], suggesting that *Scara5* may be important during the early stages of adipogenesis. In addition, the study demonstrated that *Scara5* overexpression markedly promoted adipogenesis, whilst its downregulation severely impaired adipocyte differentiation in A33 preadipocytes and C3H10T1/2 multipotent mesenchymal cells. In agreement with the association of SCARA5 with the FAK transduction pathway in human cancer studies, the authors revealed that FAK-ERK pathway was involved in the role of SCARA5 during adipogenic commitment [217]. Upregulation of *Scara5* markedly diminished phosphorylated FAK and ERK levels, whereas *Scara5* knockdown significantly increased FAK phosphorylation during early adipogenesis of adipocyte lineage commitment [217]. Alternatively, as FAK was shown to play a vital role in osteogenesis, *Scara5*-overexpressing C3H10T1/2 showed a significant decrease in osteogenic differentiation and reduced osteogenic gene expression [244, 245]. These results indicated that SCARA5

was a positive regulator for adipogenesis and negatively influenced osteogenesis.

Taken together, SCARA5 is implicated in a range of biological processes from iron transport, cancer progression, to adipocyte differentiation, functioning as a scavenger receptor or a cell signalling inhibitor. However, the role of SCARA5 in the cell fate decisions of BMSCs *in vivo*, which involves both osteogenic and particularly marrow adipocyte differentiation is currently not known. In this thesis the role of SCARA5 in BMSC lineage determination is investigated using genetically modified *Scara5*-deficient mice.

1.5 Project hypothesis and objectives

In view of the previous study by Lee *et al.* demonstrating the crucial role of SCARA5 in adipogenic commitment of MSCs *in vitro* [217], it was hypothesized that SCARA5 could affect the lineage bifurcation of BMSCs between osteogenesis and adipogenesis. The recent study by Chen *et al.* [219] showed that SCARA3 was an important modulator of the cell fate switch of BMSCs between adipocytes and osteoblasts *in vivo*, where SCARA3 deficiency impaired osteogenic differentiation yet improved adipogenesis, whilst *Scara3* overexpression alleviated bone loss and reduced marrow adipocytes in ovariectomised and ageing mice. Therefore, based on these studies, the role of SCARA5 in regulating osteogenic and adipogenic differentiation of BMSCs was postulated.

By using *Scara5* knockout mice in this project, the effect of SCARA5 on bone and marrow adipocytes *in vivo* as well as BMSCs deficient of SCARA5 can be investigated *in vitro* when isolated. It was hypothesized that the depletion of *Scara5* would increase bone formation accompanied by less marrow adipocyte accumulation in bone marrow due to the cell fate shift toward osteogenesis of *Scara5*-deficient BMSCs. Figure 1.11 briefly illustrates the stages in BMSC differentiation, additional highlights where SCARA5 may play

a role in osteogenic and adipogenic lineage differentiation.

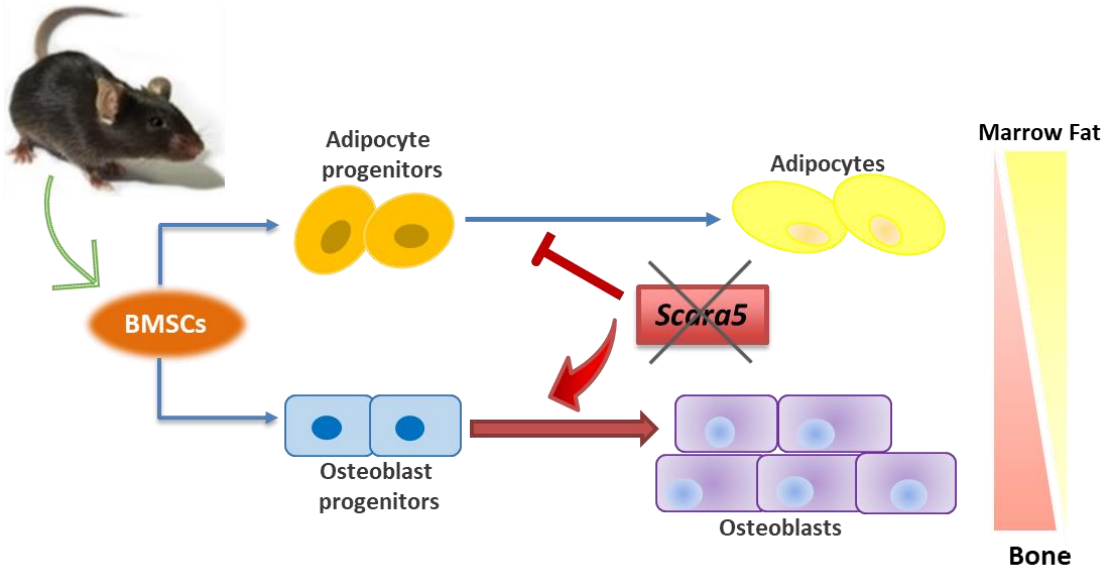

Figure 1.11 Project hypothesis on how SCARA5 affects osteogenesis and adipogenesis. Both osteogenic precursor and adipogenic precursor cells derive from a shared progenitor called bone marrow mesenchymal stromal cells (BMSCs). Adipogenic and osteogenic precursor populations can further differentiate into either mature adipocytes or osteoblasts. The working hypothesis is that the absence of SCARA5 inhibits adipogenesis and promotes osteogenic differentiation of BMSCs *in vivo*.

The aims of this thesis were to investigate SCARA5 as a potential molecular switch of BMSCs between osteogenic and adipogenic lineages. The following questions and aims are addressed:

1. Whether SCARA5 deficiency leads to an increase in bone mass *in vivo*?

2. Whether the presence of SCARA5 or its ligands affect BMSC osteogenesis?

3. Does the depletion of SCARA5 result in reduced fat development *in vivo*?

Chapter 2. Materials and Methods

2.1 Mice

All mouse colonies were maintained under specific pathogen-free conditions at University of Oxford, with food and water available ad libitum and kept in a 12 h light/12 h dark cycle. Animal studies were conducted under UK Home Office Project License numbers 30/3218 and 30/3246 in accordance with the UK Animal Scientific Procedures Act 1986. *Scara5*-deficient (*Scara5*$^{-/-}$ or KO) mice were generated in collaboration with GenOway (Lyon, France). In brief, gene deletion was achieved by replacing exons 7-9 that encode 228 bp of the collagenous domain essential for ligand binding with an IRES-NLS-lacZ cassette by homologous recombination in 129Sv/Pas embryonic stem cells and then injected into blastocysts. Crossbreeding the offspring generated KO and WT mice that were further backcrossed to the C57BL/6J strain for several generations. The mice were bred as homozygotes. Previous experiments confirmed that no functional SCARA5 protein was expressed by KO cells (unpublished). Animals were genotyped by PCR with WT (wild-type) forward primer 5'-CACCCCCGCCTTTCTGTTGTC-3' and WT reverse primer 5'-CTCCTCTCTCTCCTTTCTCTCCTTTTGG-3' to probe the *Scara5* exon 9 position 19516 to 20050; KO forward primer 5'-

AGCCCCTGATGCTCTTCGTCCAG-3' and KO reverse primer 5'-TCTGATGCCGCCGTGTTCCG-3' to probe within the LacZ cassette located in the expression vector 21126-21526 gene position). The wild-type control mice were the same generation and age as *Scara5*$^{-/-}$ mice in bone, marrow fat, body fat experiments, and mice at the same age but different generation were used in osteogenic and adipogenic differentiation assays.

2.2 Genotyping of the experimental animals

The genotyping was done by polymerase chain reaction (PCR) (Table S1) on Bio-Rad thermocycler by using DNA extracted from mouse ear clips with QIAamp DNA Mini Kit (QIAGEN). PCR reaction was carried out according to the manufacturer's instruction with the following reagents: 10x ThermoPol® Reaction Buffer, deoxynucleotide solution mix and Taq DNA Polymerase (all from New England Biolabs Ltd., UK). Primer pairs (Invitrogen™) of WT-F (forward) and WT-B (backward) were used to probe gene position 19516 to 20050 of exon 9 for WT and primer pairs of KO-F and KO-B to probe within LacZ cassette (position in expression vector 21126-21526) for *Scara5*$^{-/-}$ mice (Table S2). The PCR products were identified by DNA electrophoresis ran on 2% agarose gel (Sigma-Aldrich).

Table S1. PCR thermocycler programme

Step	Temperature	Time (seconds)	Cycles
Initial denaturation	94 °C	180	1
Denaturation	94 °C	30	35
Annealing	60 °C	60	
Extension	68 °C	60	
Final extension	68 °C	300	1
Hold	4 °C	∞	1

Table S2. PCR primers used for genotype

PCR primers	Sequence 5' – 3'	Product Length
WT-F	CACCCCCGCCTTTCTGTTGTC	535 bp
WT-B	CTCCTCTCTCTCCTTTCTCTCCTTTTGG	
KO-F	AGCCCCTGATGCTCTTCGTCCAG	401 bp
KO-B	TCTGATGCCGCCGTGTTCCG	

2.3 Body weight and fat mass measurements

The body weight and inguinal fat pads of 11-week-old and 1-year-old age- and sex-matched mice were weighed on the same day after euthanasia. Afterwards, the weight of fat pads was determined after removal.

2.4 Reverse transcription and quantitative real-time PCR (qRT-PCR)

The total RNAs were isolated using TRIzol™ Reagent (Invitrogen™)

combined with the protocol to elute RNA extracts by RNeasy mini spin column (QIAGEN) following the manufacturer's instructions. The RNA concentration of ~100 ng was used for reverse transcription to cDNA with High-Capacity cDNA Reverse Transcription Kit (Applied Biosystems) according to the manufacture's protocol. To prepare the qRT-PCR reaction mixture, the cDNA of ~1 μg as qRT-PCR template was mixed with TaqMan® Fast Advance Master Mix (Applied Biosystems) and the primers for *Scara5* (TaqMan® Assay ID: Mm00512269_m1) and *Gapdh* (TaqMan® Assay ID: Mm99999915_g1). All samples were run in triplicates and normalized to *Gapdh*. As a reference gene, *Gapdh* was constitutively and universally expressed and was used previously in three different studies regarding *Scara5* expression in murine cells [217, 233, 234]. The program for qRT-PCR is outlined in Table S3. All qRT-PCR reactions were carried out in a ViiA7 Real-Time PCR System (Applied Biosystems). Comparative CT ($\Delta\Delta C_T$) method and $2^{-\Delta\Delta CT}$ formula were applied to calculate relative levels.

Table S3. The program of qRT-PCR

Step	Temperature	Time (seconds)	Cycles
UNG incubation	50 °C	120	1
Polymerase activation	95 °C	120	1
Denaturation	95 °C	1	40
Annealing/extension	60 °C	20	

2.5 MicroCT setup and analysis

Tibias and femurs of 11-week and femurs of 12-month mice were harvested, fixed in 10% neutral-buffered formalin (VWR) for 48h, washed with PBS and stored in 70% ethanol at 4°C. Bones were scanned by a microCT system (Quantum FX; PerkinElmer), with X-ray source set to a current at 180 μA, voltage of 90 kVp and field of view of 5 mm with voxel resolution of 10 μm. Consistent criteria to select 150 serial cross-sections extending from the growth plate towards diaphysis of tibias and femurs were used for cortical and trabecular bone analysis with Bone Microarchitecture Analysis add-on of Analyze 12.0 software package (AnalyzeDirect, Inc.) in accordance with gold standard guidelines routinely used in the laboratory [246, 247].

2.6 Osmium tetroxide (OsO_4) staining of marrow adipose tissue

Mouse adipocytes were stained with OsO_4 (Sigma-Aldrich) for analysis as previously described with slight modification [248]. Briefly, after harvest the tibias were cleaned carefully cleaned of any soft tissue and were fixed in 10% neutral-buffered formalin (VWR) for 24 hours. Bones were washed with water and decalcified in 10% ethylenediaminetetraacetic acid (EDTA;

Sigma-Aldrich), pH 7.4, for 10 days by changing the EDTA solution every 3 days. After decalcification, bones were washed with water and each bone was placed in 1.5-mL microtube containing 600 μl Sorensen's phosphate buffered saline (PBS, pH 7.4). All subsequent steps involving OsO_4 were performed in the fume hood. Next, 200 μl of the 4% OsO_4 solution (Sigma-Aldrich) was added to each 1.5-mL microtube to make a final concentration of 1% OsO_4 solution. Bones were stained in the fume hood for 48 hours at room temperature. After staining, the bones were washed at least 5 times, each 12 hours, by incubating in 1 mL Sorensen's phosphate buffer at room temperature. At this point, each osmium-stained bone was moved to a fresh set of 1.5-mL microtubes, taken out of the fume hood and embedded in 1% agarose gel ready for microCT scanning. For imaging of the OsO_4 stained marrow adipocytes, the X-ray source of the Quantum microCT system was set to a current at 180 μA, voltage of 90 kVp and field of view of 20 mm to encompass the whole tibia. Analyze 12.0 software was used to calculate the volume of marrow adipose tissue.

2.7 *In vivo* bone formation assay

Bone histomorphometry was used for this assay. Calcein (Sigma-Aldrich) at a dose of 20mg/kg was injected intraperitoneally 5 days apart in 11

weeks old mice and 7 days apart in 1-year old mice. Calcein which is incorporated during bone formation as it is a calcium chelator was used to label bone mineral apposition rate. The mice were sacrificed 2 days after the 2nd calcein injection and calvarial bones were harvested, fixed in 10% neutral-buffered formalin (VWR) for 48h and kept in 70% ethanol until processing. Non-decalcified calvarial bones were plastic (polymer) embedded as described before [249]. Briefly, the bones were dehydrated by incubating them in serial concentration of acetone from 70%, 90% to 100% for at least 1h at room temperature. The dehydrated bones were subsequently infiltrated with a reagent mix of 90% destabilized methyl methacrylate (MMA), 10% dibutylphthalate (DBP) and 0.05% benzoyl peroxide (BPO) (all from Sigma-Aldrich) at 4°C for more than 3 nights. After infiltration, calvarias were embedded in 85% destabilized MMA, 15% DBP and 1.5% BPO reagent mix and induced to polymerize at 37°C. The MMA-embedded calvarial bone blocks were halved by IsoMet® Low Speed Saw machine (Buehler) and cut into 5 μm sections using a microtome (Leica RM2255). All work involving liquid form of methyl methacrylate was performed in fume hood. Finally, bone mineral apposition rate was measured from the distance between the two calcein labels under an Olympus BX51 fluorescence microscope (Olympus Corporation,)

using the OsteoMeasure software (OsteoMetrics, Inc.).

2.8 Bone histological analysis

Tibias were fixed in 10% neutral-buffered formalin (VWR) for at least 24 hours. After fixation, tibias were washed with PBS and transferred into 10% EDTA (pH 7.4) for decalcification by changing the EDTA solution every 3 days for 14 days. The decalcified tibias were paraffin embedded at the Histology Service of the Kennedy Institute and cut into 4 μm sections. Next, the paraffin sections were de-paraffined in Xylene (Sigma-Aldrich) and re-hydrated through a serial dilution of ethanol (Sigma-Aldrich) (from 100%, 90%, to 75%) with distilled water as the final step. Afterwards, the bone sections were stained with hematoxylin and eosin (H&E) (Sigma-Aldrich) or for TRAP activity (0.1 mg/ml Naphthol AS-MX phosphate, 0.5 ml dimethylformamide, and 0.4 mg/ml Fast Red Violet LB Salt in 50 ml TRAP buffer solution) with 0.2% methyl green counterstain (all from Sigma-Aldrich). TRAP buffer was made with 50mM Sodium Acetate Anhydrous plus 40mM Potassium Sodium Tartrate Tetrahydrate (Sigma-Aldrich) and mixed with distilled H_2O, and then adjusted final pH to 5.0 with Glacial Acetic Acid. Slides were mounted analyzed under Olympus BX51 microscope and micrographs were taken with an Olympus

DP71 camera (Olympus Corporation). Analysis of osteoclast and adipocyte perimeters were carried out with OsteoMeasure (OsteoMetrics Inc.) according to the guidelines of American Society for Bone and Mineral Research (ASBMR).

2.9 Mechanical Strength Testing

Three-point bending test was performed with Instron 5942 materials-testing systems (Instron Inc.), as a well-established, reproducible, and robust procedure for assessing the mechanical strength [250, 251]. Briefly, mouse femoral bones were cleaned of all the soft tissues and were immediately frozen and stored at -80°C until testing. Before three-point bending test, femurs were thawed in PBS at room temperature for 3 hours. A minimum force of 0.03 N was preloaded and calibrated to re-zeroed with the assistance of specimen protection. The load was applied at the rate of 1 mm/min directly onto the midshaft of the femur until failure. The force extension or displacement profiles were recorded and analyzed with the Bluehill 3 software package (Instron Inc.) to determine bone mechanical properties.

2.10 Inguinal fat pad histology analysis

The inguinal fat pads were dissected out of 11-weeks old WT and

Scara5-deficient mice and placed in 10% neutral-buffered formalin (VWR) and kept at 4°C for at least 72 hours. Next, the fat pads were removed and placed in 70% ethanol (VWR) for 48 hours in preparation of tissue embedding process. To prepare for the paraffin embedding, the fat pads were processed in 70% ethanol for 1 hour, followed by 1 hour in 80% ethanol, 2 times in 95% ethanol for 1 hour each, 2 times in 100% ethanol for 1 hour each, 1 hour in xylene for twice, and finally 3 times in 60°C paraffin for 1 hour each. Once processed, the fat tissues were embedded into a paraffin block and stored at 4°C. The paraffin embedded fat pads were cut into 5 μm sections, placed on slides to dry for 24 hours, and then baked at 60°C for around 1.5 hour. Subsequently, the paraffin sections were deparaffinized in xylene and rehydrated through a serial dilution of ethanol (from 100%, 90%, to 75%) with distilled water as the final step. The deparaffinized fat tissue sections were stained with H&E and analyzed with the imaging software ImageJ (National Institutes of Health, Bethesda, Maryland, USA) [252].

2.11 Osteogenic and adipogenic differentiation

Femurs and tibias were isolated from 3-4 weeks old WT and *Scara5*$^{-/-}$ mice and soft tissue was removed. Bones were crushed and digested with 0.2%

collagenase A (Roche Diagnostics) in Dulbecco's Modified Eagle *Medium* (DMEM, Sigma-Aldrich) at 37°C for 30 minutes with gentle shaking. After digestion, collagenase A was neutralized with FBS and the mixture passed through 70µm filter mesh before centrifuging 5 minutes at 1500 rpm. The supernatant was discarded, cells were resuspended in BMSC medium (DMEM + 10% FBS + 1% L-glutamine (Thermo Fisher Scientific) and 1% Penicillin-Streptomycin (Sigma-Aldrich P4333) and plated at $2x10^4$ cells/well in 96-well flat-bottom plates.

Osteogenic differentiation was induced at sub-confluence with osteogenic medium containing BMSC medium + 10 mM β-glycerophosphate + 0.05 nM Ascorbic acid + 0.1 µM dexamethasone (all from Sigma-Aldrich). The osteogenic medium was changed every 2-3 days or until the time points set in individual experiment. Ferritin (Bio-Rad 4420-4804), DKK1 (PeproTech 120-30), sFRP1 (PeproTech 120-29), SOST (PeproTech 100-49), and WNT3a (PeproTech 315-20) treatments were initiated by addition of these proteins in the osteogenic medium at the time of induced osteogenic differentiation. As for AMD3100 (CXCR4 Antagonist I, Calbiochem 239820), Fully Reduced HMGB1 [HM-116] (FR-HMGB1, HMGBiotech S.r.l. Italy) and Disulfide HMGB1 [HM-122] (DS-HMGB1, HMGBiotech S.r.l. Italy), the proteins were added either at the

time of induce osteogenic differentiation or 16 hours prior in control medium in accordance with each experimental setup.

Adipogenic differentiation was induced 2 days post confluence by using adipogenic medium (Minimum Essential Medium Alpha [αMEM, Thermo Fisher Scientific] + 1% L-glutamine + 10% MesenCult™ Adipogenic Stimulatory Supplement (STEMCELL Technologies Inc.). Adipogenic medium was changed every 3-4 days during differentiation.

2.12 Alkaline phosphatase assay and calcium content analysis by Alizarin red staining

To evaluate Alkaline phosphatase (ALP) activity, the cells were cultured in osteoinduction media with or without different additives. After incubation with ALP substrate p-nitrophenyl phosphate (pNPP) (Sigma-Aldrich) at 37 °C for 10-15 minutes, cells were washed with PBS, lysed with dH_2O and ALP activity was measured at 405 nm optical density (O.D.). The pNPP substrates, when hydrolyzed by alkaline phosphatase, develops the yellow end-product *p*-nitrophenol. The reaction was stopped with 3M sodium hydroxide solution. The colourimetric results at OD405 were read by Omega microplate reader (BMG LABTECH, FLUOstar).

Calcium content of the in vitro cultured/differentiated bone nodules were evaluated by Alizarin red S staining. Briefly, cells were fixed with cold 70% ethanol at 4 °C for 1 hour, washed twice with PBS, and incubated with 1% w/v alizarin red S (ARS, pH 4.2) (Sigma-Aldrich) solution for 15 min at room temperature to stain for calcium mineral deposition. The cells were then washed 5 times with distilled water and allowed to air dry. To quantify ARS staining intensity, the ARS stain was extracted with 10% w/v cetylpyridinium chloride buffer (Sigma-Aldrich) and measured at O.D. 550 nm with Omega microplate reader (BMG LABTECH, FLUOstar).

2.13 Oil Red O staining assay

Adipogenic differentiation was assessed by Oil red O staining. Briefly, cells were fixed with 10% neutral-buffered formalin (VWR) for 1 hour, washed 3 times with distilled water, and stained with 0.3 % w/v Oil red O solution (Sigma-Aldrich) in 40% isopropanol for 20 minutes at room temperature followed by 5 washes with distilled water. Semi-quantification of the lipid droplet volume was carried out by eluting Oil red O stain with absolute isopropanol and 200 uL eluate was measured at O.D. 500 nm. with Omega microplate reader (BMG LABTECH, FLUOstar).

2.14 Flow cytometry (FACS)

Bone marrow cells were harvested from WT and *Scara5*$^{-/-}$ mice at 11-weeks of age. Bones were crushed, digested with 0.2% collagenase A (Roche Diagnostics) and bone marrow cells were isolated as described previously in "2.11 Osteogenic and adipogenic differentiation". Cells were resuspended in FACS buffer (1x PBS with 1 % Fetal Bovine serum [FBS] and 2 mM EDTA) and stained with Zombie Aqua (BioLegend 423101), anti-mouse CD45 (BioLegend 103105), CD31 (BioLegend 102405), CD24 (BioLegend 101835), Sca1 (Ly-6A/E) (BioLegend 108113), and PDGFRα (BioLegend 135907). Stained cells were acquired on LSRFortessa™ X-20 Flow Cytometer (BD Biosciences). Data was analyzed using FlowJo V10 software (TreeStar). The gating strategy, illustrated in Supplementary Figure 3, was applied for separating bone marrow stomal cell (BMSC), osteochondrogenic progenitor cell (OPC), and adipogenic progenitor cell (APC) populations.

2.15 Indirect ELISA

The association between SCARA5 and light-chain ferritin, FR- and DS-HMGB1, WNT inhibitors (DKK1, sFRP1, SOST) and WNT3a were

examined using indirect ELISA developed in-house. To evaluate the association between SCARA5 and each proteins mentioned, various concentrations (0.1 – 250 nM) of recombinant light-chain ferritin (Bio-Techne NBC1-18546), FR-HMGB1 (HMGBiotech, HM116) and DS-HMGB1 (HMGBiotech, HM122), DKK1 (PeproTech 120-30), sFRP1 (PeproTech 120-29), SOST (PeproTech 100-49), and WNT3a (PeproTech 315-20) were coated onto ELISA microtiter wells (Falcon®) overnight at 4°C. After blocking with 5% Bovine serum albumin (BSA, Sigma-Aldrich) for 2 hours and washing three times with PBS, the wells were incubated with 100 nM of recombinant human SCARA5 protein (R&D Systems) for 1 hour at 37°C. After incubation, the wells were washed three times with PBS/Tween20 solution (PBS + 0.05% Tween20 (Sigma-Aldrich P7949) then followed by incubation with mouse anti-6x-His Tag antibody (Invitrogen 14-6657-82) for 2 hours at 37°C. Afterwards, the wells were washed three times with PBS/Tween20 solution before incubating with HRP-conjugated rabbit anti-mouse IgG (Abcam ab6728) for 1 hour. Subsequently, the wells were washed 3 times with PBS/Tween20 solution prior to developing colour assay by tetramethylbenzidine and H_2O_2 as substrates reagents (BD OptEIA™ TMB Substrate Reagent Set, BD Biosciences, Cat: BD 555214). Lastly, the reaction was stopped with 1M sulfuric acid (R&D Systems DY994, Part No. 895926).

The colorimetric results at OD450 were read by FLUOstar Omega microplate reader (BMG LABTECH Ltd).

2.16 Data Analysis and Statistics

Graphpad Prism version 7 (GraphPad software, San Diego, CA) was used to perform statistical analysis. Results are presented as mean ± SEM unless stated otherwise. Depending on data sets, statistical analyses include two-tailed unpaired t-test and two-way ANOVA tests as specified in the figure legends. The p value < 0.05 were considered statistically significant. Asterisks represent the statistical significance as *p < 0.05, **p < 0.01, ***p < 0.001, ****p < 0.0001 and 'ns' represents statistically non-significance with $p \geq 0.05$.

Chapter 3 - Bone phenotype under SCARA5 deficiency

3.1 Introduction

As a member of the class A scavenger receptors, SCARA5 sets itself apart by its inability to bind oxidized and acetylated LDLs and its ubiquitous tissue expression rather predominantly in myeloid cells as shown with SCARA1. SCARA5 is abundantly expressed in testis, adipose tissue, specific fibroblasts, and epithelial cell types, rather than macrophages or cells of the myeloid lineage [233, 234]. To date SCARA5 has not been investigated in bone or bone formation *in vivo*. Previous studies have shown that SR-A (SCARA1/MSR1) was critical to osteoclast (OC) formation and functions, and that SR-A deficiency reduced OC number and bone resorption considerably *in vitro* [218, 225, 226]. Meanwhile, a study by Lin *et al.* found that *SR-A* deletion interfered with OC functions and resulted in a significant positive effect on the mouse bone volume and development [216]. These bone related SR-A reports raised questions as to whether and how SCARA5 could alter bone properties.

A more recent study interrogating the role of SCARA5 in adipocyte lineage commitment provided a clue to the importance of SCARA5 in adipogenesis *in vitro* [217]. Lee and colleagues showed that *Scara5* knockdown

in MSC-like cells inhibited adipogenesis and favoured osteogenic differentiation. Given these studies, it was postulated that SCARA5 may play a role in bone formation due to its association with osteogenic and adipogenic lineage commitment. In this chapter, *Scara5*-deficient (*Scara5*$^{-/-}$) mice were generated to characterize and investigate their bone phenotype *in vivo*, and bone formation and osteogenic differentiation *in vitro*, in the presence and absence of SCARA5.

3.2 Results

3.2.1 *Scara5* mRNA is expressed in a range of murine tissues and cells

To start, the mRNA expression of *Scara5* was assessed in several murine tissues (Figure 3.1 A). *Scara5* was abundantly expressed in the murine testis (9.23 ± 0.43 relative fold change), as well as the white adipose tissue (2.98 ± 0.88 relative fold change). The whole bone extract also expressed *Scara5* (0.51 ± 0.07 relative fold change), although at a lower level than the other tissues in this analysis.

Scara5 mRNA expression was further investigated in murine osteoblastic 2T3 cells and BMSCs under osteogenic culture condition over a

period of 72 hours. From 0-hour to 72-hour time points, *Scara5* mRNA expression level in 2T3 cells had a significant (~ 8-fold) increase from 3.88 ± 2.02 to 30.75 ± 7.48 relative fold change under osteogenic conditions (Figure 3.1 B). Whereas *Scara5* mRNA expression of BMSCs showed no statistically significant change between 0-hour (0.13 ± 0.05 relative fold change) and 72-hour (0.30 ± 0.14 relative fold change) under the same osteogenic conditions (Figure 3.1 C). These data indicated that the murine osteoblastic 2T3 cells expressed much higher *Scara5* mRNA levels than BMSCs and expression increased considerably in response to osteogenic stimulation over the time points investigated.

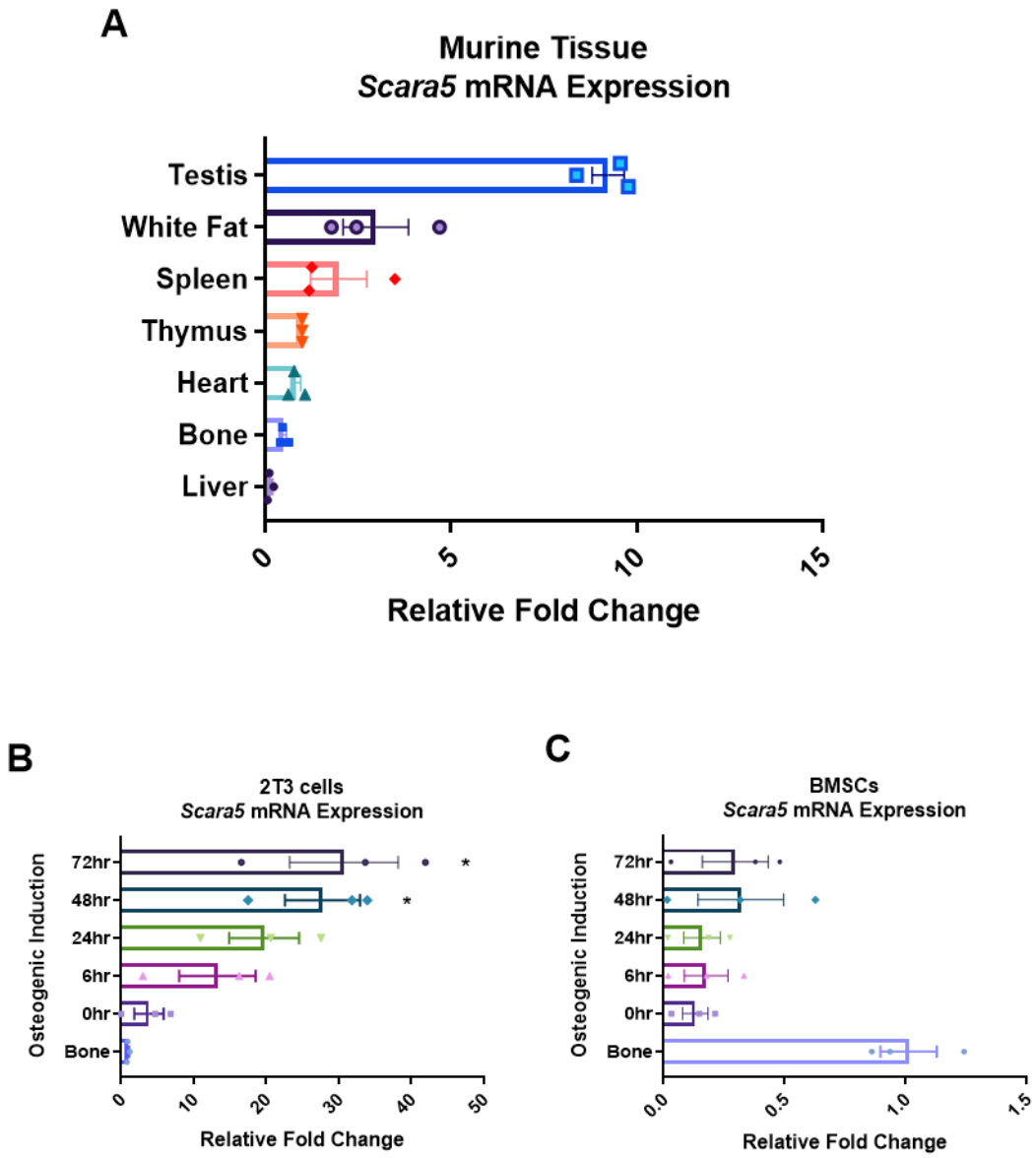

Figure 3.1 *Scara5* mRNA expression in murine tissues and cell lines.
(A) Relative mRNA expression of *Scara5* in different tissues by qRT-PCR (n = 3 biological replicates of 12 weeks old mice), normalized to *Scara5* mRNA expression of thymus with *Gapdh* as the housekeeping control gene. (B) Relative *Scara5* mRNA expression in 2T3 cells at 0, 6, 24, 48, 72 hr (hour) time points of osteogenic induction by qRT-PCR (n = 3 individual experiments), normalized to the *Scara5* expression of bone. (C) *Scara5* mRNA expression of in mouse BMSCs at 0, 6, 24, 48, 72 hr time points of osteogenic differentiation by qRT-PCR (n = 3 biological replicates), normalized to the *Scara5* expression of the whole bone. Error bars represent as mean ± SEM. *p < 0.05 by Student's t-test.

3.2.2 Genotyping *Scara5* knockout mice

Scara5-deficient (*Scara5*$^{-/-}$) mice were generated by replacing endogenous *Scara5* exons 7 to 9 with LacZ targeting vector as illustrated in Figure 3.2 A. The resulting gene sequences translate into truncated SCARA5 proteins that are unable to be expressed on the cell surface and so negate normal receptor functions. To genotype *Scara5*$^{-/-}$ mice, primer pairs were specifically designed to identify a 535bp DNA sequence within exon 9 in wild-type (WT) mice, whilst a separate primer pair for *Scara5*$^{-/-}$ mice was designed to verify 401 bp of the LacZ knock-in sequences. The PCR result from 3 WT and 3 *Scara5*$^{-/-}$ breeding pairs showed distinct DNA bands, 535bp for WT mice and 401bp for *Scara5*$^{-/-}$ mice, are shown on the agarose gel image (Figure 3.2 B).

Additionally, the body weight and femur bone length were measured to investigate if there were any obvious phenotypic differences between WT and *Scara5*$^{-/-}$ mice. The data showed that WT mice weighed significantly more than *Scara5*$^{-/-}$ animals, whilst there was no statistical difference in their femur lengths at 11-weeks old (Figure 3.2 C-D).

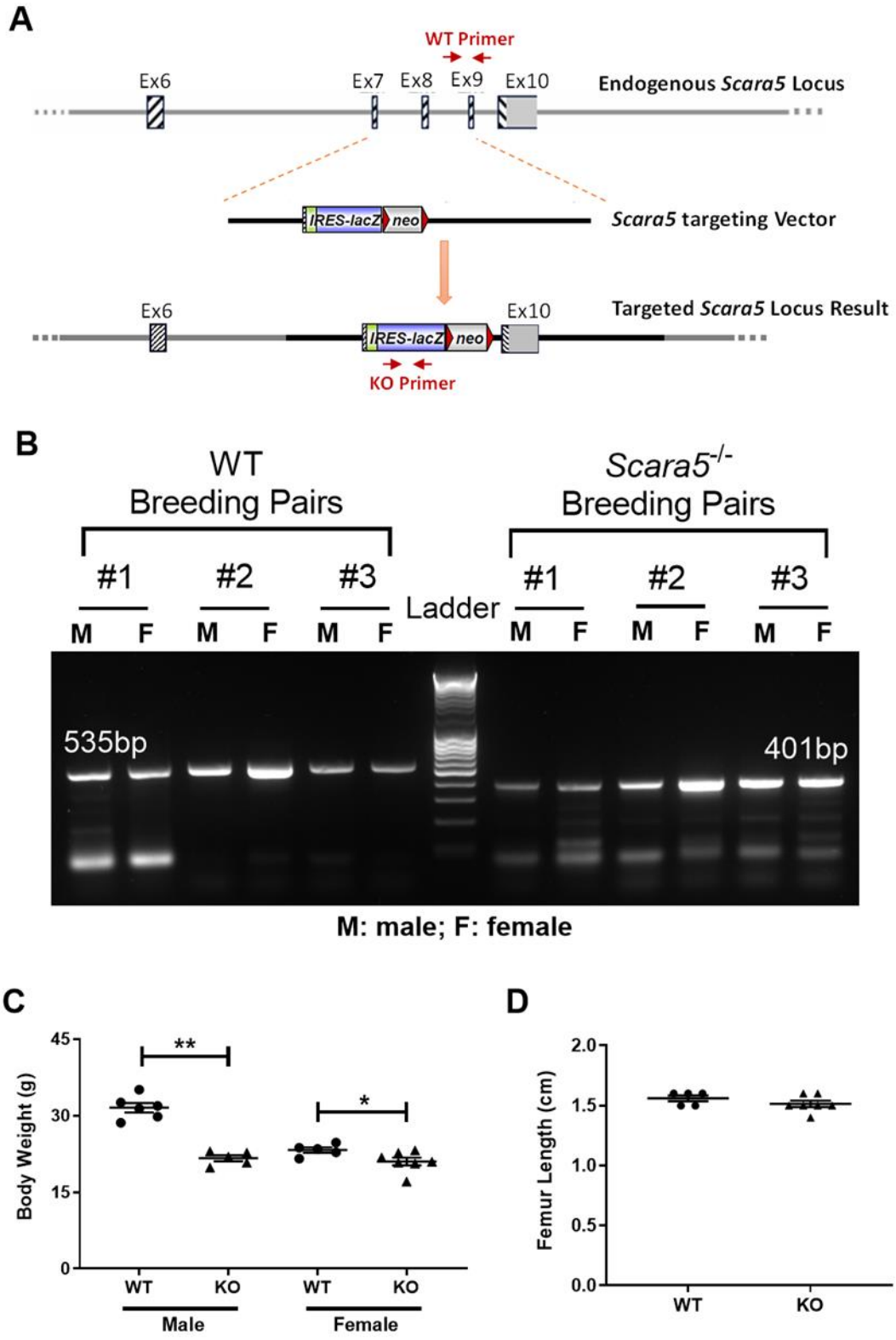

Figure 3.2 Genotype and reduced body mass of *Scara5*$^{-/-}$ (KO) mice. (A) Schematic of vector used to generate *Scara5*$^{-/-}$ mouse model. The deletion of exons 7-9 on *Scara5* locus renders a truncated and incomplete translation of SCARA5 protein that is unable to be expressed on the cell membrane. The

primer locations of WT and KO, within exon 9 and inserted vector separately, are indicated. (B) Agarose gel image of PCR products from ear clips of 3 breeding pairs (#1-3) of WT (n = 6 biological replicates) and *Scara5*$^{-/-}$ mice (n = 6 biological replicates). WT: 535 base pairs (bp) and *Scara5*$^{-/-}$: 401bp. (C) The body weight (g) of WT and *Scara5*$^{-/-}$ mice (WT = 11; *Scara5*$^{-/-}$ = 12 biological replicates) at 11-weeks of age. (D) Femur length of WT (n = 5 biological replicates) and *Scara5*$^{-/-}$ (n = 7 biological replicates) 11 weeks male mice. Error bars represent mean ± SEM. *p < 0.05; **p < 0.01 by Student's t-test.

3.2.3 Elevated bone parameters in *Scara5*$^{-/-}$ mice

MicroCT analysis of *Scara5*$^{-/-}$ and WT mice was undertaken to determine whether there were any structural differences in their bone measurements. Male and female 11-week *Scara5*$^{-/-}$ mice (Figure 3.3 A) both showed significantly higher total bone volumes relative to total volume (BV/TV, male = 31.05% ± 1.82%; female = 30.72% ± 0.97%) and enhanced trabecular parameters of trabecular number (Tb. N, male = 3.18 ± 0.12/mm; female = 3.39 ± 0.07/mm), trabecular separation (Tb. Sp, male = 0.16 ± 0.004 mm; female = 0.15 ± 0.003 mm) and trabecular thickness (Tb. Th, male = 0.093 ± 0.002 mm; female = 0.094 ± 0.003 mm), when compared to WT counterparts with BV/TV (male = 16.45% ± 1.77%; female = 12.39% ± 1.55%), Tb. N (male = 2.01 ± 0.09/mm; female = 1.64 ± 0.15/mm), Tb. Sp (male = 0.20 ± 0.002 mm; female

= 0.23 ± 0.007 mm), and Tb. Th (male = 0.088 ± 0.006 mm; female = 0.078 ± 0.004 mm).

In 3D-reconstructed micro-CT images of the proximal tibia (Figure 3.3 B), the spaces between the trabecular bone were wider and more visible in the WT tibia, whereas those in *Scara5*$^{-/-}$ tibia were much denser with narrower gaps (Figure 3.3, panel B). Besides the elevated trabecular bone density and numbers, the trabeculae (marked in red) of *Scara5*$^{-/-}$ mice extended further down from the growth plate compared to WT (Figure 3.3 B right panel). Additional bone parameters are shown in Table 3.1, followed by graphs plotted for individual parameter in Figure 3.4.

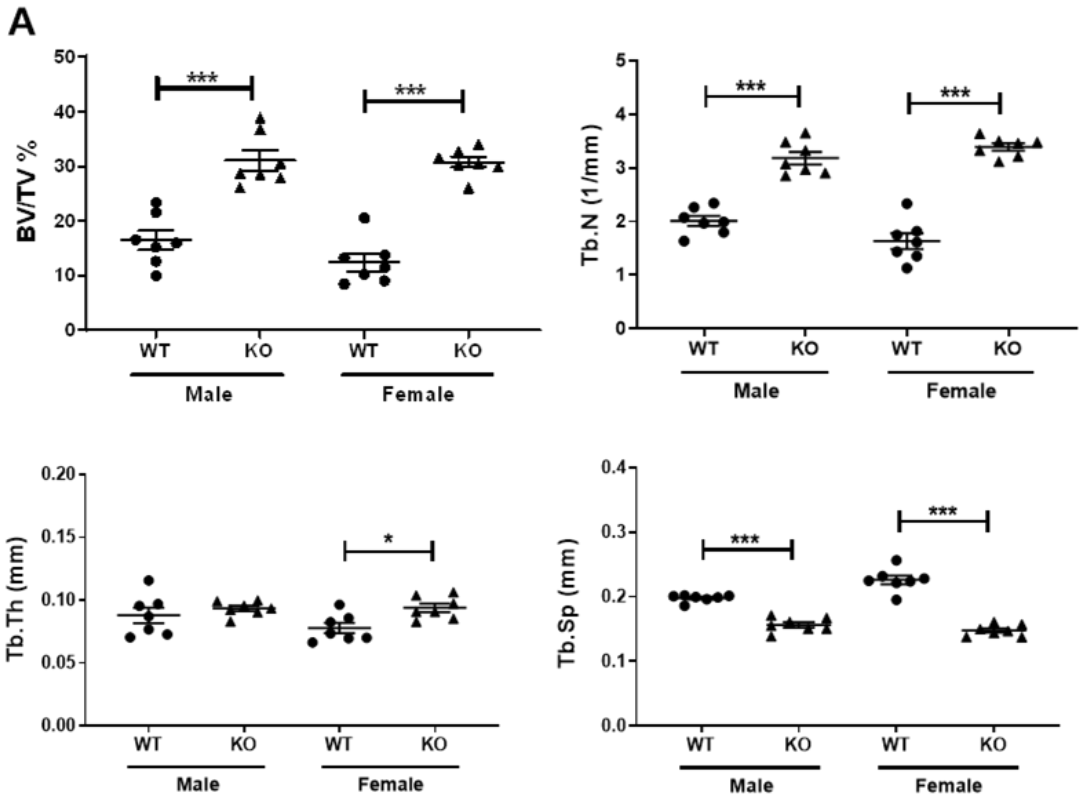

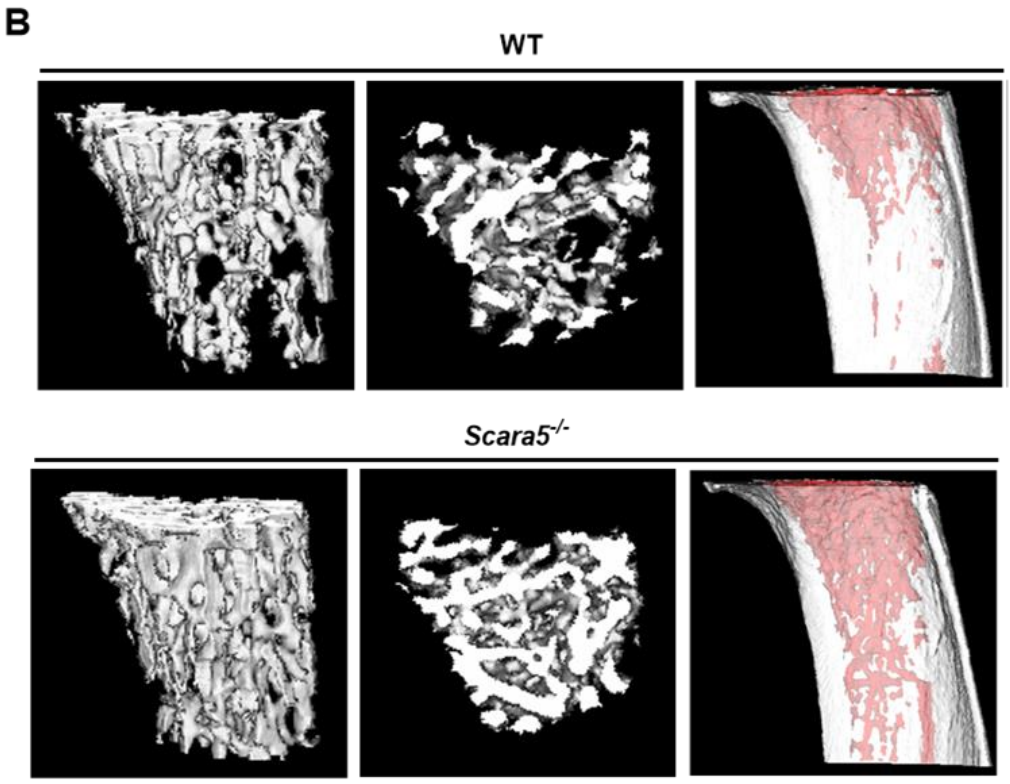

Figure 3.3 *Scara5*$^{-/-}$ mice exhibit increased bone volume. (A) Quantitative measurements of BV/TV (bone-volume/tissue volume), Tb.N, (trabecular number), Tb.Th (trabecular thickness) and Tb. Sp (trabecular separation) of tibia from 11-week-old male and female WT and *Scara5*$^{-/-}$ (KO) mice (n = 7 biological replicates). (B) Representative microCT images of trabecular bone from sagittal view (left) and horizontal view (middle) of proximal tibia, and tibia segments below the growth plate of 11-week WT and *Scara5*$^{-/-}$ mice. Tibial cortical bone is shown in white and the trabeculae are shown in red. Error bars represent mean ± SEM; *p < 0.05; **p < 0.01; ***p < 0.001 by Student t-test.

Parameters	Male		Female	
	WT	*Scara5*$^{-/-}$	WT	*Scara5*$^{-/-}$
BS/TV (mm^{-1})	7.59 ± 0.41	12.32 ± 0.42***	6.399 ± 0.55	12.84 ± 0.23*
BS/BV (mm^{-1})	48.11 ± 3.06	40.04 ± 0.97	52.95 ± 1.73**	42.02 ± 0.66
Ct.Th (mm)	0.3 ± 0.0072	0.28 ± 0.0073	0.28 ± 0.0065	0.32 ± 0.0064**
Ct.Ar/Tt.Ar (%)	58.67 ± 0.89	56 ± 0.82	60.28 ± 0.75	66.55 ± 0.52***
Conn.D (mm^{-3})	55.28 ± 4.78	146.4 ± 9.83***	50.51 ± 6.86	156.5 ± 5.83***

Table 3.1. Additional bone parameters of 11-week WT and *Scara5*$^{-/-}$ mice. Data represent mean ± SEM; n = 7 biological replicates in each group. BS/TV (bone surface/total volume), BS/BV (bone surface/bone volume), Ct.Th (cortical thickness), Ct.Ar/Tt.Ar (cortical area/total area), Conn.D (connectivity density). Data is expressed as mean ± SEM; *p < 0.05; **p < 0.01; ***p < 0.001 by Student's t-test.

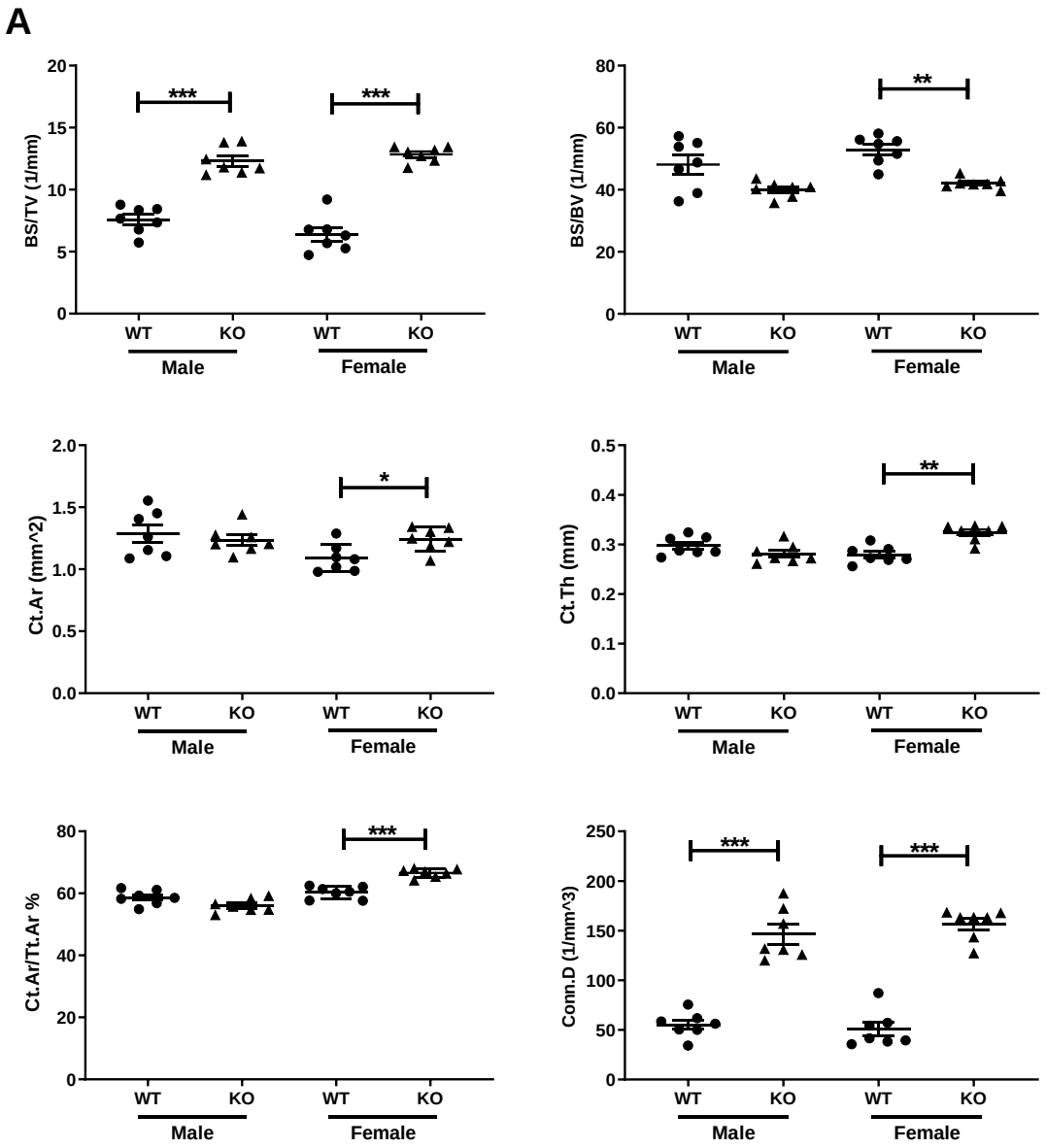

Figure 3.4 Additional bone parameters of 11-week WT and *Scara5*$^{-/-}$ mice. (A) Quantitative measurements of BS/TV, BS/BV, Ct.Ar, Ct.Th, Ct.Ar/Tt.Ar, Conn.D (n = 7 biological replicates). Data is expressed as mean ± SEM; *p < 0.05; **p < 0.01; ***p < 0.001 by Student's t-test.

Similar results were found for WT and *Scara5*$^{-/-}$ mice at 1-year of age. 3D-reconstructed images of distal femurs showed a notable decrease in trabecular bone number in the WT mice compared to *Scara5*$^{-/-}$ animals (Figure 3.5 A). Correspondingly, a higher bone volume (BV/TV, male = 9.39% ± 1.09%; female = 11.02% ± 0.9%) and an improved trabecular number (Tb. N, male = 1.1 ± 0.1/mm; female = 1.3 ± 0.07/mm) and separation (Tb. Sp, male = 0.28 ± 0.004 mm; female = 0.29 ± 0.006 mm) in *Scara5*$^{-/-}$ mice were found (Figure 3.5 B) compared to the WT animals with BV/TV (male = 5.9% ± 0.04%; female = 5.79% ± 0.73%), Tb. N (male = 0.89 ± 0.05/mm; female = 0.75 ± 0.06/mm), and Tb. Sp (male = 0.32 ± 0.001 mm; female = 0.34 ± 0.005 mm). The results of other bone parameters, including the bone surface per total volume, connectivity density, and cortical area indexes are shown in Table 3.2, with individual parameter plotted in Figure 3.6.

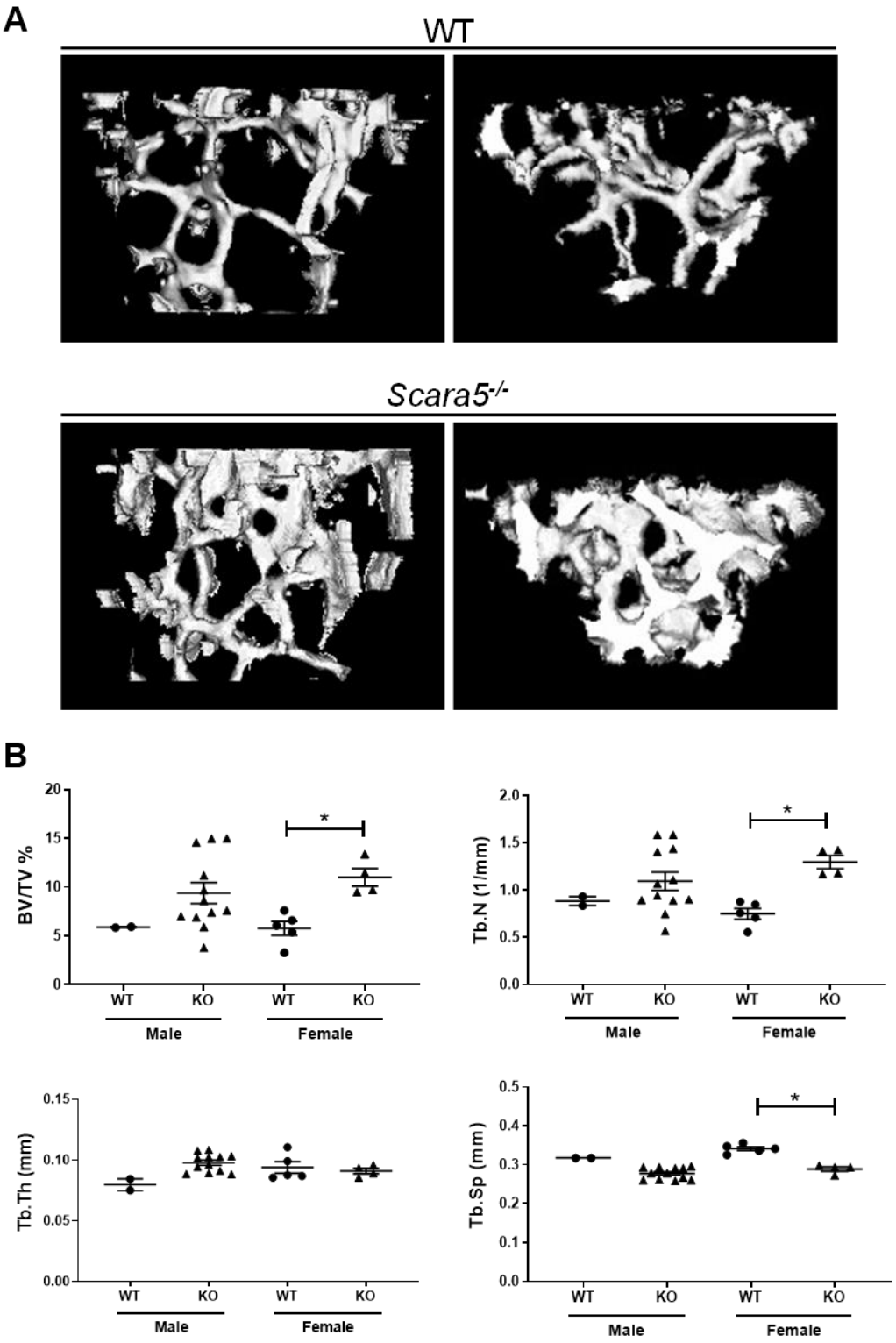

Figure 3.5 Aged *Scara5*$^{-/-}$ mice exhibit higher bone volume than WT mice. (A) Representative microCT images of trabecular bone from sagittal view (left) and horizontal view (right) of 1-year-old WT and *Scara5*$^{-/-}$ distal femurs. (B) Quantitative measurements of BV/TV, Tb. N, Tb. Th and Tb. Sp of femurs from 1-year-old WT (male, n = 2; female, n = 5 biological replicates) and *Scara5*$^{-/-}$

mice (male, n = 12; female, n = 4 biological replicates). Error bars represent mean ± SEM. *p < 0.05 by Student's t-test.

Parameters	Male		Female	
	WT	*Scara5*$^{-/-}$	WT	*Scara5*$^{-/-}$
BS/TV (mm^{-1})	3.04 ± 0.07	3.72 ± 0.338	2.691 ± 0.244	4.493 ± 0.3*
BS/BV (mm^{-1})	51.55 ± 1.48	41.22 ± 1.32	47.69 ± 2.62	41.26 ± 0.77
Ct.Th (mm)	0.24 ± 0.0098	0.26 ± 0.0031	0.27 ± 0.0062	0.3 ± 0.0083
Ct.Ar/Tt.Ar (%)	40.23 ± 2.25	47.54 ± 0.77	47.85 ± 1.01	55.0 ± 1.40*
Conn.D (mm^{-3})	14.88 ± 3.14	14.74 ± 2.07	12.02 ± 1.3	23.73 ± 3.02*

Table 3.2. Bone parameters of 12-month-old WT and *Scara5*$^{-/-}$ mice. BS/TV, BS/BV, Ct. Th, Ct.Ar/Tt.Ar, Conn.D. Data represent mean ± SEM; *p < 0.05 by Student's t-test.

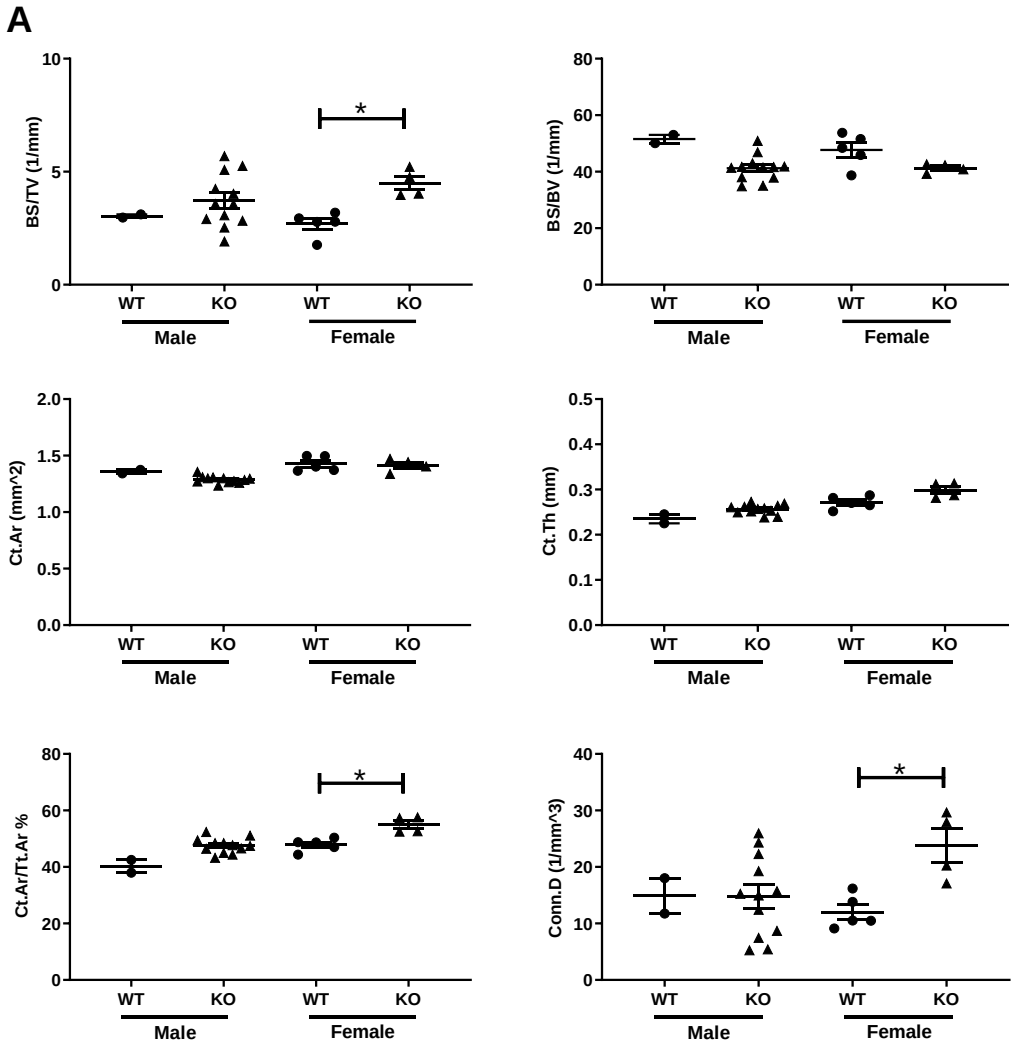

Figure 3.6 Bone parameters of 12-month-old WT and *Scara5*$^{-/-}$ mice.
(A) Quantitative measurements of BS/TV, BS/BV, Ct.Ar, Ct.Th, Ct.Ar/Tt.Ar, Conn.D WT (male, n = 2; female, n = 5 biological replicates) and *Scara5*$^{-/-}$ mice (male, n = 12; female, n = 4 biological replicates). Data is expressed as mean ± SEM; *p < 0.05 by Student's t-test.

3.2.4 Loss of SCARA5 enhances bone mineral formation

An overall increase in bone can result from more bone formation by osteoblasts, less bone resorption by osteoclasts, or a combination of both. The bone mineral apposition rate (MAR) was investigated to see whether the elevated bone volume and generally enhanced bone parameters were as a result of increased bone formation. Using the calcein double-labelling assay (Figure 3.7 A), the bone mineral apposition and formation rates were measured over the period of 5 days (11-week-old mice) or 7 days (1-year-old mice) in calvarial bones.

There was a significant increase in the calvarial MAR in both *Scara5*-deficient mice at 11-week (male = 1.56 ± 0.04 mm/day; female = 1.33 ± 0.05 mm/day) (Figure 3.7 B) and 1-year of age (1.08 ± 0.03 mm/day) (Figure 3.7 C) compared to WT control animals at 11-week of age (male = 1.20 ± 0.05 mm/day; female = 0.98 ± 0.13 mm/day) and 1-year old (0.82 ± 0.06 mm/day).

The mechanical properties of the bone were measured using a 3-point bending test. The evaluation parameters for bone strength were taken as the ‘maximal load’ until fracture, and bone structural elasticity measured as the amount of ‘extension at maximal load’. Unlike the enhanced bone parameters, no significant difference was found in the bone strength (22.77 ± 0.59 N) and elasticity (0.34 ± 0.020 mm) of *Scara5*$^{-/-}$ animals when compared to the bone strength (21.83 ± 1.18 N) and elasticity (0.35 ± 0.008 mm) of WT mice (Figure 3.7 D-E).

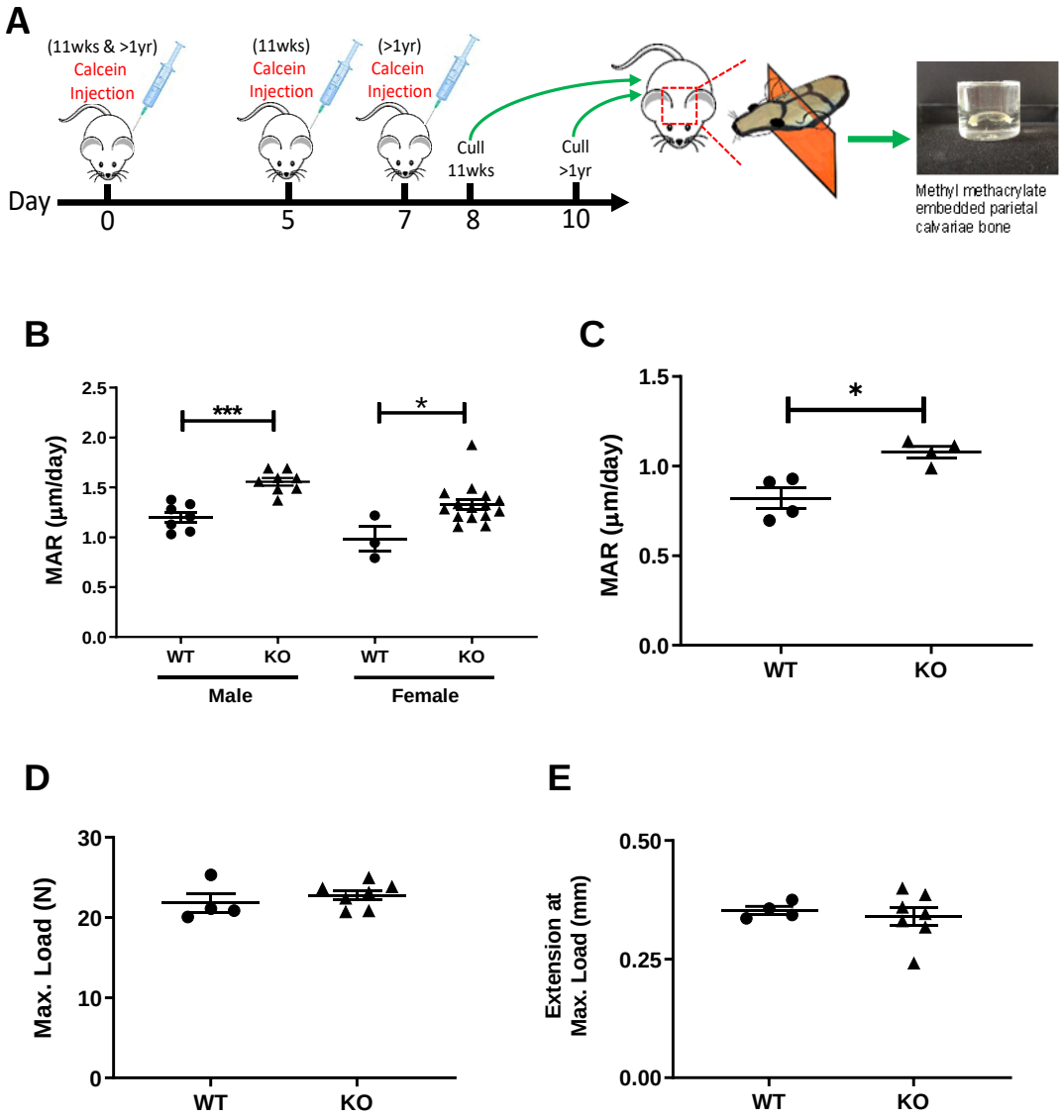

Figure 3.7 Loss of SCARA5 increases bone mineral apposition and formation rate. (A) Schematic of calcein-incorporation for measuring bone mineral apposition rate. (B) Calvarial bone mineral apposition rate (MAR) of 11-week-old WT (male, n = 7; female, n = 3 biological replicates) and *Scara5*$^{-/-}$ mice (male, n = 8; female, n = 15 biological replicates). (C) Calvarial bone MAR of 1-year-old WT (n = 4 biological replicates) and *Scara5*$^{-/-}$ females (n = 4 biological replicates). (D-E) The three-point bending test results of maximal load (D) and extension at maximal load (E) of 11-week-old WT (n = 4 biological replicates) *Scara5*$^{-/-}$ male femurs (n = 7 biological replicates). Error bars represent mean ± SEM. *$p < 0.05$; ***$p < 0.001$ by Student's t-test.

3.2.5 Comparable Osteoclast parameters between *Scara5*$^{-/-}$ and WT mice

Normal osteoclast functions are important for healthy skeletal tissue via remodeling and maintenance [30, 32]. Therefore, osteoclasts were examined in both WT and *Scara5*$^{-/-}$ animals. Paraffin embedded bone tissue sections were stained with tartrate-resistant acid phosphatase (TRAP), a key enzyme for osteoclasts' bone resorbing activity, permitting the histological analyses of osteoclast number per bone perimeter (N.Oc/B.Pm), osteoclast surface relative to bone surface (Oc.S/BS) and the number of osteoclasts per total area (N.Oc/T.Ar). Representative images of pink-red TRAP positive osteoclasts are shown in Figure 3.8 D.

Visual observation of the sections shows a greater amount of TRAP staining in the *Scara5*$^{-/-}$ mice. However, when the amount of bone present in the WT and *Scara5*$^{-/-}$ mice was calculated and applied to generate osteoclast-derived parameters, there were no significant differences between the genotypes. Osteoclast parameters included N.Oc/B.Pm (Figure 3.8 A), N.Oc/T.Ar (Figure 3.8 B) and Oc.S/BS (Figure 3.8 C). The amount of bone surface covered by osteoclast cell surface (Oc.S/BS) in WT bones (male = 19.62 ± 1.95%; female = 15.48 ± 1.55%) was comparable to *Scara5*$^{-/-}$ ones (male = 18.22 ± 1.62%; female = 18.05 ± 1.28%), showing functionally active

osteoclasts. An increase in the number of osteoclasts was noted in the WT male N.Oc/B.Pm (WT = 14.35 ± 1.35 mm^{-1}; KO = 9.99 ± 0.69 mm^{-1}) and separately in N.Oc/T.Ar of *Scara5*$^{-/-}$ female (WT = 61.65 ± 4.45 mm^{-2}; KO = 85.40 ± 5.72 mm^{-2}). Meanwhile, a noticeable, but not statistically significant difference in osteoclast parameters was seen between WT and *Scara5*$^{-/-}$ animals at 12-months of age (Figure 3.9 A-C).

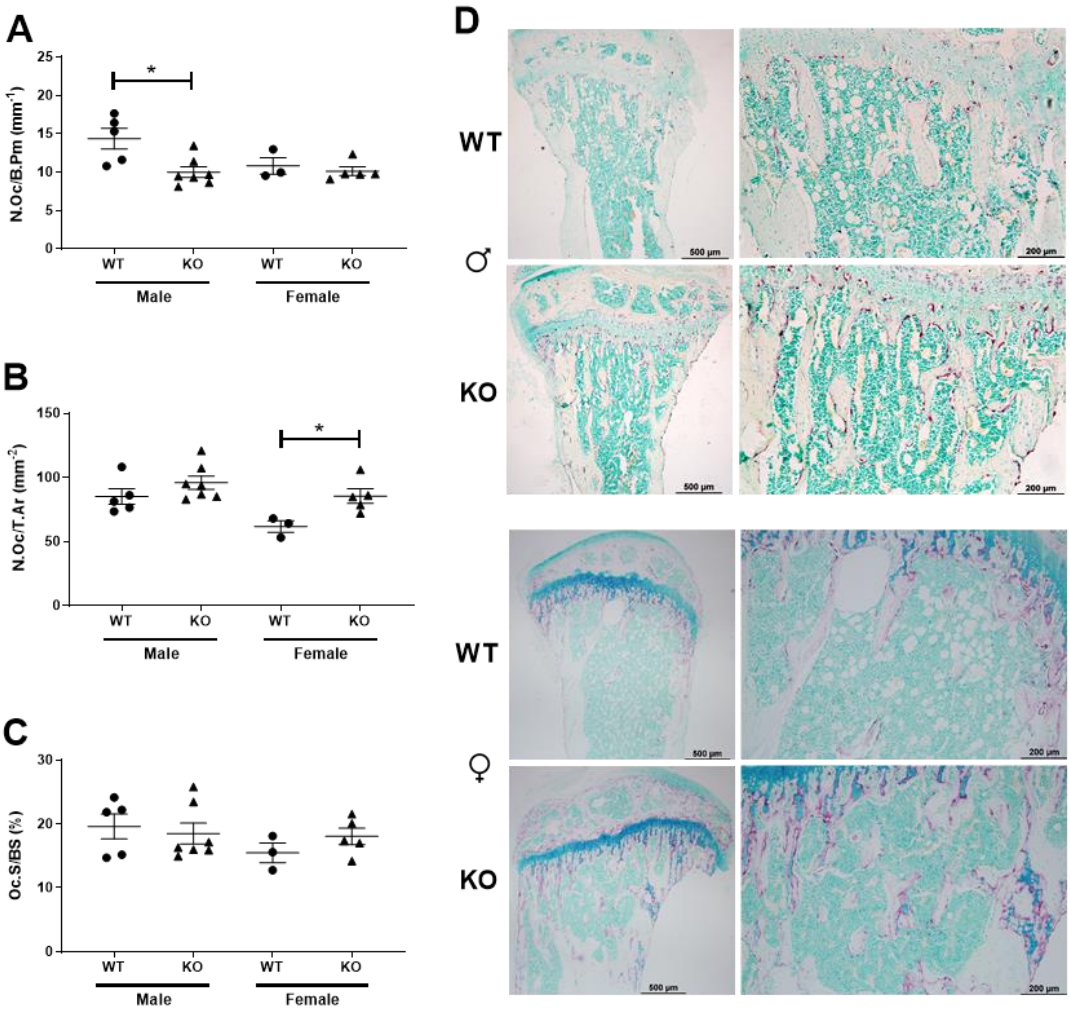

Figure 3.8 Osteoclast parameters are comparable between *Scara5*$^{-/-}$ and WT murine bones. Osteoclast parameters of N.Oc/B.Pm (A), Oc.S/BS (B) and N.Oc/T.Ar (C) of 11-week-old WT (male, n = 5; female, n = 3 biological

replicates) and *Scara5*$^{-/-}$ mice (male, n = 7; female, n = 5 biological replicates). (D) Representative micrographs of bone histology sections stained by methyl green and TRAP activity stain of 11-week-old WT and *Scara5*$^{-/-}$ bones. Scale bar = 500 µm on the left panels and 200 µm on the right panels. Bars represent mean ± SEM. *p < 0.05; by two-way ANOVA multiple comparison Sidak's test.

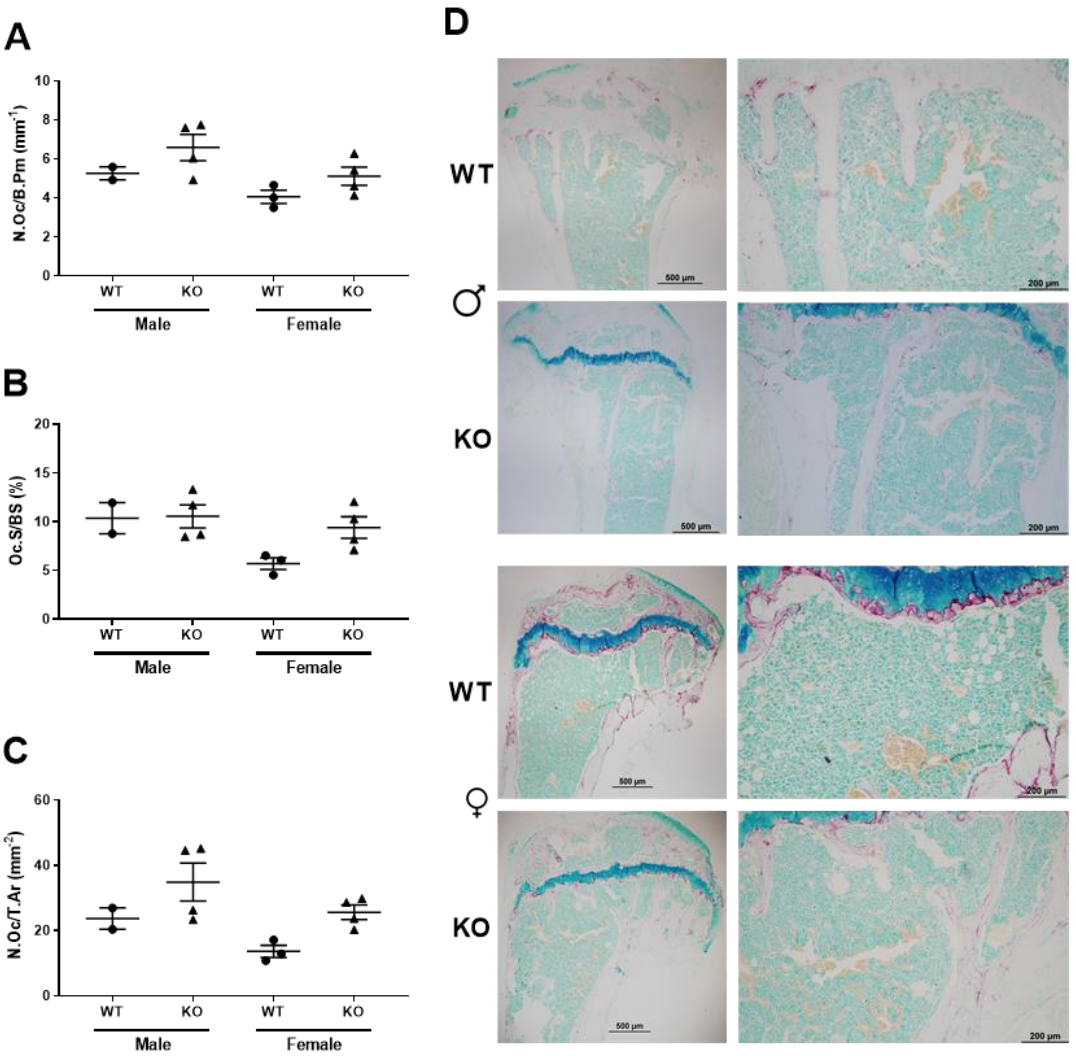

Figure 3.9 Osteoclast parameters in WT and *Scara5*$^{-/-}$ bones of 1-year mice. Osteoclast parameters showing N.Oc/B.Pm (A), Oc.S/BS (B) and N.Oc/T.Ar (C) of WT (male, n = 2; female, n = 3 biological replicates) and *Scara5*$^{-/-}$ mice (male, n = 4; female, n = 4 biological replicates) at 1-year of age. (D) Representative micrographs of bone histology sections stained by methyl green and TRAP activity stain of 1-year-old WT and *Scara5*$^{-/-}$ bones. Scale bar = 500 µm on the left panels and 200 µm on the right panels. Data is expressed as mean ± SEM.

There was no statistical significance by two-way ANOVA multiple comparison Sidak's test.

3.2.6 No difference in osteogenic progenitor cell frequency in WT and *Scara5*$^{-/-}$ bone marrow progenitor populations

The increase of bone volume and bone formation in *Scara5*$^{-/-}$ animals prompted the investigation as to whether there was a difference in the size of the osteogenic progenitor population between WT and *Scara5*$^{-/-}$ mice. Using cell surface markers defined by Ambrosi and colleagues [64], marrow cell populations were identified as multipotent BMSCs (CD45^{-} CD31^{-} Sca1^{+} CD24^{+}) and osteochondrogenic lineage progenitors (CD45^{-} CD31^{-} Sca1^{-} PDGFRα^{+}) by FACS analysis. Bone marrow cells were isolated from tibias and femurs of 11-week-old WT and *Scara5*$^{-/-}$ mice and stained with cell surface markers CD45**,** CD31**,** Sca1, CD24, and PDGFRα. Representative plots are shown in Figure 3.10 A to illustrate the gating strategy that was employed to identify BMSC and osteochondrogenic progenitor cell (OPC) populations.

Both BMSC and OPC populations were identified initially by absence of the haematopoietic and endothelial cell markers CD45 and CD31. BMSCs were identified further by expression of the molecules Sca1 and CD24 (Figure

3.10 A lower middle panel - green box). OPCs were determined by positive staining for PDGFRα (Figure 3.10 A lower right panel - purple box). There was no statistically significant difference in the frequency of BMSCs and OPCs between WT and *Scara5*$^{-/-}$ mice (Figure 3.10 B). Although there was no statistical significance, the size of the BMSC population in WT (male = 0.072 ± 0.018%; female = 0.081 ± 0.011%) was somewhat higher than *Scara5*$^{-/-}$ mice (male = 0.058 ± 0.003%; female = 0.066 ± 0.004%). The OPC population in *Scara5*$^{-/-}$ females (0.473 ± 0.029%) was moderately larger than that of WT females (0.261 ± 0.076%), whereas the number of OPCs in male WT (0.435 ± 0.079%) and *Scara5*$^{-/-}$ (0.407 ± 0.017%) mice was comparable (Figure 3.10 C).

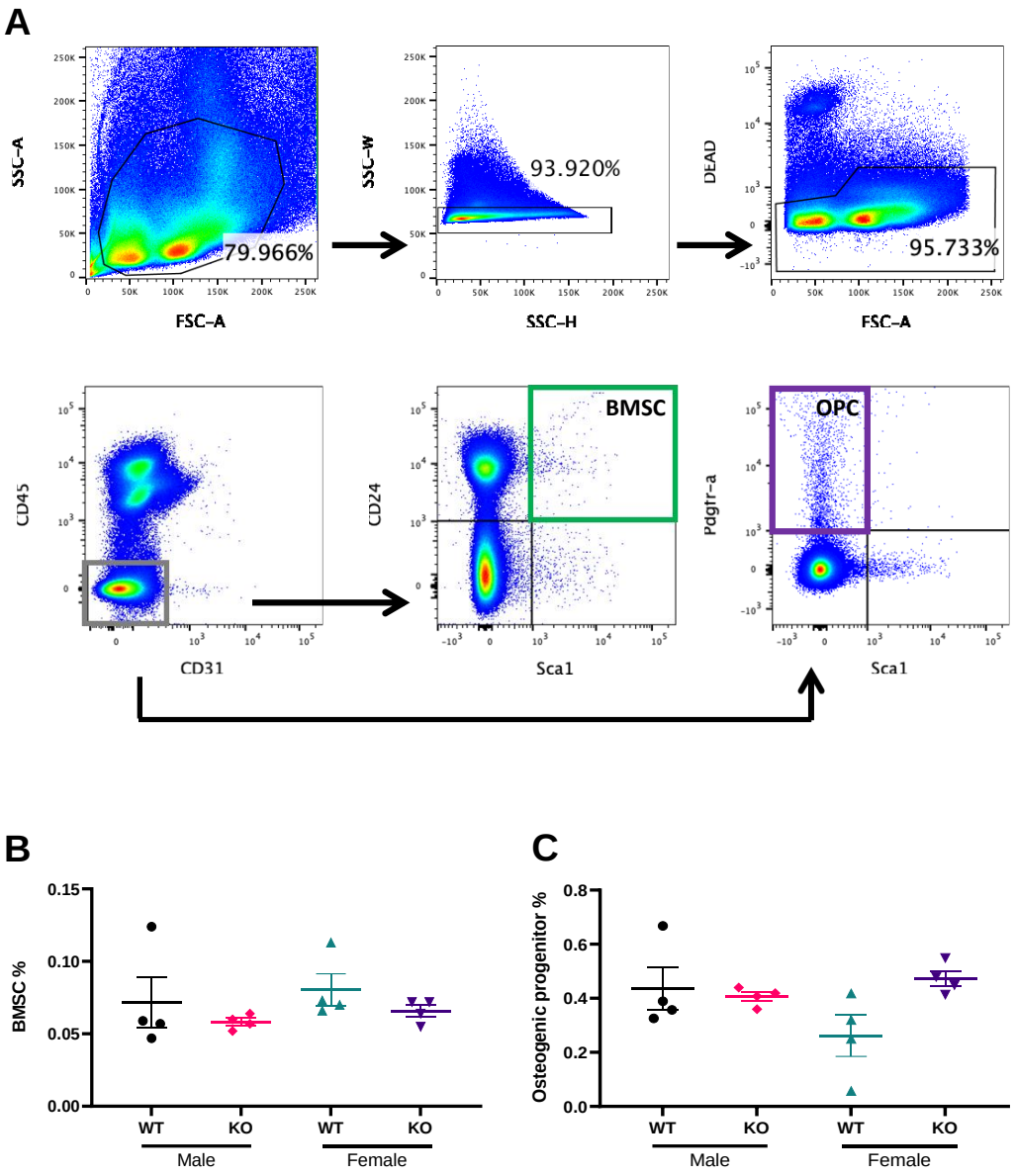

Figure 3.10 FACS analysis of BMSC and osteogenic progenitor cells in WT and *Scara5*$^{-/-}$ mice. (A) Gating strategy of FACS analysis for BMSC and osteogenic progenitor cell (OPC) populations. Lower panel: grey box is CD45^{-} CD31^{-}cells; green box is CD45^{-} CD31^{-} Sca1^{+} CD24^{+} BMSC population; purple box is CD45^{-} CD31^{-} Sca1^{-} Pdgfrα^{+} OPC population. (B-C) The percentage of BMSCs and OPCs from 11-week WT and *Scara5*$^{-/-}$ (KO) long bones (n = 4 biological replicates in each group). Data represents mean ± SEM.

3.2.7 SCARA5 deficiency in BMSCs enhances osteogenesis

Although a significantly elevated bone volume and improved bone formation rate were exhibited in mice lacking SCARA5, no significant change in populations of BMSCs or OPCs was found. These results lead to the question of whether the absence of SCARA5 affects the osteogenic differentiation capacity of bone marrow progenitors and thereby bone formation. To investigate this, BMSCs isolated from WT and *Scara5*$^{-/-}$ mice were cultured in osteogenic medium *in vitro* and alkaline phosphatase (ALP) levels assessed as an early indicator of osteoblast formation.

The substrate *p*-nitrophenylphosphate interacts with ALP in the cells and yields a yellow soluble product and its relative intensity correlates to the amount of ALP activity. This colourimetric ALP assay was optimised by varying cell density and making measurements at multiple time points between day 1 and day 7 of osteogenic culture (Figure 3.11 A-D). Initial trials confirmed that after plating $1x10^4$ cells the earliest increase in ALP was detected on day 3, after which ALP levels plateaued through day 5 and day 7. Hence, $1x10^4$ cells on day 3 was selected to assess osteogenic cultures.

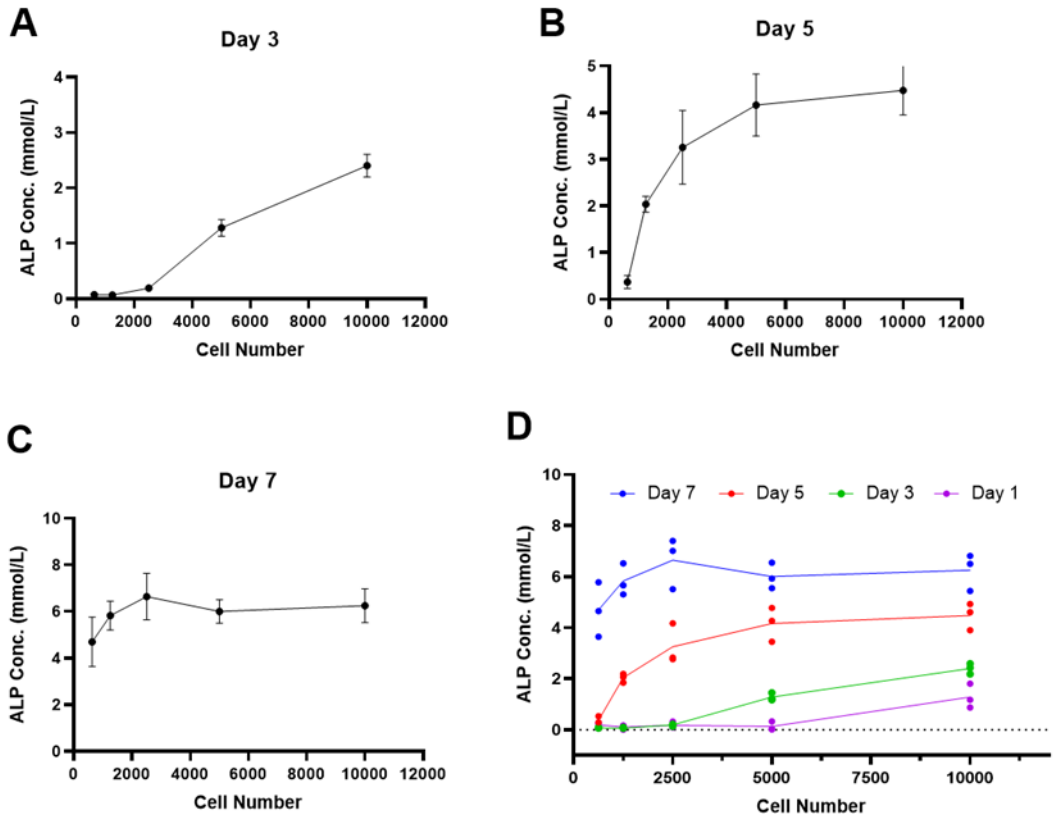

Figure 3.11 Optimization of ALP assay using different cell densities and assessment at different time points. (A-C) Optimization of ALP assay. ALP concentration was measured at Day 1, day 3 (A), day 5 (B) and day 7 (C) at 2T3 cell density of 625, 1250, 2500, 5000, 10000 cells/well of 96-well plate. (D) The merge of graphs D-F of the ALP concentration at different 2T3 cell numbers at day 1, 3, 5, 7 of osteogenic induction.

Under osteogenic conditions, ALP activity was significantly greater in *Scara5*$^{-/-}$ BMSCs (2.44 ± 0.23 mmol/L) in comparison to WT BMSCs (1.60 ± 0.13 mmol/L) (Figure 3.12 A). Assays were subsequently established to investigate bone nodule formation from *Scara5*$^{-/-}$ and WT BMSCs. After 28 days in culture, plates were stained with Alizarin Red S (ARS) to visualize the bone

nodules before eluting ARS for quantification. There was a significant increase in bone nodule staining of *Scara5*$^{-/-}$ BMSCs (0.90 ± 0.07 mM) as compared to WT BMSCs (0.53 ± 0.03 mM) (Figure 3.12 B). Images (Figure 3.12 C) of bone mineral nodule deposition (indicated by red stain with ARS) confirmed that they were markedly lower in WT BMSCs (0.529 ± 0.025 mM) than in *Scara5*$^{-/-}$ (0.904 ± 0.074 mM) cell cultures, indicating enhanced osteogenesis of BMSCs at the absence of SCARA5.

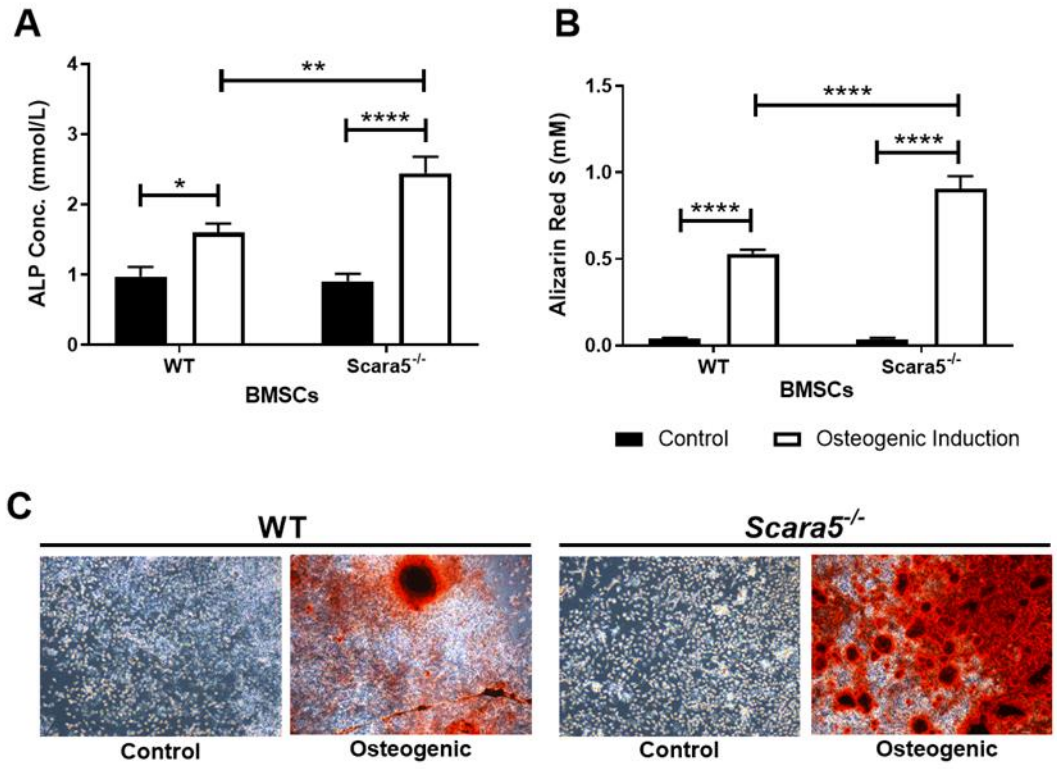

Figure 3.12 *Scara5*$^{-/-}$ BMSCs display an enhanced osteogenic differentiation capacity. (A) ALP concentration levels of WT and *Scara5*$^{-/-}$ BMSCs at day 3 under control and induced osteogenesis (n ≥ 5 triplicate experiments). (B) ARS concentration from eluates of stained WT (n = 4 biological replicates) and *Scara5*$^{-/-}$ (n = 5 biological replicates) BMSCs at day 28 under control and induced osteogenesis. (C) Representative micrographs of

Alizarin Red staining of WT and *Scara5*$^{-/-}$ BMSCs in control and osteogenic culture conditions at day 28. Error bars represent mean ± SEM. *p < 0.05; **p < 0.01; ****p < 0.0001 by two-way ANOVA multiple comparison Sidak's test.

3.3 Discussion

The established paradigm of healthy bone remodelling and maintenance reflects a balance between bone resorption by osteoclasts and bone formation by osteoblasts [29, 30]. Recent evidence has indicated that osteoblast and adipocyte lineage determination of BMSCs is a key contributing mechanism to bone loss during aging and osteoporosis, giving rise to the phenotypic presentation of low bone mass and high marrow adiposity [106, 148]. Therefore, molecules that contribute to the functions of osteoclasts, osteoblasts, or BMSCs can influence bone mass and development. In this chapter, SCARA5 was considered as a promising factor important to bone formation and differentiation, where its loss of function was investigated in murine long bones and under osteogenic differentiation *in vitro*.

Jiang and colleagues showed that primarily populations of epithelial cells expressed *Scara5*, rather than cells of the haematopoietic system [233]. *Scara5* expression was examined in a small number of mouse tissues in this

chapter, including bone and white fat by qRT-PCR. In agreement with previous studies [233, 234], testis expressed the highest level of *Scara5* in C57/BL6 WT mice, whilst expression of *Scara5* mRNA was much lower in liver. Interestingly, *Scara5* mRNA expression level in liver tissue can vary moderately between distinct mouse strains, which may be the same for other tissues [234]. By immunocytochemical methods that utilised antibodies against SCARA5, the macrophage marker F4/80 and reagents that were specific for fibroblasts (PDGFRα and vimentin), endothelia (CD31) and myofibroblasts (α-SMA), Ojala *et al.* observed that the SCARA5 was expressed by a subset of fibroblasts in mice [234]. In addition, it was revealed by Lee and colleagues that *Scara5* was more abundantly expressed in SVF (stromal vascular fraction) compared with the epididymal white fat fraction. Meanwhile, analysis into different mouse tissues found that white adipose tissue showed the highest level of *Scara5* expression in comparison to the other tissues that were investigated [217]. As a result, it was suggested in this study that SCARA5 was involved in adipogenesis by the authors. However, expression of *Scara5* in bone has not been reported previously.

Scara5 mRNA expression in various cell lines has been previously investigated [233, 234, 243]. The fibroblast cell lines NIH3T3 and L929

consistently express *Scara5*, whereas no significant expression was reported in the macrophage cell lines IC-21 and RAW 264.7. Moreover, Lee and colleagues found that *Scara5* expression was upregulated in 3T3-L1 and A33 preadipocytes at the early stage of adipocyte differentiation but subsequently decreased, whilst the level of *Scara5* remained low in multipotent C3H10T1/2 cells [217]. During adipocyte differentiation, *Scara5* expression increased in A33 preadipocytes along with other key differentiation markers, including C/EBPβ, C/EBPα and PPARγ2. Conversely, genetically knocking down *Scara5* during adipogenic differentiation severely blunted C/EBPβ, C/EBPα, PPARγ2 and aP2/422 expressed in 3T3-L1 and A33 preadipocytes [217]. On the other hand, *Scara5* upregulation enhanced adipocyte differentiation and formation whilst osteoblastic gene markers, such as *Alp*, *Runx2* and *Osteocalcin*, were suppressed in C3H10T1/2 cells [217]. These results indicated that SCARA5 may play a critical role in regulating differentiation and commitment of osteoblast and adipocyte lineage.

Here *Scara5* expression in osteoblastic 2T3 cells and primary mouse BMSCs was investigated during early osteogenic differentiation. The results showed that the level of *Scara5* mRNA increased approximately 8 folds in 2T3 cells at the 72-hour time point, whilst a 2-fold increase was seen in the primary

BMSCs 72-hour after osteogenic induction. The different extent of increase in the *Scara5* expression may be due to their cell differentiation stage, where BMSCs are uncommitted cells and 2T3 cells are committed osteoblastic cells. Therefore, it will be interesting to further investigate *Scara5* expression of BMSCs for longer and more time points in osteogenic culture.

In general, aside from being highly enriched in testis, white fat tissue and SVF, SCARA5 is also known to be regulated under osteogenic and adipogenic differentiation. These findings provide an important insight to its effects on the lineage determination between osteoblasts and adipocytes and the potential role of SCARA5 in bone *in vivo*. Through investigating the bone phenotype and osteogenic differentiation between WT and *Scara5*$^{-/-}$ mice, the results in this chapter identified SCARA5 as a negative mediator in bone formation and differentiation. It was found that in the absence of SCARA5, bone volume, trabecular bone and connectivity index were significantly greater than the WT control group at 11-week and 1 year of age. Following investigations showed an enhanced osteogenic differentiation ability as well as higher MAR and BFR, indicating an increase in osteoblast activities in *Scara5*$^{-/-}$ animals. To better understand the elevated bone formation in *Scara5*$^{-/-}$ mice, a further analysis of osteogenic marker gene expression during osteogenesis, such as

Runx2, Alp, *Col1a1* and *Osteocalcin*, will be especially supportive for future mechanistic studies.

The contributions of other scavenger receptors to bone formation and differentiation have been reported. In the study by Lin *et al.*, the authors found that 129/SvJ mice with SR-A (MSR1/SCARA1) deletion (*SR-A*$^{-/-}$) had a significantly greater bone volume, trabecular number and thickness than WT counterparts at 4 weeks of age, but there was no difference in bone formation rate between WT and *SR-A*$^{-/-}$ mice [216]. SR-A is expressed predominantly by macrophages and unsurprisingly osteoblast-related histomorphometric parameters of *SR-A*$^{-/-}$ mice, such as bone formation rate were not altered. However, a significant decrease in osteoclast-dependent parameters was found in *SR-A*$^{-/-}$ mice, confirming that SR-A was important to the osteoclast activities that derive from the monocyte-macrophage lineage *in vivo*. In brief, Lin and colleagues found the increase of bone mass in *SR-A*$^{-/-}$ mice was at least in part due to the significant reduction in osteoclast frequency, probably as a result of impaired osteoclast differentiation [216]. In contrast, *Scara5*$^{-/-}$ mice showed higher bone mineral deposit and formation rates than WT animals, but showed no significant difference in osteoclast parameters, indicating that SCARA5 plays a different role in bone development than SR-A.

Class B scavenger receptor 1 (SCARB1) is a mediator of glycoprotein production in the adrenal gland and a main receptor of high-density lipoprotein (HDL) essential for normal osteoblast differentiation and bone formation [229, 253]. In contrast to the increase bone volume observed in SR-A and SCARA5 deficiency, *Scarb1*$^{-/-}$ mice had a bone phenotype with lower bone mass and trabecular density than the WT controls [216, 230]. In addition, as a consequence of the role of SCARB1 in glucocorticoid production and HDL receptor, *Scarb1*-deficient mice have normal glucocorticoid level but produce high levels of adrenocorticotropic hormone (ACTH). This study showed that *Scarb1* deficiency in MSCs inhibited osteoblast differentiation *in vitro*, and that the positive effect on bone formation was only observed at low ACTH concentrations (<10 nM). As a result, *Scarb1*$^{-/-}$ animals showed decreased bone formation and osteoblast differentiation *in vitro* and a reduced bone volume *in vivo* relative to WT mice.

Focusing specifically on the role of SCARA5 in osteogenic differentiation, the influence of SCARA5 in osteoblast differentiation of MSC-like cells C3H10T1/2 was considered in the study by Lee and colleagues [217]. Whilst their investigation was primarily on SCARA5 in adipocyte lineage commitment, their findings showed that *Scara5* overexpression significantly

reduced C3H10T1/2 osteogenesis and osteogenic gene expressions (*Runx2*, *Alp* and *Osteocalcin*). Their data correspond to the results presented in this chapter, in which SCARA5 has a negative or inhibitory contribution to osteoblast differentiation and that BMSCs exhibit an increase in osteogenesis and enhanced calvaria osteoblast activity at the absence of SCARA5. One possible explanation could be a change in the frequency of osteogenic precursors in the bone marrow of WT and *Scara5*$^{-/-}$ mice. However, FACS analyses did not reveal significant differences in the percentage of osteogenic progenitor population (Figure 3.10 C). Considered together, these data indicated that SCARA5 was important to osteoblast differentiation and bone development as a consequence of altered cell lineage differentiation propensity of BMSCs.

Defects in osteoclasts are one of the most common causes of altered bone mass [5, 39]. Takemura *et al.* determined that immature mononuclear osteoclasts and macrophages expressed SR-A, whilst mature multinucleated osteoclasts were negative [218]. In addition, they showed that osteoclast differentiation was enhanced by SR-A via increased expression of RANK and RANK-related differentiation molecules. Conversely, though the expression of c-fms, a M-CSF receptor, were not affected, RANK and RANK-related

molecules were markedly decreased in *SR-A* depleted animals [218]. This effect was replicated *in vivo*; the number of multinucleated mature osteoclasts was significantly diminished with elevated femoral bone density in *SR-A*$^{-/-}$ mice as compared to WT animals. Gao and colleagues reported that the number of multinucleated osteoclasts and bone resorption was significantly reduced in *SR-A*$^{-/-}$ mice and demonstrated that administrating recombinant IL-6 restored the frequency of osteoclasts to that of WT control mice [226]. Additional investigations of *in vitro* osteoclast formation assay found that RANKL-induced MAPK signalling pathways, including c-Jun N-terminal protein kinase (JNK) and extracellular signal-regulated kinase (ERK), but not p38, were significantly downregulated in *SR-A*$^{-/-}$ osteoclasts. Meanwhile, ERK or JNK inhibitor significantly reduced the generation of osteoclasts from WT bone marrow macrophages, concomitantly with reduced expression of IL-6. This study demonstrated that SR-A played an important role in supporting osteoclastogenesis via activation of ERK and JNK signals and inducing IL-6 expression [226].

Although other class A scavenger receptors are primary expressed by myeloid cells which includes the osteoclast lineage, the evidence to date is that SCARA5 is not, but rather expressed ubiquitously in other cell types [254, 255].

To further exclude the possibility that *Scara5* expression in osteoclasts may be transient, we used TRAP staining to identify active osteoclasts within the bone marrow of WT and *Scara5*$^{-/-}$ tibia. In agreement with the absence of *Scara5* expression in osteoclasts, the osteoclast parameters in *Scara5*$^{-/-}$ animals were not different as compared to WT, both in terms of frequency and density per bone surface. The difference between the bone phenotypes in SR-A and SCARA5 deficiency are implicated by their cell expression profile. In addition, unlike *SR-A*$^{-/-}$ mice, bone mineral deposition rate, controlled by osteoblast activities, were significantly accelerated in *Scara5*$^{-/-}$ animals as compared to WT control mice. Therefore, these data are consistent with distinct roles for SR-A and SCARA5 in murine bone remodelling [234, 256].

In summary, the findings presented and discussed in this chapter suggested a novel role of SCARA5 in bone biology and the potential for SCARA5 to affect bone formation and differentiation.

Chapter 4 – SCARA5 receptor-ligand associations in bone biology

4.1 Introduction

One of the main functions of scavenger receptors is to mediate the cellular uptake of soluble ligands (e.g. modified lipoproteins) through receptor-mediated endocytosis. The ligand is bound by the scavenger receptor and internalised in a vesicle formed from the cell membrane [214]. SCARA5 shares sequence and structural similarity with other class A scavenger receptor family members [214]. However, SCARA5 may therefore have distinctive functions, with its specificity to bind and transport L-ferritin and direct association with FAK [235, 236, 241]. Here, the function of SCARA5 was explored via its established and potential ligands that has been shown to affect bone formation, thereby linking SCARA5's function to bone biology.

SCARA5 was identified by Li and colleagues as a ferritin receptor that was part of a non-transferrin receptor iron delivery pathway in the developing murine embryonic kidney [241]. They confirmed that SCARA5 bound and endocytosed serum ferritin which was subsequently delivered into the cytosol. Another study found that SCARA5 expressed by endothelial cells helped transport light-chain ferritin (L-ferritin) across the blood-retinal barrier [235]. A

more recent study showed that the C-terminal cysteine-rich domain of SCARA5 was responsible for ferritin binding in a Ca^{2+}-dependent manner [257]. The interaction between SCARA5 and ferritin provided the basis for the development of an ELISA, that could be utilised for the identification of other ligands for the receptor (in this thesis). It is pertinent that a previous study has shown that iron overload completely abolished the osteogenic differentiation of human BMSCs via ferritin upregulation, with similar effect applied to exogenous ferritin administration under BMSC osteogenic condition [258]. Thus, in this chapter, the effect of ferritin on BMSC osteogenesis in the presence and absence of SCARA5 was briefly investigated.

Guo *et al.* showed a direct receptor interaction with high mobility group box 1 (HMGB1) in SCARA5-mediated clearance of HMGB1 in fish models under inflammatory challenges [259]. The 25 kDa nuclear protein, HMGB1, plays an essential role in immunity as a mediator of tissue damage and inflammation [260, 261]. There are two active redox forms of HMGB1 under physiologic conditions; fully-reduced (FR-HMGB1) and disulfide (DS) forms (DS-HMGB1), which differ in the redox status of cysteine residues within the protein [262]. FR-HMGB1 acts as a chemoattractant, whilst partially oxidized DS-HMGB1 with a disulfide bond induces proinflammatory cytokines and

further cysteine oxidation to sulfonates abrogates both activities during inflammation [261, 262]. Interestingly, it was demonstrated recently that HMGB1 stimulation, especially with the fully-reduced form of HMGB1, accelerated mouse bone fracture healing and tissue regeneration [263], whilst others have reported that HMGB1 is an active cytokine involved in bone resorption signals of the bone microenvironment [264, 265]. Given the associations of HMGB1 with SCARA5 and bone healing, this chapter looked into possible interactions between the two redox forms of HMGB1 and SCARA5 and whether they played a part in BMSC osteogenic differentiation in the presence and absence of SCARA5.

WNT proteins and WNT signalling pathways are one of the most robustly investigated and diverse mechanisms that are involved in multiple biological processes, including osteogenic and adipogenic lineage differentiation of BMSCs [148, 266, 267]. Numerous studies have emphasized the significant role of WNT pathways in bone development, fracture repair and regeneration, and osteogenic differentiation [14, 268, 269]. Nevertheless, the relationship between WNT and SCARA5 has not been investigated to date. Therefore, this chapter explored the potential link between SCARA5 and WNT and the involvement of WNT-related signalling in BMSC osteogenesis in the presence

and absence of SCARA5. The canonical WNT/β-catenin pathway plays a major role in cell fate decision and osteogenic differentiation of BMSCs [14, 148, 270]. Due to the variety of WNT ligands and related proteins, WNT inhibitors and a WNT ligand known to be strongly associated with the WNT/β-catenin pathway and osteogenesis were selected for the experiments described in this chapter.

4.2 Results

4.2.1 Light chain ferritin binds to recombinant SCARA5 using self-designed indirect ELISA

To investigate receptor-ligand interaction of SCARA5 with candidate ligands, an indirect ELISA was designed as illustrated in Figure 4.1; the assay components and sequential steps leading to the colourimetric readout of the final enzyme reaction step. Since the positive binding ability of SCARA5 to L-ferritin had been established previously [259], the efficacy of this indirect ELISA was determined using different concentrations of L-ferritin as the target ligand. Recombinant human SCARA5 (hSCARA5) bound to L-ferritin in a concentration-dependent manner, that correlated with increased OD 450nm absorbance intensity (Figure 4.3 A). Validation of the ELISA indicated that the

highest concentration 500 nM of L-ferritin gave an average value of 0.704 ± 0.087 absorbance, and the lowest concentration 0.1 nM of L-ferritin gave an average of 0.181 ± 0.059 absorbance at OD 450nm (Figure 4.3 A).

Figure 4.2. illustrated the study rationale of ferritin in the presence and absence of SCARA5. To determine whether there was an effect of ferritin on osteogenic differentiation of BMSCs, assays were established for the detection of ALP in response to increasing concentrations of native human ferritin (purified from liver and composed of L-ferritin and H-ferritin). Briefly, WT and *Scara5*$^{-/-}$ BMSCs were treated under osteogenic medium with native human ferritin at concentrations of 1.8, 18, and 180 ug/mL (Figure 4.3 B); media lacking exogenous ferritin was used as a negative control to ensure that the cells responded to the osteogenic media appropriately. Native human ferritin significantly suppressed ALP activity of *Scara5*$^{-/-}$ BMSCs at 18 and 180 ug/mL at day 3 under osteogenic culture conditions, with ALP levels decreased by ~2.5 fold to 0.695 ± 0.05 and 0.898 ± 0.098 nmol/L respectively, compared to the osteogenic culture without ferritin treatment (Figure 4.3 B). In contrast, there was no statistically significant change in ALP levels of WT BMSCs treated with native human ferritin in osteogenic differentiation medium (Figure 4.3 B).

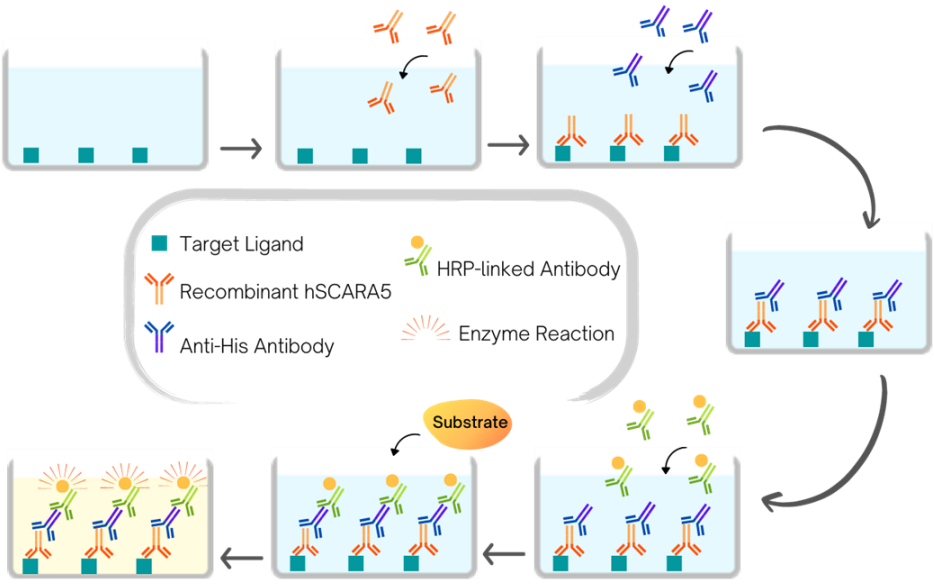

Figure 4.1 Schematic of SCARA5-ligand binding ELISA. The step-by-step guide to self-designed ELISA assay to interrogate target ligands interacting with SCARA5 receptor. Target ligands are bound to the plate and blocked with BSA prior to adding His-tagged recombinant hSCARA5. After washing, anti-His antibodies bind to recombinant hSCARA5 followed by Horseradish Peroxidase (HRP)-linked antibodies which bind to the anti-His antibodies and allow colorimetric ELISA assay readout.

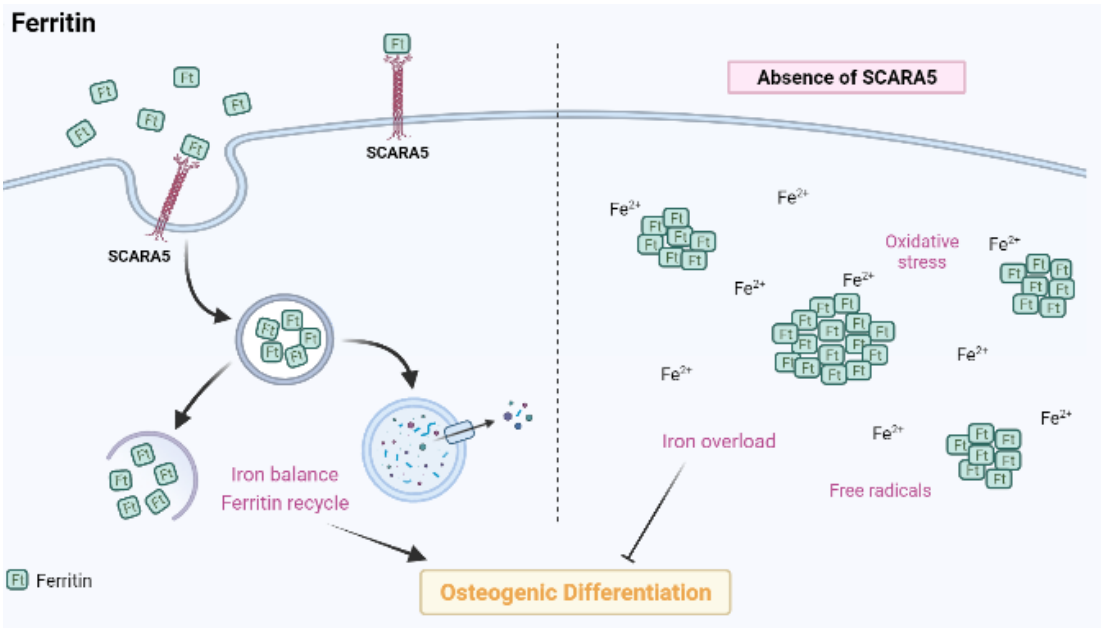

Figure 4.2 Schematic for the study rationale of ferritin and their effects on osteogenesis. Working hypothesis is that the presence of SCARA5 takes up

and recycle excess ferritins or dispose harmful iron particles, whereas excess iron particles and ferritins at the absence of SCARA5 causes cellular damage due to iron overload and oxidative stress.

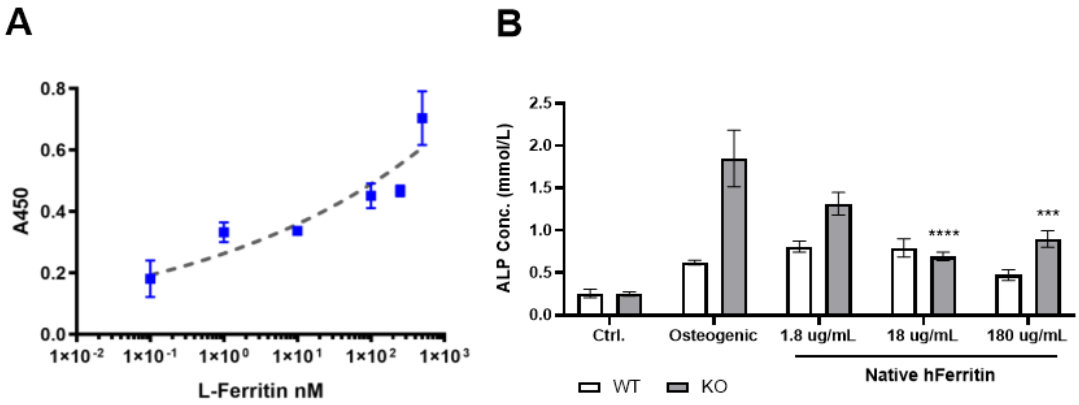

Figure 4.3 The positive interaction of Ferritin light chain with recombinant hSCARA5 confirmed using the in-house designed ELISA. (A) The level of OD 450 nm absorbance positively correlates with the relative amount of protein interaction between recombinant hSCARA5 and light-chain Ferritin (L-Ferritin) in the ELISA (n ≥ 3 duplicate experiments). (B) The ALP concentration of WT and *Scara5*$^{-/-}$ BMSCs treated with native Ferritin at day 3 under osteogenic culture condition (n = 6 biological replicates of duplicate experiments). Data represent mean ± SEM. ***p < 0.001; ****p < 0.0001 by 2-way ANOVA multiple comparison Sidak's test compared to the osteogenic condition.

4.2.3 HMGB1 is recognised by SCARA5 and can suppress osteogenic differentiation of murine BMSCs *in vitro*

Although it has been shown that SCARA5 facilitated HMGB1 clearance and attenuated inflammatory reactions in fish models [259], it was unknown whether mammalian SCARA5 would be able to bind to HMGB1 and whether HMGB1 involvement in BMSC osteogenic differentiation would be

affected by SCARA5. Figure 4.4 illustrated the study hypothesis of the HMGB1 interaction with SCARA5 and potential functions in the absence and presence of SCARA5.

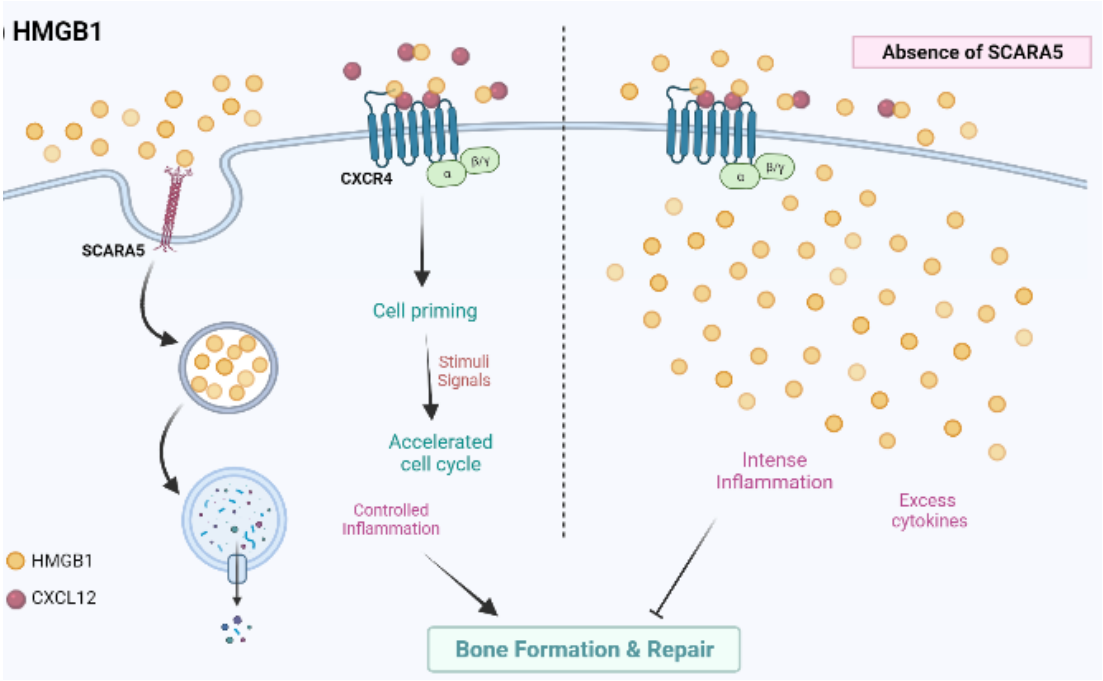

Figure 4.4 Schematic illustrations of the study rational for HMGB1 and its reported effects on osteogenesis. Potential interaction with HMGB1 in the presence and absence of SCARA5. The working hypothesis is that the presence of SCARA5 takes up and degrades excess HMGB1 to achieve a controlled cellular response, whereas excess HMGB1 at the absence of SCARA5 leads to over reactions. Alternatively, HMGB1 can form a complex with CXCL12 and binds to CXCR4 on the cell membrane, which triggers cell priming state and responds quickly when receiving stimuli and signals to promptly start the cell cycle.

Interaction of SCARA5 with fully-reduced HMGB1 (FR-HMGB1) and disulfide HMGB1 (DS-HMGB1) was investigated using ELISA. The binding of

recombinant hSCARA5 to FR-HMGB1 was concentration-dependent: from an average OD 450nm readout of 0.071 ± 0.058 at 0.1 nM FR-HMGB1, it increased to 0.319 ± 0.047 at 100 nM FR-HMGB1 (Figure 4.5 A).

Previously, Lee *et al.* demonstrated that HMGB1 pre-treatment *in vivo* accelerated bone fracture repair and increased the ALP activity of hMSCs *in vitro* under osteogenic conditions [263]. It was found here that pre-treatment of 1 ug/mL FR-HMGB1 for 16 hours before osteogenic differentiation significantly inhibited ALP levels in *Scara5*$^{-/-}$ BMSCs, whereas there was no significant change for WT BMSCs under osteogenic conditions (Figure 4.5 B). Similarly, continuous treatment of *Scara5*$^{-/-}$ BMSCs, with FR-HMGB1 in osteogenic medium significantly suppressed ALP activity, with an approximate 3-fold decrease occurring with all FR-HMGB1 concentrations (Figure 4.5 C). However, continuous FR-HMGB1 treatment of WT BMSCs, as opposed to pre-treatment, greatly diminished ALP activity more than 3-fold under osteogenic culture conditions (Figure 4.5 C). There was only a modest difference in ALP activity between WT and *Scara5*$^{-/-}$ BMSCs in osteogenic culture condition due to duplicate experiments with three mice in each experiment group with (Figure 4.5 C).

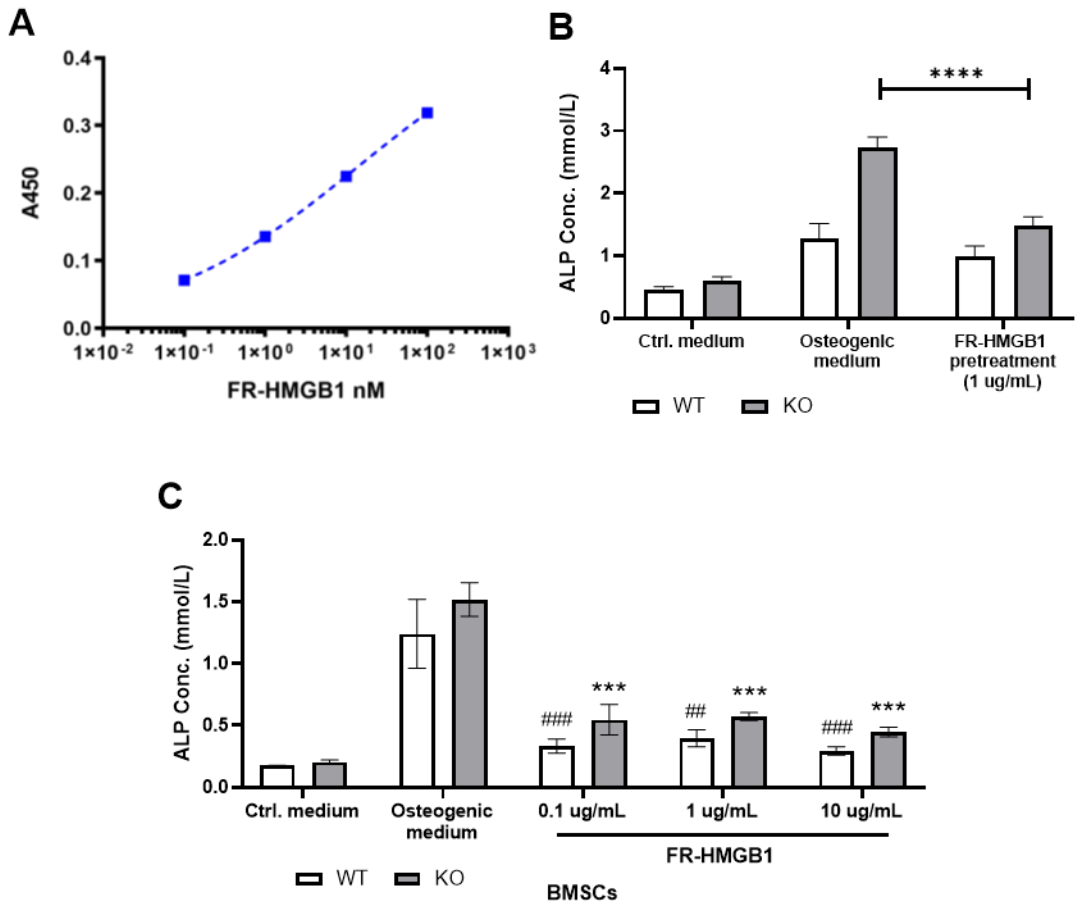

Figure 4.5 FR-HMGB1 interacts with SCARA5 and inhibits osteogenic differentiation of BMSCs. (A) A representative assay showing the relative SCARA5 binding activity to FR-HMGB1 at concentrations 0.1, 1, 10 and 100 nM (n ≥ 3 duplicate experiments). (B) ALP concentration of WT and *Scara5*$^{-/-}$ BMSCs at day 3 after 16 hours of pre-treatment with FR-HMGB1 at 1ug/mL under control and induced osteogenesis conditions (n = 3 biological replicate of triplicate experiments). (C) The level of ALP activity of WT and *Scara5*$^{-/-}$ BMSCs at day 4 treated with 0.1, 1, or 10 ug/mL of FR-HMGB1 under control and induced osteogenic conditions (n = 3 biological replicate of duplicate experiments). Error bars represent mean ± SEM. Against WT osteogenic medium ##p < 0.01; ###p < 0.001; against KO osteogenic medium ***p < 0.001; by 2-way ANOVA multiple comparison Sidak's test.

The interaction between SCARA5 and DS-HMGB1 was investigated using the in-house designed ELISA protocol illustrated in Figure 4.2. It was shown that recombinant hSCARA5 recognized DS-HMGB1, with concentration-dependent intensity increase of OD 450nm from 0.067 ± 0.066 at 0.1 nM to 0.205 ± 0.031 at 100 nM DS-HMGB1 (Figure 4.6 A). Pre-treatment of 1 ug/mL DS-HMGB1, before osteogenic induction for 16 hours, inhibited ALP level significantly in *Scara5*$^{-/-}$ BMSCs under osteogenic differentiation conditions (Figure 4.6 B). However, no significant change in the ALP level of WT BMSCs was found under the same conditions (Figure 4.6 B). Similar to pre-treatment of DS-HMGB1 on *Scara5*$^{-/-}$ BMSCs, treating *Scara5*$^{-/-}$ BMSCs continuously with DS-HMGB1 in osteogenic medium markedly suppressed ALP activity at 0.1 and 1 ug/mL DS-HMGB1 (Figure 4.6 C). Contrary to pre-treatment on WT BMSCs, continuous DS-HMGB1 treatment on WT BMSCs significantly diminished the ALP activity under osteogenic culture condition, with the greatest decrease to 0.22 ± 0.039 mmol/L ALP at 0.1 ug/mL of DS-HMGB1 (Figure 4.6 C). It was noted that only moderate differences were found in ALP activity between WT and *Scara5*$^{-/-}$ BMSCs in osteogenic culture due to the duplicate experiments using three mice in each experiment group (Figure 4.6 C).

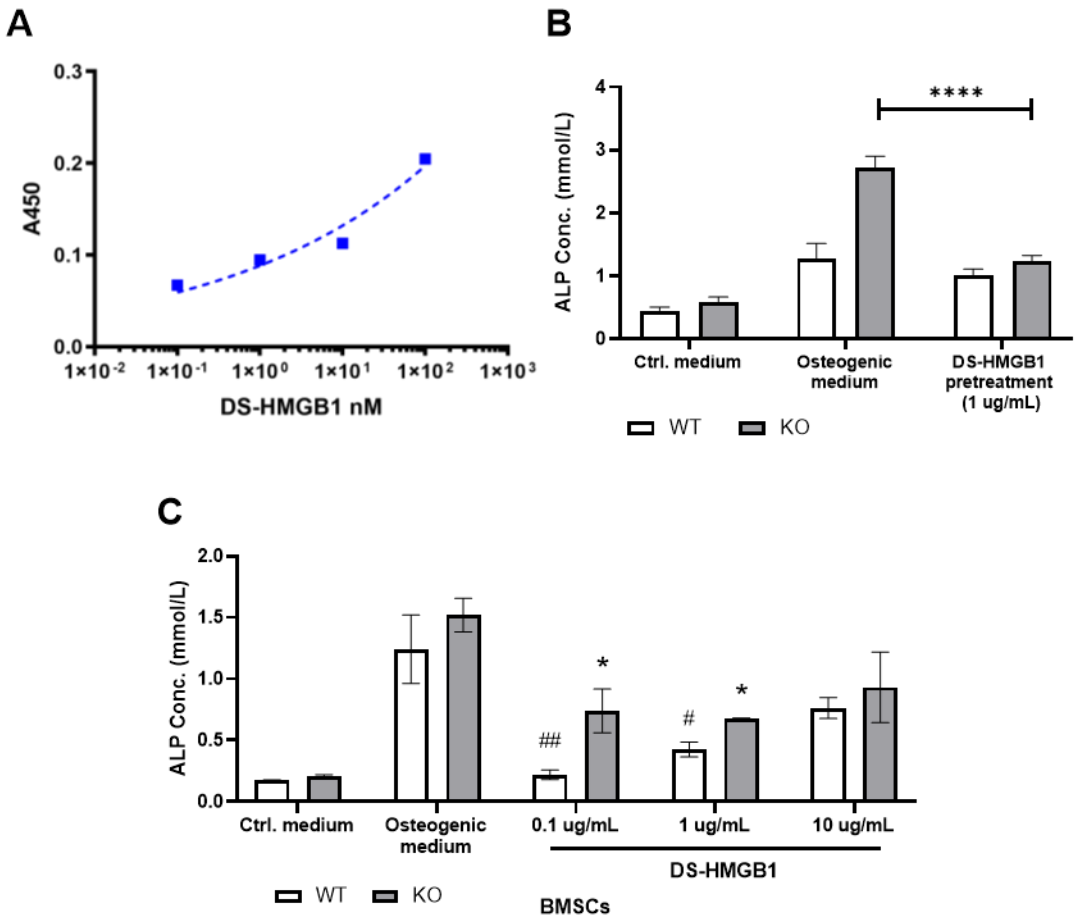

Figure 4.6 DS-HMGB1 binds to SCARA5 and inhibits osteogenic differentiation of BMSCs. (A) A representative result showing the relative SCARA5 binding activity to DS-HMGB1 at concentration 0.1, 1, 10 and 100 nM (n ≥ 3 duplicate experiments). (B) The ALP concentration of WT and *Scara5*$^{-/-}$ BMSCs at day 3 after 16 hours of pre-treatment with DS-HMGB1 at 1ug/mL under control and induced osteogenesis condition (n = 3). (C) The level of ALP activity of WT and *Scara5*$^{-/-}$ BMSCs at day 4 treated with 0.1, 1, or 10 ug/mL of DS-HMGB1 under control and osteogenic conditions (n = 3 biological replicates of duplicate experiments). Error bars represent mean ± SEM. Against WT osteogenic medium #$p < 0.05$; ##$p < 0.01$; against KO osteogenic medium *$p < 0.05$; by 2-way ANOVA multiple comparison Sidak's test.

4.2.4 Blocking CXCR4, the HMGB1-CXCL12 receptor, had no effect on osteogenic differentiation of *Scara5*$^{-/-}$ BMSCs

It is known that HMGB1 forms a heterocomplex with CXCL12 that then interacts with CXCR4 to elicit downstream signalling events in the cell [261, 263]. To investigate further the effect of HMGB1 in the presence and absence of SCARA5, the CXCR4 inhibitor, AMD3100, was used to inhibit HMGB1 signalling. In the first instance, cells were treated with AMD3100 for 16 hours before osteogenic induction. AMD3100 pre-treatment did not have an effect on WT and *Scara5*$^{-/-}$ BMSCs in control and osteogenic medium (Figure 4.7 A). Subsequently, WT and *Scara5*$^{-/-}$ BMSCs were treated continuously with or without AMD3100 for the duration of the culture conditions; there was no significant effect on BMSC differentiation as measured by ALP (Figure 4.7 B). Thus, both pre-treatment and continuous treatment of AMD3100 made no significant impact upon osteogenesis of WT and *Scara5*$^{-/-}$ BMSCs.

Lastly, AMD3100 was added 16 hours before FR- and DS-HMGB1 treatment of WT and *Scara5*$^{-/-}$ BMSCs (Figure 4.7 C). In the presence of AMD3100, FR- and DS-HMGB1 continued to suppress The ALP activity in *Scara5*$^{-/-}$ BMSCs, however the inhibitory effect of FR- and DS-HMGB1 on WT

BMSCs observed previously was abolished, with ALP levels remaining equivalent to that of the osteogenic media control (Figure 4.7 C).

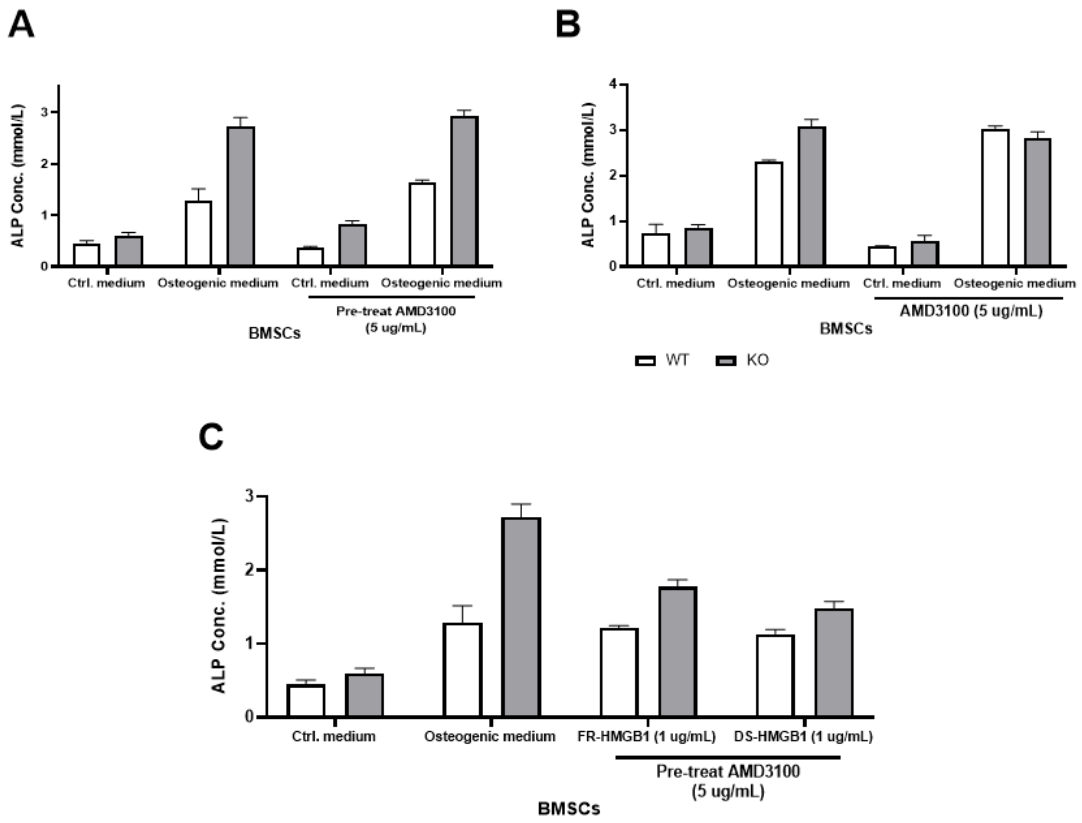

Figure 4.7 AMD3100 does not alter osteogenic differentiation of *Scara5*$^{-/-}$ BMSCs in the presence of HMGB1. (A) ALP activity of WT and *Scara5*$^{-/-}$ BMSCs pre-treated with AMD3100 for 16 hours followed by 3 days of incubation under control and osteogenic culture conditions (n = 3 biological replicates of triplicate experiments). (B) ALP concentration of WT and *Scara5*$^{-/-}$ BMSCs treated with AMD3100 for 3 days of culture under control and osteogenic conditions (n = 3 biological replicates of triplicate experiments). (C) ALP level of WT and *Scara5*$^{-/-}$ BMSCs pre-treated with AMD3100 for 16 hours followed by 3 days incubation with FR- and DS-HMGB1 at 1 ug/mL under control and osteogenic conditions (n = 3 biological replicates of triplicate experiments). Error bars represent mean ± SEM.

4.2.5 The WNT inhibitors, DKK1 and sFRP1 but not SOST, significantly suppressed the osteogenic differentiation of *Scara5*$^{-/-}$ BMSCs

WNT signalling is a major pathway regulating osteoblast and adipocyte differentiation of BMSCs [148, 269, 271]. Since the cysteine-rich domain on frizzled receptors and the LRP5 co-receptor is required for WNT ligand and antagonist interaction in WNT pathway [272, 273], it is speculated that the cysteine-rich domain of SCARA5 [274] may interact similarly with WNT inhibitors and ligands. Three WNT inhibitors, DKK1, sFRP1, and SOST, were investigated for their association with SCARA5 using the in-house designed ELISA protocol described previously in Figure 4.2. DKK1, sFRP1, and SOST were individually interrogated under osteogenic differentiation conditions in the presence and absence of SCARA5 in BMSCs. Figure 4.8 depicted the study hypothesis for WNT inhibitors and SCARA5 interaction and potential effects in the absence and presence of SCARA5.

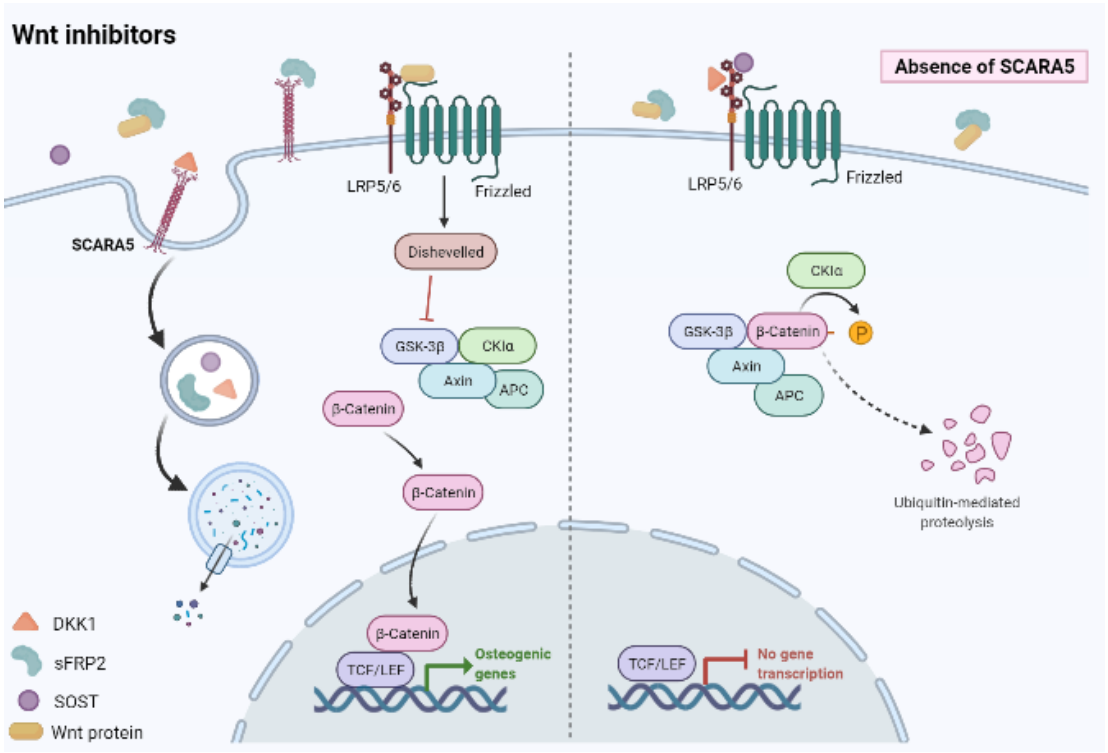

Figure 4.8 Schematic illustrations of the study rational for WNT inhibitors and their recognised effects on osteogenesis. Potential interaction of SCARA5 with WNT inhibitors (DKK1, sFRP1, SOST). Working hypothesis is that SCARA5 endocytoses and degrades WNT inhibitors to balance WNT signal activation, whereas in the absence of SCARA5 excess WNT inhibitors result in WNT signal inhibition.

Recombinant hSCARA5 captured DKK1 *in vitro* with increasing OD 450nm absorbance correlating with increasing DKK1 concentration (Figure 4.9 A). Subsequently, DKK1-treated *Scara5*$^{-/-}$ BMSCs showed a significant inhibition of ALP activity under osteogenic condition at 10 and 100 ng/mL DKK1, whilst WT-BMSCs showed moderate but not statistically significant decrease in ALP level at 100 ng/mL DKK1 (Figure 4.9 B). Similarly, sFRP1 positively bound to

recombinant hSCARA5 in a concentration-dependent manner (range 0.1 to 150 nM sFRP1) (Figure 4.9 C). WT-BMSCs treated with sFRP1 showed a modest decrease in ALP level under osteogenic differentiation conditions, whereas sFRP1 significantly suppressed ALP activity in *Scara5*$^{-/-}$ BMSCs at 10 and 100 ng/mL sFRP1 (Figure 4.9 D). In contrast, SOST did not reduce ALP of both WT and *Scara5*$^{-/-}$ BMSCs significantly, even though it exhibited comparable binding with recombinant hSCARA5 in the ELISA (Figure 4.9 E-F).

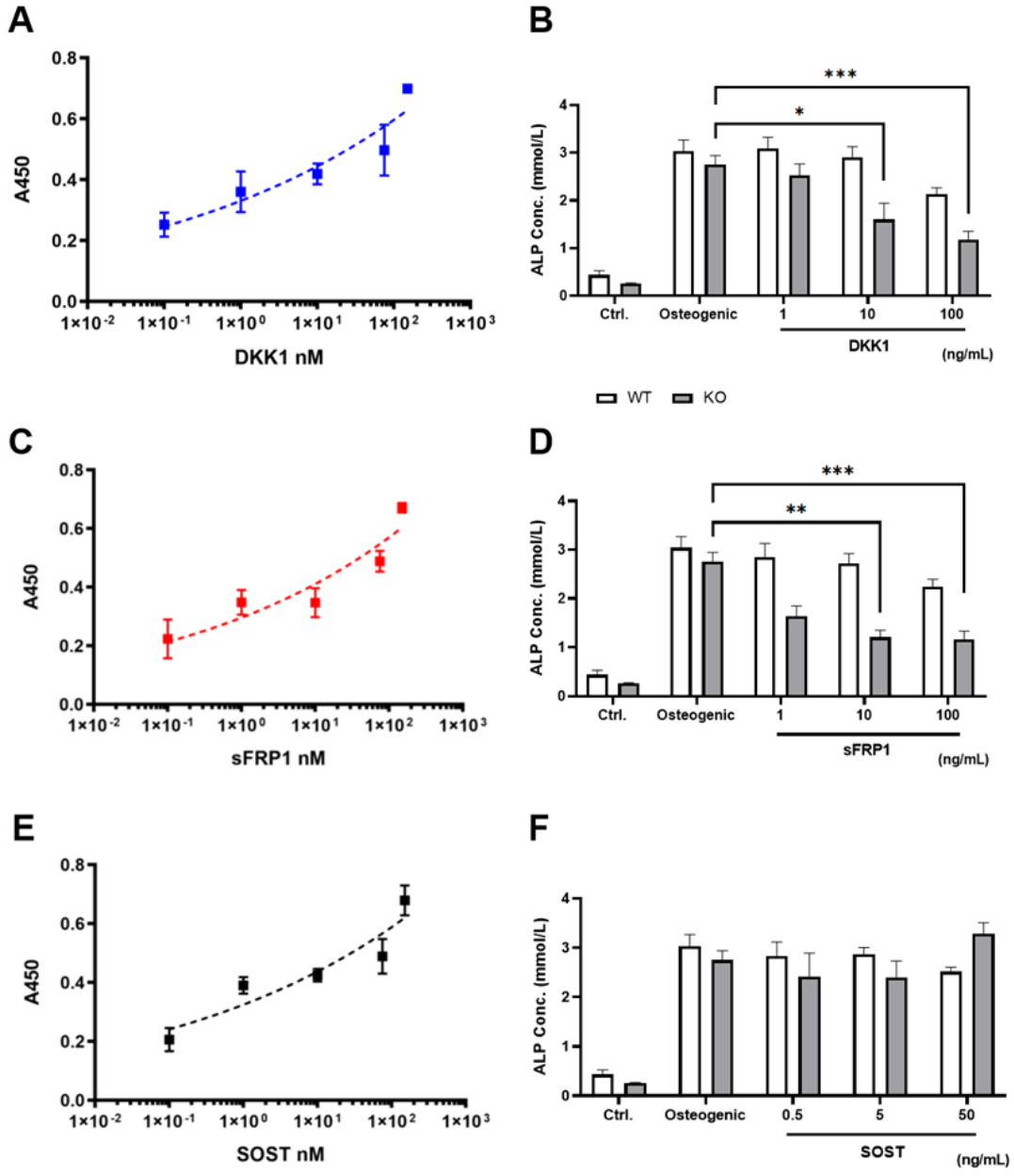

Figure 4.9 DKK1 and sFRP1, but not SOST, inhibit ALP expression in *Scara5*$^{-/-}$ BMSCs. (A) Interaction between DKK1 and recombinant SCARA5 via relative OD 450nm absorbance in ELISA (n ≥ 3 duplicate experiments). (B) The concentration of ALP of WT and *Scara5*$^{-/-}$ BMSCs at day 4 treated with DKK1 in control or osteogenic differentiation conditions containing 2% FBS (n = 3 biological replicates of duplicate experiments). (C) Relative binding activity between sFRP1 and SCARA5 recombinant protein as determined by ELISA (n ≥ 3 duplicate experiments). (D) ALP concentration of WT and *Scara5*$^{-/-}$ BMSCs at day 4 treated with sFRP1 under control or osteogenic differentiation condition with 2% FBS (n = 3 biological replicates of duplicate experiments). (E) The

relative interacting activity between SOST and SCARA5 recombinant protein measured by ELISA (n ≥ 3 duplicate experiments). (F) ALP concentration of WT and *Scara5*$^{-/-}$ BMSCs at day 4 treated with SOST in control or osteogenic differentiation condition with 2% FBS (n = 3 biological replicates of duplicate experiments). Error bars represent mean ± SEM. *p < 0.05; **p < 0.01; ***p < 0.001 by two-way ANOVA Sidak's test.

4.2.6 WNT3a supports BMSC osteogenic differentiation in the absence of SCARA5

Separate studies reported that WNT3a enhanced important regulators in early osteogenic differentiation and was associated with osteoblast metabolism (e.g. glycolysis), osteogenic signals (e.g. FGF-2 and LRP5/6) and transcription factors (e.g. LEF and TAZ) [182, 185-187]. Given its involvement in bone metabolism and differentiation, WNT3a was selected as a potential ligand of SCARA5 for investigation. The possibility of direct binding between WNT3a and SCARA5 was examined using the ELISA and the requirement for SCARA5 for WNT3a-dependent activities during osteogenic differentiation of BMSCs was also studied. The study hypothesis of WNT3a and its functions in the presence and absence of SCARA5 was illustrated in Figure 4.10.

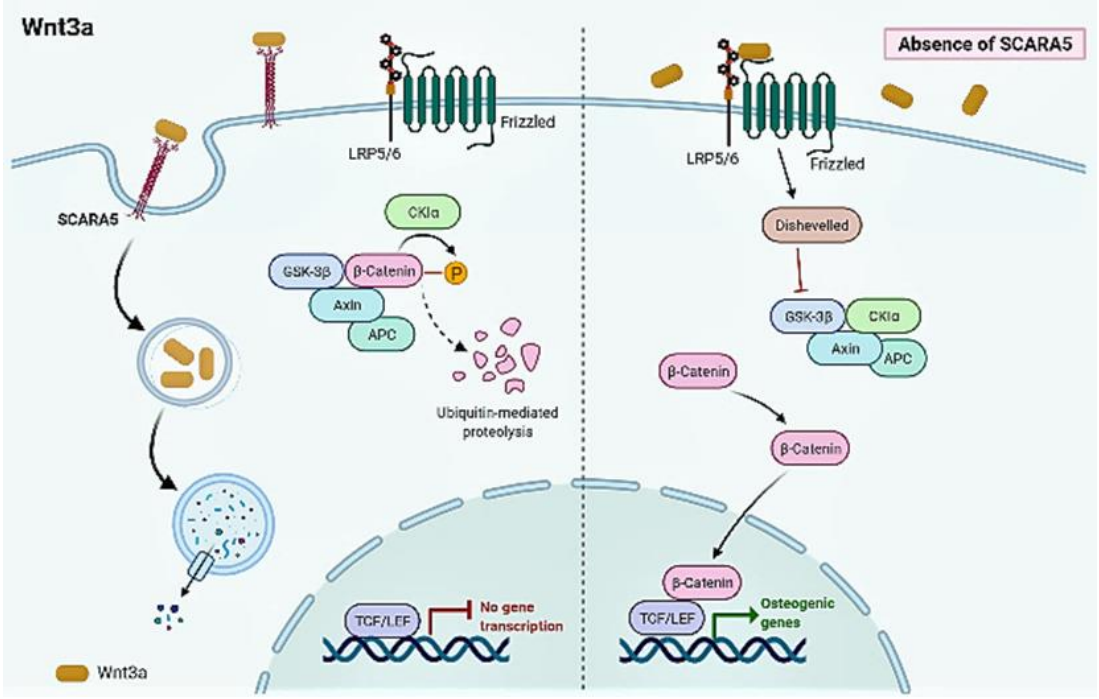

Figure 4.10 Schematic of the study hypothesis of WNT3a and its known effects on osteogenesis. Potential interaction of SCARA5 with WNT3a. Working hypothesis is that the presence of SCARA5 can compete with WNT receptors and endocytose WNT3a, whereas the absence of SCARA5 allows higher WNT signal activity.

Recombinant hSCARA5 recognised WNT3a *in vitro*, as shown by OD 450nm absorbance correlating with increasing WNT3a concentration (Figure 4.11 A). WNT3a treated *Scara5*$^{-/-}$ BMSCs in osteogenic medium showed a moderate, statistically insignificant increase in ALP activity (1.406 ± 0.176 mmol/L and 1.523 ± 0.136 mmol/L at 10 and 100 ng/mL WNT3a respectively in comparison to *Scara5*$^{-/-}$ osteogenic control BMSCs of 1.098 ± 0.125 mmol/L) (Figure 4.11 B). There was no significant change in ALP for WT BMSCs under

osteogenic conditions treated with WNT3a at all concentrations tested. Under different cell culture condition, where WT and *Scara5*$^{-/-}$ BMSCs were treated with WNT3a in control medium, a significant increase in ALP activity was found in *Scara5*$^{-/-}$ BMSCs treated at 100 ng/mL WNT3a, with ALP level of 0.873 ± 0.138 mmol/L related to no treatment *Scara5*$^{-/-}$ control which was at an average of 0.397 ± 0.048 mmol/L ALP level (Figure 4.11 C). Meanwhile, WT BMSCs exhibited no significant difference in ALP activity between WNT3a treated and non-treated WT BMSCs at the concentrations investigated (Figure 4.11 C).

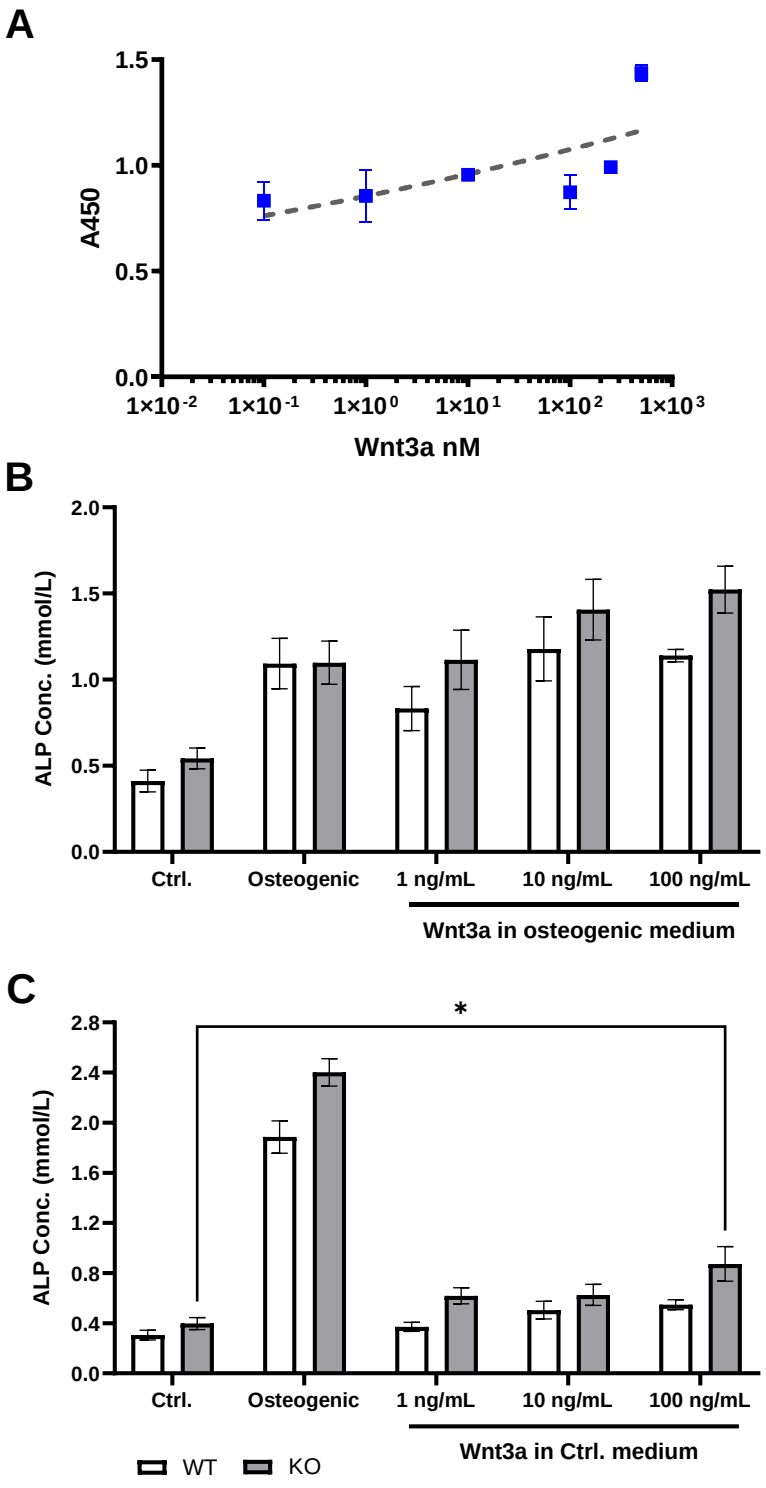

Figure 4.11 WNT3a can bind to SCARA5 and support osteogenic differentiation in absence of the receptor. (A) Relative binding activity between WNT3a and recombinant SCARA5 measured by ELISA (n ≥ 3 duplicate experiments). (B) ALP levels at day 3 of WT and *Scara5*$^{-/-}$ BMSCs treated with 1, 10, 100 ng/mL WNT3a in osteogenic medium (n = 3 biological replicates of duplicate experiments). (C) ALP concentration at day 3 of WT and

Scara5$^{-/-}$ BMSCs treated with 1, 10, 100 ng/mL WNT3a in control medium (n = 6 biological replicates of duplicate experiments). Error bars represent mean ± SEM. *p < 0.05 by two-way ANOVA multiple comparison Sidak's test.

4.3 Discussion

The activities of SCARA5 have been investigated to a much lesser extent than those of the other class A scavenger receptors SCARA1 and SCARA2. In particular, the potential involvement of SCARA5's ligands in osteogenesis and other skeletal-related mechanisms have not been reported. This chapter aimed to explore this subject and to identify ligands for the receptor that may mediate such processes.

Li and colleagues identified ferritin as a ligand for SCARA5 in the context of a non-transferrin receptor-mediated iron delivery pathway [241]. The interaction between SCARA5 and ferritin, especially L-ferritin, was demonstrated by the internalization of ferritin by Trvb cells that had been transiently transfected with SCARA5, in addition to the colocalization of SCARA5 with ferritin on the surface of MSC-1 cells [241]. In a subsequent study Mendes-Jorge *et al.* found SCARA5 was expressed by retinal endothelial cells and could transport L-ferritin across the blood-retinal barrier in mice [235]. In this chapter, native ferritin (containing both heavy and light chain ferritin)

significantly suppressed ALP levels of *Scara5*$^{-/-}$ BMSCs, but had no effect on WT BMSCs, indicating that SCARA5 may mediates significant uptake of ferritin by BMSCs. The effect of iron and ferritin on bone has been reported previously [258, 275]; excess iron inhibited MSC osteogenic differentiation and mineralization through induction of ferritin induction and that the same effects were seen with exogenous ferritin [258]. However, in their study, very high doses of ferritin (≥ 1 mg/mL) were used. In this chapter, much lower concentrations of ferritin were sufficient enough to suppress ALP expression of *Scara5*$^{-/-}$ BMSCs under osteogenic conditions, but no significant effect was observed on WT BMSCs at the same concentrations. Thus, the presence of SCARA5 possibly helps sequester ferritin allowing the cells to withstand higher levels of ferritin.

HMGB1 was investigated for possible interactions with SCARA5 and its potential contribution to bone phenotype at the absence of SCARA5. Lee *et al.* demonstrated that HMGB1, specifically FR-HMGB1, pre-treatment or administered at the time of injury improved bone fracture healing and tissue regeneration via CXCR4 signalling [263]. In addition, Gao and colleagues showed a direct interaction between HMGB1 and SCARA5 in a fish model of induced inflammation response [259]. Internalization and clearance of HMGB1

by SCARA5 reduced inflammatory reactions triggered by CpG-oligodeoxynucleotides [259]. These studies suggested that HMGB1 and SCARA5 interaction played a role in inflammatory response and HMGB1 may be involved in osteogenic bone formation.

In this chapter, it was shown that SCARA5 was able to bind to both FR- and DS-HMGB1 and that HMGB1 negatively regulated ALP activity under osteogenic conditions at the absence of SCARA5 (Figure 4.5 and 4.6). Meanwhile, transient (pre-treatment only) and continuous treatment with HMGB1 induced differential responses in WT BMSCs, where constant HMGB1 treatment suppressed whereas HMGB1 pre-treatment had no effect on ALP levels. It will be interesting in future studies to evaluate if continuous and pre-treatments influence osteogenic gene expression (e.g., *Runx2, Sp7, Bsp, Ocn*) and mineral nodule formation.

Previously, studies have reported HMGB1 as an active cytokine triggering bone resorption signal within the bone marrow [264, 265]. Such responses found on BMSCs under continuous HMGB1 treatment may resemblance inflammation that triggered bone resorption and bone loss [260, 276]. Unfortunately, investigations to the osteogenic outcomes of BMSCs under inflammatory challenge at the presence and absence of SCARA5 were beyond

the scope of this thesis. Nonetheless, further studies investigating cytokine expression, such as TNFα, IL-1 and IL-6, under prolonged HMGB1 exposure during osteogenic differentiation will be insightful to understand the effect of HMGB1 on osteogenesis in the presence and absence of SCARA5.

The WNT signalling pathway is one of the key and best-understood regulatory pathways with respect to bone development, regeneration and homeostasis [14, 268, 277]. Canonical WNT pathway has been shown to enhance osteoblast differentiation and proliferation, promote maturation and mineralization, and prevent apoptosis, whilst the same pathway has been found to exert inhibition on osteoclast differentiation [278-280]. Nevertheless, there have been no published reports into associations between WNT and SCARA5. This chapter made an initial investigation into whether the responses of BMSCs to key canonical WNT inhibitors (DKK1, sFRP1, and SOST) and WNT3a change during osteogenic differentiation in the presence and absence of SCARA5.

DKK1 and SOST can act as potent inhibitors of canonical WNT signalling by binding to LRP5 and LRP6 WNT co-receptors and preventing WNT proteins interaction and signal transmission [281, 282]. SOST interacts with the first two β-propeller/EGF-like domain repeats of the four β-

propeller/EGF-like domain repeats on LRP6 [283, 284]. Meanwhile, it was revealed that DKK1 can bind to two separate sections of the four β-propeller/EGF-like domain repeats on LRP6, including the first two repeats and the remaining two repeats, and thereby inhibit different WNTs through binding at different locations [283, 285, 286]. Since canonical WNT signal activation is critical during osteogenic differentiation of BMSCs, inhibition by DKK1 and SOST can considerably diminish osteogenesis and disrupt bone growth [287, 288]. Human bone pathologies such as low bone mass (osteopenia and osteoporosis pseudoglioma syndrome), high bone mass, sclerosteosis, and van Buchem's disease are associated with aberrant WNT signalling that links to altered DKK1 or SOST inhibition [289-292].

In light of the elevated bone volume and enhanced osteogenic differentiation of BMSCs in *Scara5*$^{-/-}$ animals, the interaction with SCARA5 and effects of DKK1 and SOST on osteogenesis were investigated at the presence and absence of SCARA5 in this project. It was found that both DKK1 and SOST were able to be recognized and captured by SCARA5 (Figure 4.9 A and E), although only DKK1 significantly suppressed the ALP level of *Scara5*$^{-/-}$ BMSCs at day three of the assay compared to WT BMSCs which showed a modest decrease in ALP expression at DKK1 100 ng/mL (Figure 4.9 B and F). It will

require further investigations into structural interaction of DKK1 and SOST with SCARA5 and the mechanisms as to how DKK1 and SOST mediate osteogenic differentiation differently in the absence of SCARA5. Additional analyses of osteogenic marker genes (e.g., *Runx2, Osx, Col1, Ocn*) and mineral nodule formation in further experiments will provide understanding of the mechanistic effect of DKK1 and SOST on osteogenesis in *Scara5*$^{-/-}$ BMSC.

Secreted FRPs (sFRP) are a group of WNT signalling modulators that can act by binding to both soluble WNT proteins and cell membrane Frizzled receptors, thus modulating WNT signalling cascades [293, 294]. It has been established that sFRPs are not simply just antagonists, but that they can inhibit or activate WNT pathways depending on the cellular context and concentration [294, 295]. For example, at 1 to 10 nM concentrations in combination with WNT3a, sFRP1 enhanced WNT/β-catenin signalling in HEK293 cells, whilst sFRP1 at higher concentrations inhibited the WNT3a signalling activity. In contrast, sFRP1 exerted antagonizing function in L929 fibroblasts at corresponding concentrations [294]. Studies have indicated that sFRP1 was associated with osteogenesis, bone mass, and bone formation [296-298]. Bodine *et al.* showed that *sFRP1* ablation in mice resulted in increased trabecular bone volume, mineral density and apposition rate compared to

control mice [297]. In addition, heightened trabecular bone mass of *sFRP1*$^{-/-}$ mice was observed in multiple skeletal sites of adult animals of both sexes between 13 - 52 weeks of age [297]. Another study also reported that glucocorticoid treatment augmented sFRP1 expression, which was associated with inhibited osteogenic activities, reduced trabecular bone density, bone volume, midshaft cortical bone areas, and biomechanical properties in rat femurs [298]. As a negative modulator in bone, overexpressing sFRP1 resulted in a decrease in bone mass of distal femurs and lumbar vertebrae at 3-month-old *sFRP1* transgenic mice [299].

Due to sFRP1's ability to bind WNT ligands and Frizzled receptors and its differences from DKK1 and SOST, the present chapter also investigated the association between SCARA5 and sFRP1. SCARA5 was able to capture sFRP1 as demonstrated by ELISA with corresponding increase of sFRP1 concentrations (Figure 4.9 C). Meanwhile similar to DKK1, sFRP1 significantly inhibited the ALP activity of *Scara5*$^{-/-}$ BMSCs at day three of osteogenic induction compared to WT BMSCs that showed a moderate decrease in ALP level at sFRP1 100 ng/mL (Figure 4.9 D). Although sFRP1 appears to exert a similar inhibitory function as the DKK1 results in *Scara5*$^{-/-}$ BMSCs during osteogenic induction, the mechanism will require elucidation by further studies.

Additionally, it will be interesting to compare the long term osteogenic inhibitory effect of DKK1, SOST and sFRP1 in *Scara5*$^{-/-}$ BMSCs regarding changes in osteogenic gene expression, mineral nodule deposition, and WNT signalling molecules (e.g. Axin2, GSK3, and β-catenin).

To gain a better insight into whether the presence and absence of SCARA5 impact WNT signalling, WNT3a was investigated. Previous studies have shown that WNT1, WNT3a and WNT10b preferentially activate canonical WNT signalling pathway and promote bone formation [277, 300-303]. By activating WNT/β-catenin canonical pathway, WNT3a enhanced osteogenic differentiation and significantly upregulated the expression of *Runx2*, *Osterix* and *Osteocalcin* in BMSCs [304]. Additionally, local WNT3a administration restored bone formation via canonical WNT pathway activation for defects due to post-traumatic osteomyelitis [184]. Given the role of WNT3a in WNT signalling, it was speculated that WNT3a may have an effect on osteogenic differentiation of BMSCs in the absence of SCARA5.

Here we showed that WNT3a treatment of *Scara5*$^{-/-}$ BMSCs in osteogenic medium seemed to promote ALP activity during osteogenic differentiation yet no statistically significance was found (Figure 4.11 B). On the other hand, treating WNT3a in control cell culture medium significantly

increased the ALP level of *Scara5*$^{-/-}$ BMSCs at 100ng/mL of WNT3a on day 3, whereas there was no significance in WT BMSCs at all concentrations investigated (Figure 4.11 C). These results suggest that WNT3a could affect BMSC osteogenesis and WNT signalling sensitivity might be altered under SCARA5 depletion. Thus, further investigations for a longer time frame during osteogenic differentiation will allow better understandings of the impact of SCARA5 deficiency on WNT3a and WNT signal activation.

Overall, the investigations in this chapter have found that SCARA5 is able to recognise ferritin, HMGB1, WNT3a, and WNT inhibitors (DKK1, sFRP1, and SOST). In general, the proteins investigated, except WNT3a, played a negative role which suppressed ALP activity level during osteogenic differentiation of *Scara5*$^{-/-}$ BMSCs. Further studies are required to understand the molecular interactions of SCARA5 with these proteins as well as the mechanisms involved in osteogenesis at the absence of SCARA5.

Chapter 5. SCARA5 deficiency reduces bone marrow adipocytes and body fat accumulation

5.1 Introduction

There is a plasticity in the development of osteoblasts and adipocytes from MSC whereby fat-inducting factors inhibit osteogenesis whilst bone-inducing factors hinder adipogenesis [148] This is supported by robust evidence from clinical and scientific studies showing that the inverse relationship between bone mass and marrow adiposity is contributed, in part, to the unbalanced distribution and/or differentiation of osteoblast and adipocyte lineages of BMSCs [106, 201].

Lee *et al.* demonstrated that the loss of function of SCARA5 greatly inhibited adipogenic differentiation in preadipocyte and MSC-like cell lines, however the involvement of SCARA5 in adipocyte development *in vivo* is unknown [217]. Recently SCARA3 has been described as a determinant of BMSC fate that favours osteoblast differentiation. The authors demonstrated *in vitro* that siRNA to *Scara3* inhibited osteoblasts and promoted adipogenesis. Conversely, overexpression of SCARA3 promoted osteogenesis and reduced adipocytes. *In vivo*, the intra-bone marrow injection of an adeno-associated virus overexpressing SCARA3 promoted bone formation in aged mice and

reduced bone loss in ovariectomy-induced osteoporosis [219]. In another study by Lin *et al.*, the authors attributed the increased bone volume in *SR-A*$^{-/-}$ mice to the decrease in OC function and number yet there was no difference in both osteoblast and adipocyte number between control and *SR-A*$^{-/-}$ mice [216]. SCARA5 and SCARA3 are known to be expressed in a wide range of tissues, unlike SR-A which is restricted to haematopoietic cells such as monocytes and macrophages [217, 233].

The effects of SCARA5 on bone marrow adipocyte formation have not been described *in vivo*. Since Lee and colleagues showed that SCARA5 plays a significant role in adipocyte commitment of preadipocytes and MSC-like cells in vitro [217], and given that the increased bone mass observed in *Scara5*$^{-/-}$ mice (Chapter 3), it was postulated that the absence of SCARA5 would reduce bone marrow adipose tissue (BMAT) due to a cell fate shift between osteoblasts and adipocytes during BMSC differentiation (Figure 5.1). This chapter characterizes further alterations in the bone marrow composition, including BMAT and a change in bone marrow vascularity in the presence and absence of SCARA5.

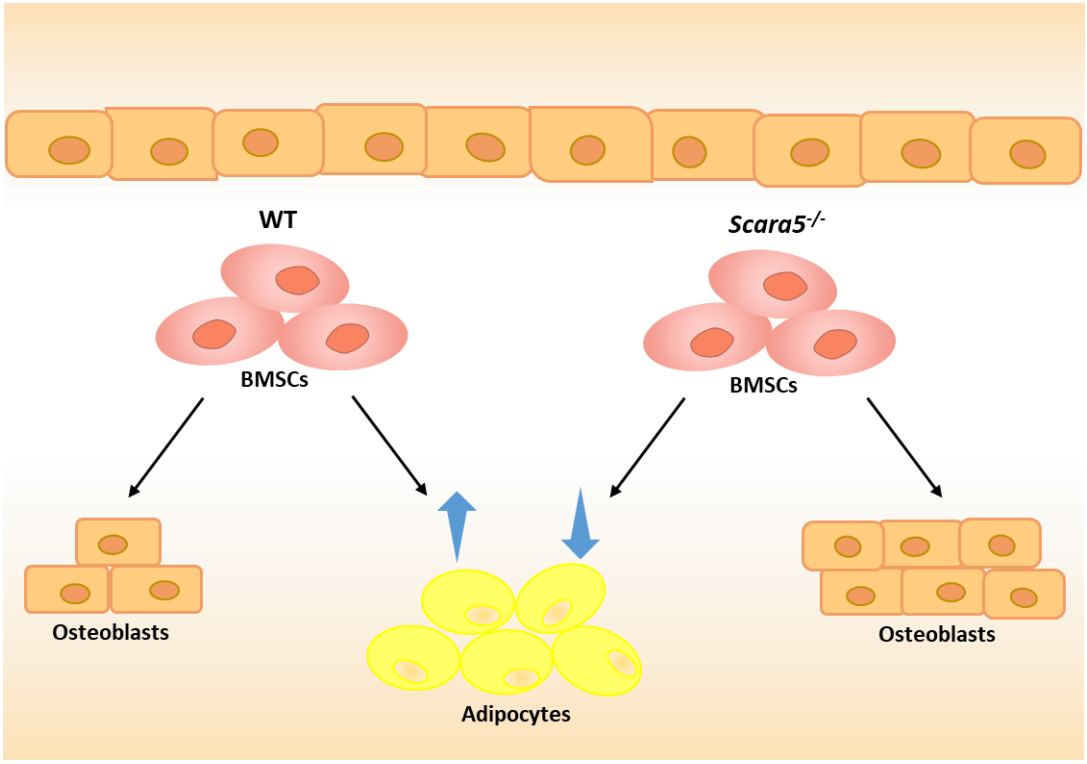

Figure 5.1 Potential role of SCARA5 in adipocyte development. In Chapter 3 it was demonstrated that osteoblast differentiation was less abundant in WT BMSCs than *Scara5*$^{-/-}$ BMSCs. Given the plasticity between osteoblasts and adipocytes, it is hypothesized that there will be less adipocyte development in the absence of SCARA5.

5.2 Results

5.2.1 SCARA5 expression supports body fat accumulation in mice

The global gene ablation of *Scara5* allowed for the interrogation of the effect of SCARA5 on body fat. 11-week WT mice stored significantly more inguinal fat than *Scara5*$^{-/-}$ animals, such that the average inguinal fat of WT males was >1.5 times heavier (0.356 ± 0.028 g) than *Scara5*$^{-/-}$ males (0.23 ±

0.012 g) and that of WT females was >2 times heavier (0.521 ± 0.01 g) than *Scara5*$^{-/-}$ females (0.242 ± 0.011 g) (Figure 5.2A). Correspondingly, the average percent of inguinal fat as a function of total body weight in WT males was ~1.5 times heavier (1.172 ± 0.092 g) than *Scara5*$^{-/-}$ males (0.755 ± 0.08 g) and that of WT females was ~2 times heavier (2.245 ± 0.086 g) than *Scara5*$^{-/-}$ females (1.161 ± 0.073 g) (Figure 5.2 B). The size of inguinal fat pads was larger in WT control animals compared to that of the *Scara5*$^{-/-}$ ones as shown in the representative photo (Figure 5.2 D).

It was also interesting to find that the control mice accumulated a considerable amount of inguinal fat weight during aging in both males (1.039 ± 0.234 g) and female s (1.372 ± 0.131 g) (Figure 5.2 C). Conversely, in comparison to WT mice, the inguinal fat volume remained consistently low in both male (0.182 ± 0.023 g) and female (0.153 ± 0.008 g) *Scara5*$^{-/-}$ animals (Figure 5.2 C). Respectively, it was clear from the representative photo that the size of inguinal fat pads was much larger in control animals compared to that of the *Scara5*$^{-/-}$ ones as shown in Figure 5.2 D.

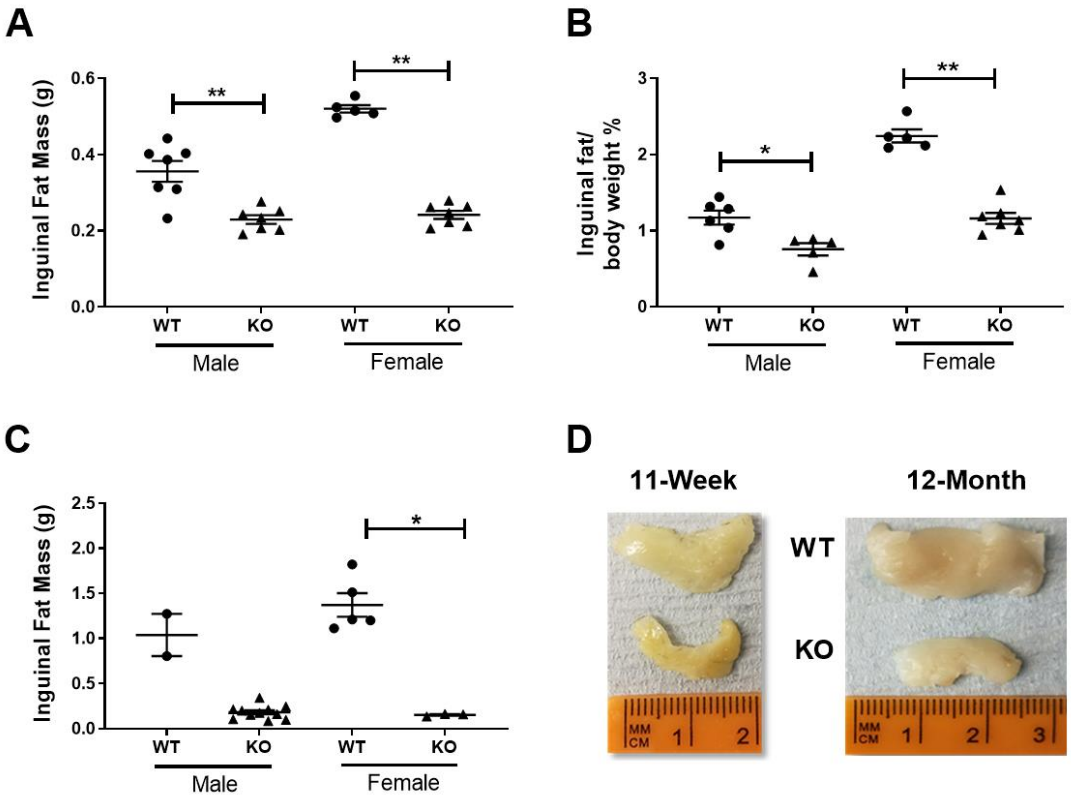

Figure 5.2 SCARA5 deficiency reduces inguinal fat accumulation. (A) Inguinal fat weight of 11-week WT (male, n=6; female, n=5 biological replicates) and *Scara5*$^{-/-}$ (male, n=5; female, n=7 biological replicates) mice. (B) The percentage of inguinal fat/body weight of 11-week WT (male, n=6; female, n=5 biological replicates) and *Scara5*$^{-/-}$ (male, n=5; female, n=7 biological replicates) animals. (C) Inguinal fat mass of 12-month-old WT (male, n=2; female, n=5 biological replicates) and *Scara5*$^{-/-}$ mice (male, n=11; female, n=3 biological replicates). (D) Representative photos of the inguinal fat pads from WT and *Scara5*$^{-/-}$ mice at 11-week and 12-month of age. Data show as mean ± SEM. *p < 0.05; **p < 0.01 by Student's t-test.

5.2.2 SCARA5 deficiency in inguinal fat development

The inguinal fat pads from both WT and *Scara5*$^{-/-}$ animals were examined further using tissue staining and histology (Figure 5.3 A). It was shown that there was no statistical significance between WT and *Scara5*$^{-/-}$ mice of both sexes in adipocyte count and adipocyte diameter at 11 weeks of age (Figure 5.3 B-C). Nevertheless, there were somewhat noticeable differences between WT and *Scara5*$^{-/-}$ mice, where the adipocyte number and diameter in the WT animals for both sexes appeared to be higher in the absence of statistical significance. The average number of adipocytes of WT males (129.8 ± 7.49) was marginally higher than *Scara5*$^{-/-}$ males (117.8 ± 10.77); likewise, WT females (85.5 ± 8.67) had slightly more adipocytes compare to *Scara5*$^{-/-}$ females (67.22 ± 16.06) (Figure 5.3 B). In terms of adipocyte diameter, both WT and *Scara5*$^{-/-}$ female mice exhibited an average of wider adipocyte diameter relative to that of the male mice at 11 weeks old (Figure 5.3 C). Similarly, both WT males (28.91 ± 0.75 μm) and females (35.07 ± 1.39 μm) presented an average of slightly bigger inguinal adipocytes (diameter) than those in *Scara5*$^{-/-}$ males (22.01 ± 1.16 μm) and females (26.29 ± 1.03 μm) (Figure 5.3 C).

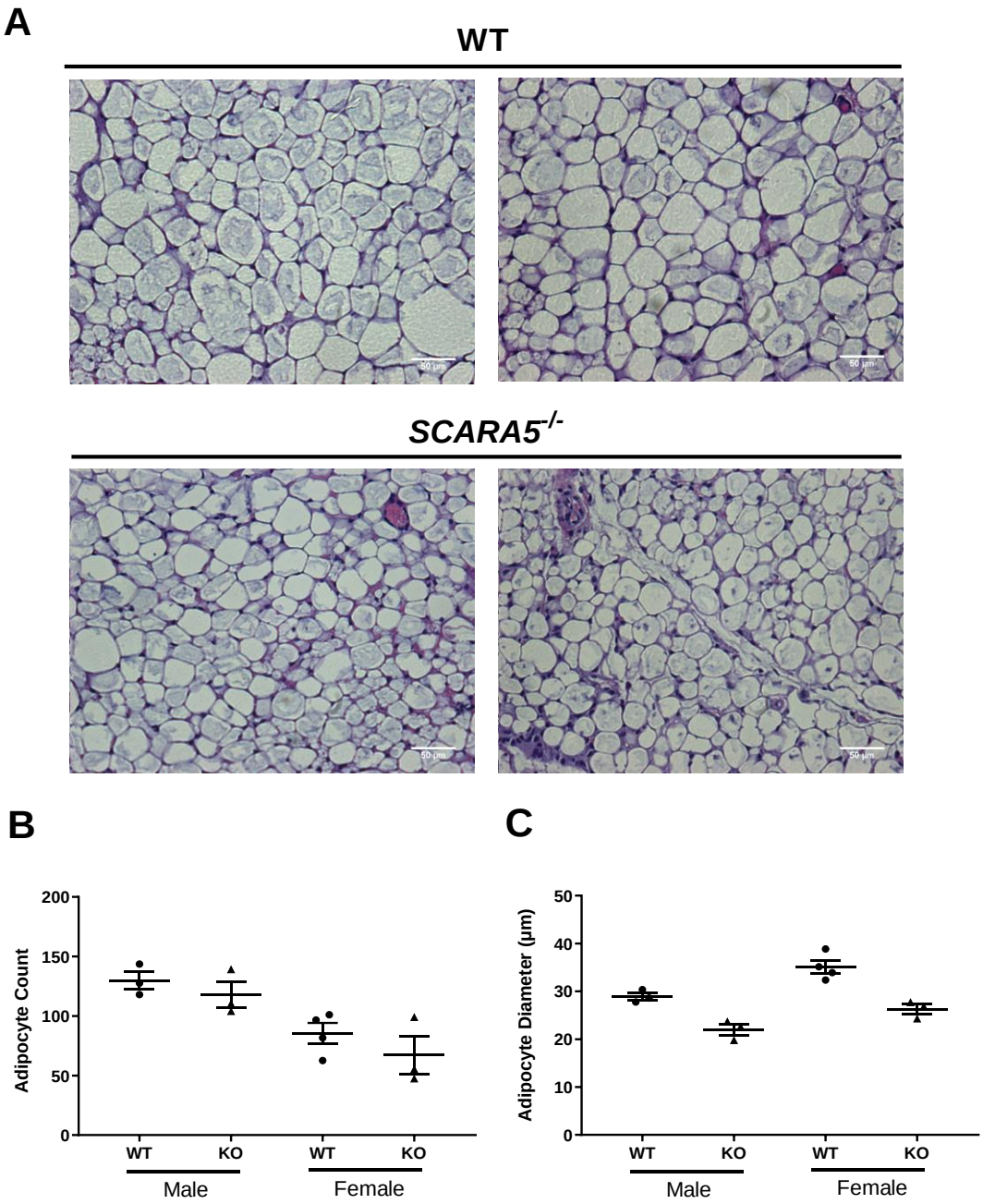

Figure 5.3 The absence of SCARA5 in inguinal adipocyte development in mice. (A) Representative H&E staining images of inguinal fat tissue sections of WT and *Scara5*$^{-/-}$ mice at 11-weeks old. Scale bar is 50 μm. (B) The average number of adipocytes of WT and *Scara5*$^{-/-}$ mice at 11 weeks of age (WT males, n=3; WT females, n=4; *Scara5*$^{-/-}$ males, n=3; *Scara5*$^{-/-}$ females, n=3 biological replicates of three slides) (C) The average diameter of adipocytes of WT and *Scara5*$^{-/-}$ mice at 11 weeks old (WT males, n=3; WT females, n=4; *Scara5*$^{-/-}$ males, n=3; *Scara5*$^{-/-}$ females, n=3 biological replicates of three slides). Data show as mean ± SEM. No significance was found by Student's t-test.

5.2.3 *Scara5* expression supports bone marrow adipocyte accruement

BMAT within the yellow marrow of the distal tibia and caudal vertebra is called constitutive BMAT (cBMAT). These adipocytes develop soon after birth and are observed by one week of age in rodents. Development of regulated BMAT (rBMAT) occurs later than cBMAT and is located in the red marrow of the tibia proximal to the fibula junction, in the femur and in the axial skeleton [58].

The loss of SCARA5 significantly diminished the total amount of BMAT in *Scara5*$^{-/-}$ mice compared to WT littermates at 11 weeks old (Figure 5.4A). MicroCT 3D-reconstructed images showed a notable accumulation of rBMAT cluster(s) near WT tibial growth plate, whereas rBMAT in the *Scara5*$^{-/-}$ tibia was not discernible. On the other hand, cBMAT near the distal tibia in both WT control and *Scara5*$^{-/-}$ animals was clearly identified in the 3D-reconstructed images (Figure 5.4A). Quantification of the microCT data showed that total BMAT (cBMAT + rBMAT) volume as a function of total bone volume (BMAT/BV) of WT mice was significantly greater than that of *Scara5*$^{-/-}$ animals (WT male = 6.89 ± 0.45%; WT female = 13.74 ± 1.15%; *Scara5*$^{-/-}$ male = 5.19 ± 0.18%; *Scara5*$^{-/-}$ female = 9.68 ± 0.45%) (Figure 5.2B). Separately, the amount of rBMAT, located below the growth plate to the juncture with the distal fibula, was

significantly lower in *Scara5*$^{-/-}$ mice (male, 0.07 ± 0.03% and female, 1.35 ± 0.12%) than in the WT animals (male, 1.01 ± 0.27% and female, 3.59 ± 0.73%) (Figure 5.4C). Similarly, there was a significantly higher percentage of cBMAT in WT mice than in *Scara5*$^{-/-}$ animals, with WT and *Scara5*$^{-/-}$ males at 5.88 ± 0.35% and 5.12 ± 0.17%; and WT and *Scara5*$^{-/-}$ females at 10.15 ± 0.46% and 8.33 ± 0.48%, respectively (Figure 5.4D).

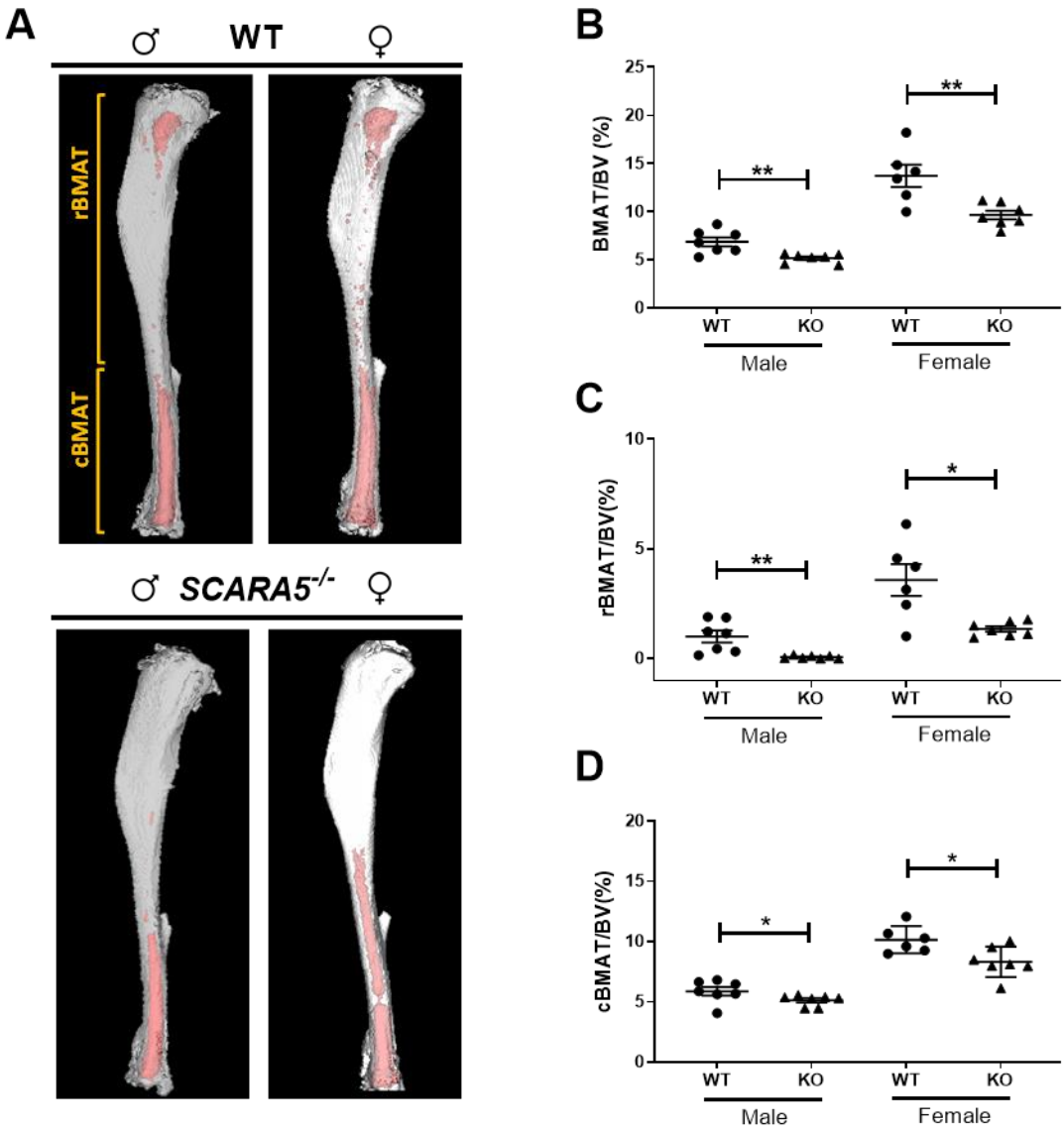

Figure 5.4 *Scara5*-deficient mice exhibit decreased marrow adiposity. (A) Representative microCT reconstructed images showing rBMAT (in yellow bracket) near the proximal tibia and cBMAT around the distal tibia marked in red, of 11-week WT and *Scara5*$^{-/-}$ mice. (B-D) Quantitative measurements of total BMAT/BV (bone marrow adipocyte tissue volume/total bone volume) ratios (B); rBMAT/BV volume (C) and cBMAT/BV (D) of 11-week WT (males, n=7; females, n=6 biological replicates) and *Scara5*$^{-/-}$ tibias (males, n=7; females, n=7 biological replicates). Error bars represent mean ± SEM. *$p < 0.05$; **$p < 0.01$ by Student's t-test.

In one year old mice, histological analysis by H&E staining followed by identification of adipocyte 'ghosts' showed that the WT adipocyte cell count (40.33 ± 11.55) and adipocyte perimeter (4.92 ± 1.45 mm) were higher than the adipocyte count (7.44 ± 2.60) and adipocyte perimeter (0.63 ± 0.21 mm) of *Scara5*$^{-/-}$ ones (Figure 5.5 A-B). The representative images of both WT and *Scara5*$^{-/-}$ tibia sections with H&E stain were shown in Figure 5.5 C. Due to a low number of WT male mice in the sample it was not possible to perform statistics on the male mice.

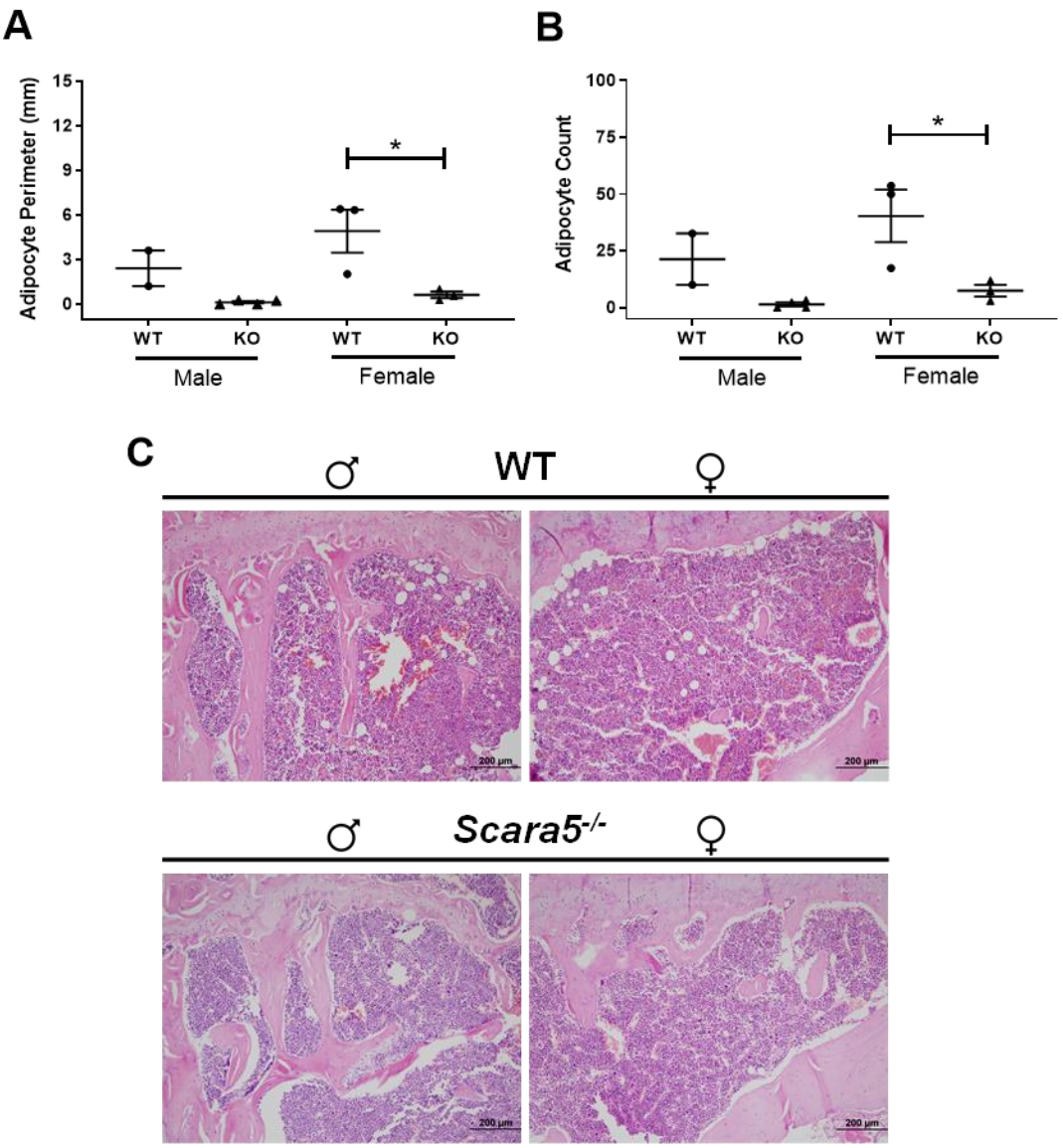

Figure 5.5 *Scara5* expression supports marrow adipocyte deposition in aged mice. (A-B) Quantitative analysis of adipocytes perimeter (A) and adipocyte counts (B) of WT (males, n = 2; females, n = 3 biological replicates) and *Scara5*$^{-/-}$ (males, n = 4; females, n = 3 biological replicates) tibia at 1-year of age. (C) Representative micrographs of H&E stained bone sections of WT and *Scara5*$^{-/-}$ tibia at 1-year of age. Scale bars represent 200 mm. Data is expressed as mean ± SEM. *p < 0.05 by Student's t-test.

5.2.4 The loss of SCARA5 suppresses adipocyte differentiation of BMSCs

Following the stark differences observed between the BMAT of control and *Scara5*$^{-/-}$ mice, the adipocyte differentiation capacity of WT control and *Scara5*$^{-/-}$ BMSCs was investigated. It was found that *Scara5*$^{-/-}$ BMSCs differentiated into significantly less adipocytes with noticeable decrease in lipid droplet formation when compared to WT BMSCs, as shown by an increase in lipid droplets staining by Oil red O (ORO) (Figure 5.6 A). The relative concentration of ORO in adipogenic cell eluate of WT BMSCs (4.12 ± 0.59) was ~2 times higher than the concentration of adipogenic cell eluate of *Scara5*$^{-/-}$ BMSCs (Figure 5.6 B).

One factor that could contribute to the differences between the adipogenic differentiation capacity of WT and *Scara5*$^{-/-}$ BMSCs would be an alteration to adipogenic progenitor cells (APC). On this note, BMSCs as well as the adipogenic progenitor populations were investigated further. The cell surface markers $CD45^{-}$ $CD31^{-}$ $Sca1^{+}$ $CD24^{+}$ distinguished multipotent BMSCs and $CD45^{-}$ $CD31^{-}$ $Sca1^{+}$ $CD24^{-}$ to distinguish adipogenic lineage progenitors [64]. FACS analyses showed that there was no statistically significant difference between the frequency of BMSCs and APCs in WT and *Scara5*$^{-/-}$ mice (Figure 5.6 C-D). The percentage of BMSC population in WT (male, 0.072 ± 0.018%;

female, 0.081 ± 0.011%) was comparable to *Scara5*$^{-/-}$ mice (male, 0.058 ± 0.003%; female, 0.066 ± 0.004%). Correspondingly, the frequency of *Scara5*$^{-/-}$ APCs (male, 0.046 ± 0.008%; female, 0.034 ± 0.003%) was moderately higher but not statistically significant than WT APCs (male, 0.025 ± 0.006%; female, 0.023 ± 0.006%) (Figure 5.6 D).

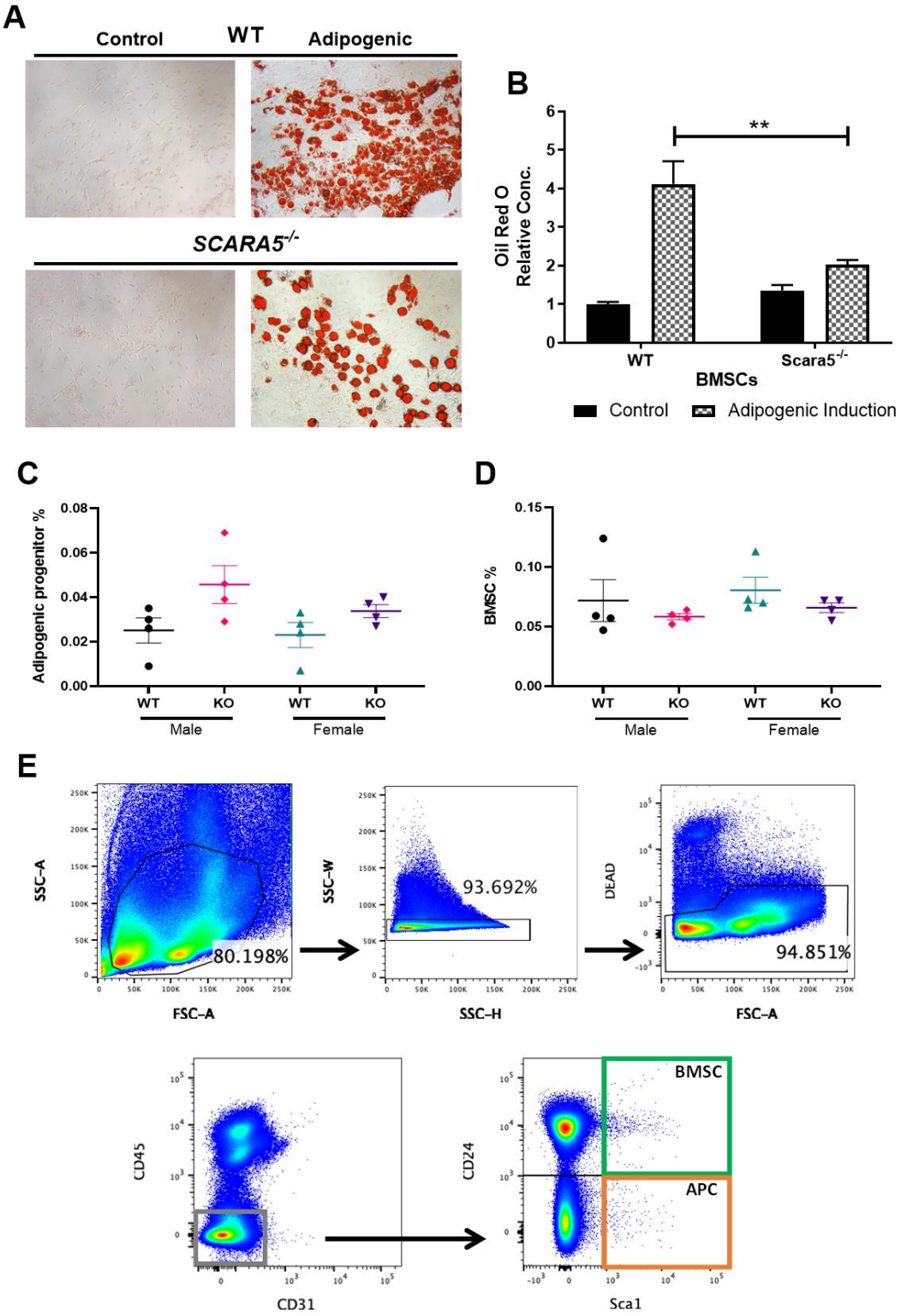

Figure 5.6 SCARA5 deficiency in BMSCs attenuated adipogenic differentiation activity whilst maintaining the adipocyte progenitor level in the bone marrow. (A) Representative micrographs of Oil Red O staining of WT and *Scara5*$^{-/-}$ BMSCs under control and adipogenic differentiation culture conditions. (B) Semi-quantification measurements of cell eluates from ORO-

stained WT and *Scara5*$^{-/-}$ (n = 6 biological replicates) under control and adipogenic cell cultures. Data were normalized to the WT control sample values. (C-D) The percentage of APCs and BMSCs from 11-week-old WT and *Scara5*$^{-/-}$ long bones (n = 4 biological replicates). (E) Gating strategy of FACS analysis for BMSC and adipogenic progenitor cells (APC) populations. Lower panel: grey box is $CD45^{-}$ $CD31^{-}$ cells; green box is BMSC population $CD45^{-}$ $CD31^{-}$ $Sca1^{+}$ $CD24^{+}$; orange box is APC population $CD45^{-}$ $CD31^{-}$ $CD24^{-}$ $Sca1^{+}$. Error bars represent mean ± SEM. **p < 0.01 by Student's t-test.

5.2.5 The absence of SCARA5 promotes bone marrow vascularity

Whilst examining the osteoclasts in tibia sections, it was noted that blood vessels appeared to be more prevalent in *Scara5*$^{-/-}$ bone sections than the WT control ones. As shown in Figure 5.7 A, representative images demonstrated that adipocyte 'ghosts' (marked with blue letter A) were widespread in WT tibia section (left) compared to *Scara5*$^{-/-}$ bone section (right). In contrast, blood vessels (marked with red letter V) were predominant in *Scara5*$^{-/-}$ tibia compared to the WT bone section (Figure 5.7 A). The magnified insets of Figure 5.7 A provided a closer look at the adipocyte and blood vessel distinctions that were separately identified in the images. The number of blood vessels and adipocyte ghosts in the representative images were individually counted and analysed. Indeed, the average number of blood vessels in *Scara5*$^{-/-}$ tibia (male = 60 ± 6.658; female = 49.67 ± 1.856) was significantly higher than

those in WT control tibia (male = 36.33 ± 1.856; female = 26 ± 2.887) (Figure 5.7B). On the other hand, and in agreement with the microCT data, the average number of adipocyte ghosts in WT control tibia (male = 27.67 ± 5.044; female = 39.67 ± 28.88) were significantly higher than those in *Scara5*$^{-/-}$ tibia (male = 1 ± 0.577; female = 3.667 ± 1.453) (Figure 5.7 C).

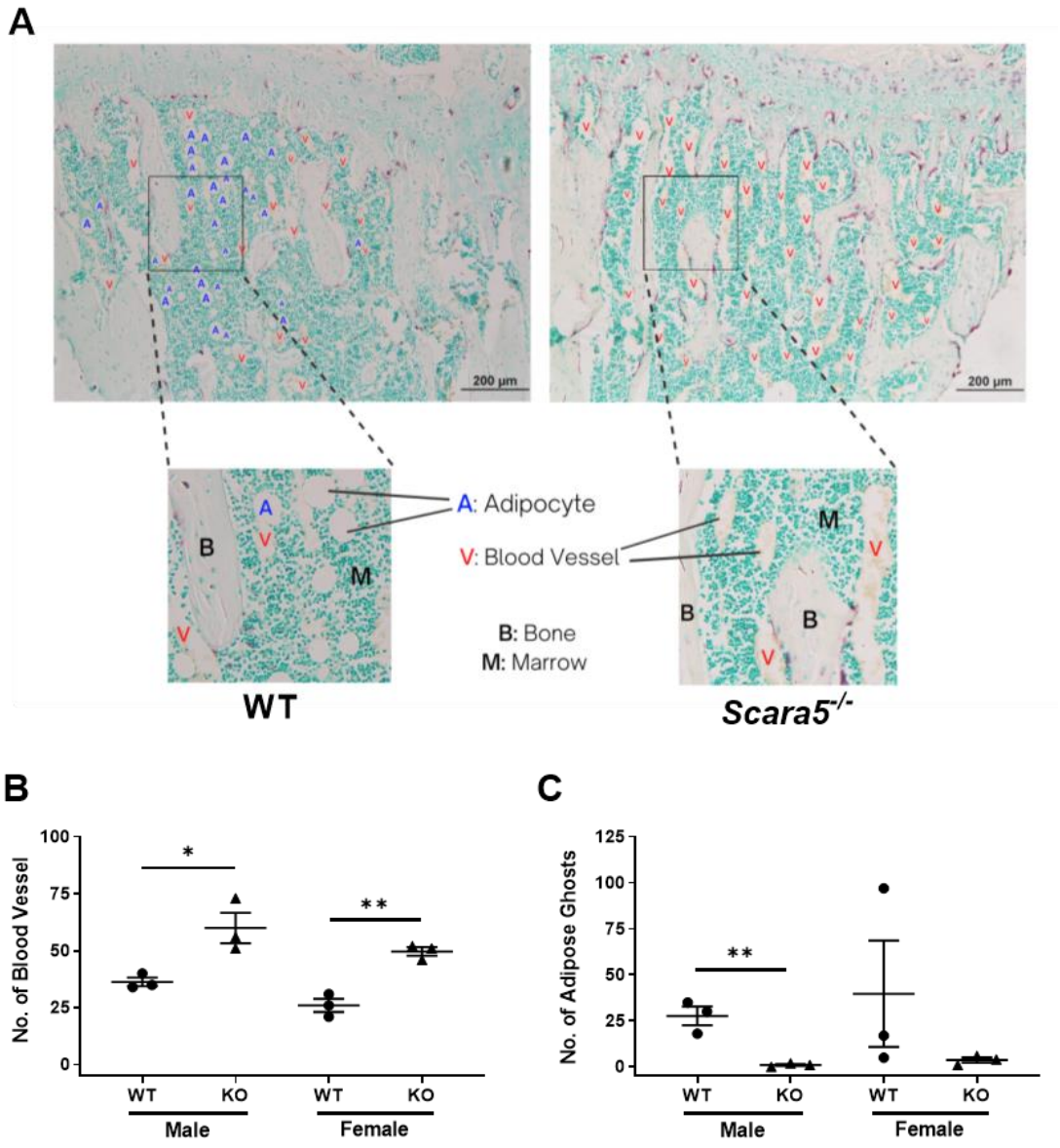

Figure 5.7 The absence of SCARA5 promotes bone marrow vascular development in mice. (A) Representative images and inset images of TRAP

stained 11-week-old WT and *Scara5*$^{-/-}$ tibia. A: adipocyte; V: blood vessel; B: bone; M: Marrow. (B) The number of blood vessel counts in TRAP stained 11-week-old WT and *Scara5*$^{-/-}$ tibia (n=3 biological replicates). (C) The number of adipocyte ghosts counted in TRAP stained 11-week-old WT and *Scara5*$^{-/-}$ tibia (n=3 biological replicates). Error bars represent mean ± SEM. *p < 0.05 and **p < 0.01 by Student's t-test.

5.3 Discussion

In this investigation, *Scara5*$^{-/-}$ mice were lighter and considerably leaner than WT control mice when comparing the percentage of inguinal fat mass at 11 weeks old (Figure 5.2 A). A previous study of class A scavenger receptor deletion (*SR-A*$^{-/-}$) in 129/SvJ mice by Lin *et al.* showed that *SR-A*$^{-/-}$ mice exhibited significantly higher bone volume, trabecular number, thickness, and connectivity whilst their physical growth was considered proportional between WT control and *SR-A*$^{-/-}$ mice [216]. Since there was no difference found in marrow adipocyte count and osteoblast-related histomorphometric parameters between WT and *SR-A*$^{-/-}$ mice, the study did not investigate the effect of *SR-A* deletion on osteoblast and adipocyte differentiation. Alternatively, the effect of *Scara5* depletion on osteoblast differentiation, which showed a negative regulator role, have been investigated in chapter 3.

Conversely unlike *SR-A*$^{-/-}$ mice, the current project observed a significant decrease in bone marrow adipocyte and body fat volume in *Scara5*$^{-/-}$ animals. As predicted, based on earlier literature by Lee *et al.*, the absence of SCARA5 resulted in a reduced capacity to differentiate into adipocytes *in vitro* [217]. The weight of literature in the osteoblast/adipocyte arena indicates that an increase in one will result in a decrease in the other; the increase bone mass in the *Scara5*$^{-/-}$ mice did indeed correlate with a reduction in fat mass of both inguinal fat (white adipose tissue) and BMAT. As cell lines were used solely in the study by Lee and colleagues [217], the present result chapter provided firmer evidence of SCARA5's function *in vivo*. Therefore, further analyses into the expression of adipocyte-lineage transcription factors (e.g. *Pparg*, *Cebpa/b*, *Fabp4*), and adipokines (e.g. leptin and adiponectin) will be an important insight to understand the mechanism of SCARA5 in adipogenesis.

A recent study showed that SCARA3 was a critical modulator of the cell fate switch of BMSCs between adipocytes and osteoblasts [219]. SCARA3 was found positively associated with osteogenic-related genes, whilst its expression was downregulated significantly in BMSCs during adipogenesis. The role of SCARA3 as a crucial regulator of BMSC cell fate was robustly demonstrated with both *in vitro* and *in vivo* experiments in the study [219]. *In*

vitro, overexpressing SCARA3 using *Scara3* plasmid or knocking down with *Scara3* siRNAs in primary BMSCs significantly promoted osteogenic differentiation and bone mineralization at the expense of adipogenesis, whilst the latter downregulated *Scara3* and resulted in an impaired osteogenesis and an enhanced adipocyte differentiation and formation [219]. *In vivo*, AAVs (adeno-associated viruses) expressing *Scara3* were administered through intra-bone marrow injection in aged and ovariectomy-induced osteoporotic mice, alleviating bone loss in both ovariectomised and aging mice with increased bone formation and reduced marrow fat accumulation [219].

Similarly to SCARA3's expression profile, SCARA5 was found ubiquitously expressed in multiple tissues; however, unlike SCARA3, SCARA5 was positively involved in adipogenic commitment and differentiation at the expense of osteoblasts [217, 219]. Lee *et al.* demonstrated that *Scara5* expression increased in A33 preadipocytes along with key adipogenic differentiation markers during adipocyte differentiation and this was significantly disrupted by knocking down *Scara5* expression [217], but the authors did not explore the functional roles of SCARA5 further in bone and fat formation. Based on these studies, it was hypothesized that SCARA5 played a role in the balance between bone and fat. Indeed, it was shown in Chapter 3 that *Scara5* depletion

enhanced bone formation (Figure 3.3) and osteogenic differentiation (Figure 3.10) and that *Scara5* expression in BMSCs supported marrow adipocyte formation (Figure 5.4) and adipogenic differentiation (Figure 5.6 A-B) in the current chapter.

A number of bone related factors have been shown to associate with body fat volume, distribution as well as adipocyte metabolism [305, 306]. The receptor, low-density lipoprotein receptor-related protein 5 (LRP5), is a critical component of bone development and WNT signalling pathway. Interestingly, LRP5 has been reported as an important regulator of human body fat accumulation and distribution [305]. As a key WNT co-receptor, the mechanism of LRP5 was attributed to WNT/β-catenin pathway activity in separate fat depots [305]. Previous studies have linked reduced marrow fat to LRP5 gain-of-function high bone mass phenotype in human and mice mutation, whilst *Lrp5*-deficient mice exhibited an increased marrow adiposity with low bone mass [181, 201, 307]. In comparison to LRP5, *Scara5* deficiency in mice promoted bone formation and increased bone volume whilst exhibiting a reduced inguinal and BMAT fat phenotype. This could indicate that SCARA5 has functional associations yet to be revealed linking bone and fat development.

Another well-known, yet traditionally viewed as a bone specific cytokine, Sclerostin (SOST), has been shown to contribute to whole-body metabolism and marrow adipogenesis [306, 308]. The mechanism of SOST was established as a negative regulator of bone acquisition via WNT/β-catenin signalling suppression [309, 310] which in return can induce marrow adipocyte differentiation in preadipocytes [308]. Thus, reducing SOST via both pharmaceutical and genetic methods *in vivo* significantly diminished BMAT formation. Meanwhile, study by Kim *et al.* found that *Sost*-deficient mice had reduced body fat mass and adipocyte size relative to littermate controls [306]. It was found that the decrease in white adipose tissue volume in $Sost^{-/-}$ mice was due to an increased WNT/β-catenin signalling associated with a reduction of *de novo* fatty acid synthesis and enhanced fatty acid oxidation [306]. These studies provided a crucial link between body fat and bone development.

Other studies also revealed important regulating factors that influence lineage bifurcation of BMSCs with significant representations of bone or marrow fat phenotypes and mechanisms. Conditional deletion of *Pgc1α* (peroxisome proliferator-activated receptor gamma coactivator 1 alpha) in mesenchymal progenitor cells resulted in an enhanced bone loss and marrow adipocyte volume [311]. The mechanism was attributed to the loss of *Pgc1α* which

inhibited the induction of TAZ (transcriptional co-activator with PDZ-binding motif) functioning as a co-activator of RUNX2 to promote osteogenic differentiation, whilst as a co-repressor of PPARγ to suppress adipogenesis in MSC lineage determination. Furthermore, *Thy1* (thymus cell antigen 1) deficient mice exhibited a reduced bone mass and increased marrow fat phenotype [312]. This was associated with an altered WNT signalling regulation, where WNT inhibitors increased and WNT ligands reduced at the absence of *Thy1*. On the other hand, *Shp1* (SH2-domain-containing phosphatase 1) depletion enhanced adipogenesis and attenuated osteogenic differentiation by facilitating β-catenin destabilization, which in return hampered the WNT/β-catenin signalling that supports bone formation [313]. Intriguingly, significant higher fat mass to body weight ratios were reported in *Shp1*- and *Thy1*-deficient murine models, with both mechanisms relating to disturbed WNT signalling pathway [312, 313].

The current findings of *Scara5*$^{-/-}$ animals in this chapter showed phenotypic changes in not only bone and marrow fat but also body fat deposition with age. Due to the established relationship between bone and body fat development with WNT signalling pathway [306, 312, 313], future studies into WNT signalling pathway under SCARA5 deficiency may potentially

build a novel association and mechanistic insight. Meanwhile, although it would be reasonable to suspect the involvement of WNT signalling, it is likely that SCARA5 is also associated with other mechanisms.

A recent study revealed an important role of SCARA5 in adipogenic commitment of MSCs *in vitro*, where SCARA5 overexpression considerably induced adipocyte differentiation through suppressing FAK phosphorylation and deactivating FAK-ERK signalling pathway [217]. This study demonstrated the critical mechanistic association between SCARA5 and FAK-ERK pathway during MSC adipocyte lineage differentiation. However, this association was not investigated in bone marrow adipocytes nor *in vivo*. The experiments in this chapter have established further that *Scara5* depletion led to increased body fat and marrow adipocyte deposition in mice and the latter was aided by enhanced adipogenesis of *Scara5*$^{-/-}$ BMSCs. Given these results, further investigations into FAK signal activation (e.g. AKT, JNK and ERK) in *Scara5*$^{-/-}$ BMSCs during adipocyte and osteoblast differentiation will be highly beneficial to understand the principal mechanism of *Scara5* involved in bone and BMAT development *in vivo*.

Recent advances have expanded our understanding of the importance of the skeletal homeostasis and marrow microenvironment, where

heterogeneous interfaces and functional niches of bone, fat, and blood vessels reside closely in the bone marrow. A study by Zhong and co-workers recently identified a unique subpopulation of marrow adipocytes named marrow adipogenic lineage precursors (MALPs) that were able to regulate bone marrow environment [314]. MALPs are adipocyte precursors that contain no lipid droplet, but express genes associated with adipocytes and form a 3D-network as pericytes and stromal cells surrounding marrow blood vessels. Although it was reported by RNA-seq experiments that a considerable amount of marrow progenitor cells express adipocyte-associated genes [147, 315, 316], it was Zhong and colleagues that further demonstrated the functional roles of MALPs in suppressing bone formation and maintaining marrow vasculature [314]. The weight of the study underscored the importance of marrow fat differentiation and formation in bone marrow homeostasis. Whilst this current chapter found no significant difference between WT and *Scara5*$^{-/-}$ bones in either adipogenic progenitor cells or BMSCs (Figure 5.6 C-E), a finer dissection to better define mesenchymal progenitors may provide insight into the bone, fat and marrow vasculature phenotypes under SCARA5 deficiency.

Blood vessels in skeletal system not only serve as a conduit for gases, nutrients, cells or waste transport but also play an essential role in the

maintenance and regulation of haematopoiesis, skeletal development and homeostasis [317, 318]. Abundant evidence has confirmed that the coupling of osteogenesis and angiogenesis, the process of new blood vessel formation from existing vessels, is crucial for bone formation and regeneration [319-321]. It was shown in this chapter that the blood vascular density was significantly higher in *Scara5*$^{-/-}$ tibias than WT tibias (Figure 5.7 A-B). Elevated bone volume alongside greater vascularity found in *Scara5*$^{-/-}$ bone marrow is in agreement with previous research. Although further efforts are required to interrogate the exact mechanism, the enhanced expansion of bone marrow capillaries could be the consequence of high energy and nutrient demands [322, 323] due to increased bone generation in the absence of SCARA5. That said, it was found that pro-angiogenic factors, including vascular endothelial growth factor (VEGF), hypoxia-inducible factor-α, and C-X-C motif chemokine ligand 12 (CXCL12), were expressed by osteolineage cells at all differential stages [73, 324, 325]. In this sense, enhanced osteogenic differentiation of *Scara5*$^{-/-}$ BMSCs could potentially recruit and promote blood vessel formation by producing pro-angiogenic factors. Reciprocally, endothelial and perivascular cells of bone vasculature can release factors that act on osteoblasts,

chondrocytes and osteoclasts to support osteogenesis thus bone formation and repair [319, 320, 326].

In summary, it has been revealed that SCARA5 plays an important role in white adipocyte accumulation as well as adipogenic differentiation of BMSCs. The positive regulator function of SCARA5 in adipogenesis was shown when comparing WT and *Scara5*$^{-/-}$ animals, where WT animals presented a higher white fat volume and elevated marrow adiposity as opposed to a lower body fat and marrow adipocyte volume in *Scara5*-deficient mice. Similarly, the expression of SCARA5 supported adipogenesis of BMSCs *in vitro*. These results could simply be due to the fact that adipogenic differentiation was favoured at the expense of osteogenesis in the presence of SCARA5. Although a previous study has shown that FAK/ERK signalling as one of the pathways found involved with SCARA5 in adipocyte commitment of MSCs *in vitro*, it is critical to investigate whether the mechanism of SCARA5 is different concerning bone marrow adipocyte differentiation and in the cell fate switch between osteoblasts and adipocytes of BMSCs *in vivo*.

6. Discussion

6.1 SCARA5 mediates the balance of osteoblast and adipocyte formation

An imbalance between osteoblast and adipocyte differentiation of BMSCs with age can result in low bone volume and increased marrow adiposity; a mechanism underlying bone disorders such as osteopenia, osteoporosis, and fragility fracture [106, 119, 123, 149]. This project revealed that SCARA5 is a negative regulator of bone mass and osteogenic differentiation of BMSCs. Mice lacking *Scara5* expression exhibited greater bone volume due to an elevated bone mineral deposition rate as compared to WT animals. *Scara5*$^{-/-}$ BMSCs formed more bone nodules *in vitro*. This phenotype persisted with age leading to similar differences in bone and body phenotypes of older mice at one year of age. Conversely, there was no change in either bone structural integrity or osteoclast activity as a result of SCARA5 deficiency, indicating that primarily cells of the mesenchymal lineage are affected.

In agreement with phenotypic observations, the absence of SCARA5 in BMSCs promoted osteogenic differentiation and suppressed adipocyte formation *in vitro*. However, no statistical difference was found in pre-adipocyte and pre-osteoblast frequencies in primary bone marrow cell populations of

Scara5$^{-/-}$ and WT mice. *Scara5*$^{-/-}$ animals were leaner with a smaller inguinal fat mass and had significantly lower BMAT volume than WT control mice at 11 weeks of age. A closer examination of inguinal adipocytes demonstrated a slight, but not statistically significant, reduction in the size and number in *Scara5*$^{-/-}$ animals; more samples will be required to confirm this result. Interestingly, blood vessel density in *Scara5*$^{-/-}$ bone marrow was significantly higher than that of WT mice, implying the possible involvement of SCARA5 in bone vasculature. These results indicate that SCARA5 is an important regulator of osteoblast and adipocyte formation and may play a role in whole-body fat metabolism.

Five class A scavenger receptors, that are encoded by different and unrelated genes, have currently been identified [327]. These class A scavenger receptors are type II membrane proteins and have similar structure as shown in Figure 6.1. The expression of SR-A1 and SR-A6 (also known as MARCO or SCARA2) is relatively abundant on macrophages, whilst SR-A3 (also known as cellular stress response/CSR), SR-A4 (scavenger receptor with C-type lection/SRCL), and SR-A5 (SCARA5) are expressed in a variety of other tissues and cell types [213]. Members of this class can recognise a diverse range of ligands, such as β-amyloid, heat shock proteins, lipopolysaccharides, and modified and oxidized LDL [213, 327]. In general, their functions are diverse,

non-redundant and involved in multiple diseases and organ systems [213, 215, 327].

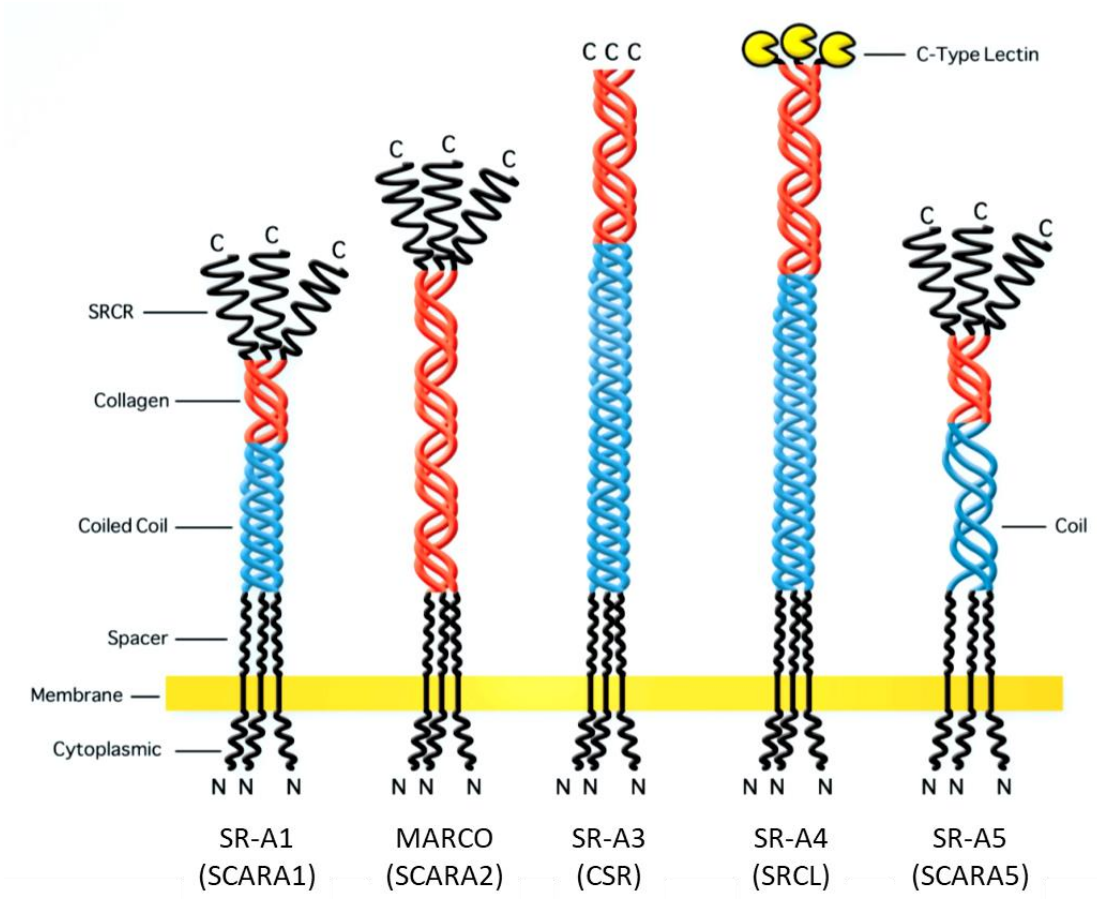

Figure 6.1 Schematic of structures of class A scavenger receptors. The class A scavenger receptors form homo trimeric transmembrane proteins with similar structure comprised of an N-terminal cytoplasmic tail, transmembrane sequence, spacer region, α-helical coiled coil domain, collagenous domain, and a C-terminal scavenger receptor domain. Differences are in the presence of coiled-coil, collagenous, and C-terminus structures. A c-type lectin, scavenger receptor cysteine-rich (SRCR), or absent SRCR structure may locate at the C-terminus of class A scavenger receptors. Abbreviations: Scavenger receptor class A (SCARA), scavenger receptor class A member 1 (SR-A1/SCARA1); macrophage receptor with collagenous structure (MARCO); cellular stress response (CSR); scavenger receptor with C-type lection (SRCL), scavenger receptor class A member 5 (SCARA5). (Adapted from [327])

A common cause of altered bone mass in bone disorders is aberrant osteoclast function [5]. SR-A (SR-A1) is a receptor predominantly expressed in macrophage/monocyte lineage that includes osteoclasts, which differentiate via RANK expression and IL-6 mediated ERK and JNK signalling [218, 226]. Studies on SR-A$^{-/-}$ animals showed that increased bone volume was partly due to a significant decrease in osteoclast number and differentiation [216, 218, 226]; no changes were reported in osteoblast-related or adipocyte parameters. However, osteoclast numbers in *Scara5*$^{-/-}$ animals remained unchanged relative to WT control mice, with equivalent osteoclast parameters. Thus, the underlying cause of increased bone parameters is fundamentally different and likely to be due to the different cellular expression of the various Class A scavenger receptors.

Other classes of scavenger receptors have also been shown to influence bone phenotypes in mice. For example, mice lacking lectin-like oxidized low-density lipoprotein receptor-1 (LOX-1 also known as SCARE1) have decreased trabecular bone mass due to elevated bone resorption resulting from enhanced cell-cell fusion during osteoclast differentiation [328]. On the other hand, *Scarb1* and *CD36* (also known as SR-B2; Figure 1.10) influenced bone mass primarily through alterations in osteoblast differentiation

[220, 230]. Deletion of either *Scarb1* or *CD36* reduced osteoblast differentiation resulting in lower bone volume and trabecular density with a reduced bone formation rate [220, 230]. Bone marrow adipocytes were not investigated in these studies. Nonetheless, the absence of published studies on other scavenger receptors means that at this time we cannot exclude the potential involvement of other scavenger receptors in bone formation and adipocytes.

Within the Class A scavenger receptors, SCARA3 is the only other family member that has been confirmed as an important modulator of BMSC cell fate determination [219]. *Scara3* overexpression in BMSCs significantly enhanced osteogenic differentiation and inhibited adipogenic differentiation, with a corresponding increase in osteoblast-related genes and reduced adipocyte-related gene expression. Moreover, *Scara3* overexpression ameliorated the bone loss and reduced marrow adipocyte number in ovariectomized and ageing mice [219]. Overexpressing *Scara3* upregulated FOXO1, a positive regulator of osteoblast differentiation [329] associated with SIRT1/FOXO1/PGC1α pathway that promotes osteoblast activities [330].

Both SCARA5 and SCARA3 were initially reported as critical regulators of adipocyte differentiation [217, 331]. The apparent opposite roles of these two receptors, whereby overexpression of *Scara3* enhances

osteogenesis whilst *Scara5* upregulation promotes adipogenesis, suggest that BMSC differentiation may be dependent upon the relative expression levels or activities of these two receptors and that they are maintained in an equilibrium. It could be hypothesised that an imbalance in the receptor expression ratio of SCARA3 and SCARA5 may predispose BMSCs towards either osteogenic or adipogenic lineage cell fate (Figure 6.2). The similar concept, like that of the RANKL/OPG ratio and RANKL/RANK/OPG system operating to regulate bone resorption and formation, has aided our understanding of disorders of bone and bone remodelling [332, 333].

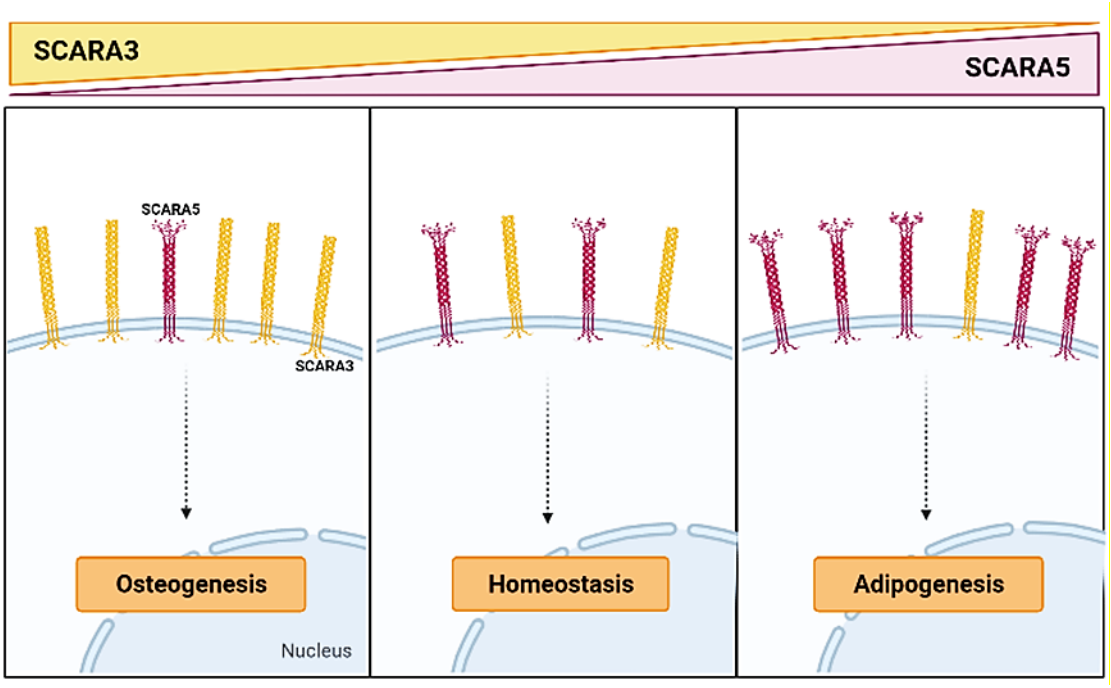

Figure 6.2 Schematic of potential influence of SCARA3/SCARA5 ratio in osteogenic and adipogenic differentiation of BMSCs. It is hypothesized that an equilibrium of SCARA3 and SCARA5 expression exists to regulate BMSC cell fate. This hypothesis indicates increased expression of SCARA3 favours osteogenesis, whilst SCARA5 overexpression skews BMSC differentiation

towards adipogenesis.

The different roles of individual scavenger receptors in bone may be due to structural differences and the presence or absence of specific protein domains [257]. For example, the C-terminal scavenger receptor cysteine-rich domain of SCARA5 facilitates ferritin binding, whereas the same domain in SCARA3 does not [257]. The N-terminal intracellular and C-terminal domains differ ~~significantly~~ between specific scavenger receptors and may be responsible for receptor-specific signal transduction and trafficking [215]. Expression of individual scavenger receptors may be restricted to specific cell types in the bone marrow or found more broadly. Certain cell types may express multiple scavenger receptors and further complexity could be added by temporal differences in receptor expression during cellular differentiation. Such data will require comprehensive analyses of the bone marrow at both transcriptional and proteomic levels. In a comparable way, the distribution and abundance of receptor ligands that may be unique or bound by multiple scavenger receptors have the potential to be the basis for how these receptors affect cellular differentiation and bone formation. Ligands associated with osteogenic differentiation, such as ferritin and specific antagonists (e.g. DKK1, SOST and sFRP1) were investigated for their potential involvement in

SCARA5-dependent mechanisms.

Various molecular factors have been identified to influence osteoblast and adipocyte lineage bifurcation, with some studies addressing regulatory factors that present phenotypic and reciprocal changes in bone mass and marrow adiposity in different mouse models during skeletal aging [123, 311, 334-336]. Conditional deletion of *Pgc1α* in mesenchymal progenitor cells resulted in enhanced bone loss and marrow adipocyte accumulation in aged mice [311]. The loss of PGC1α inhibited TAZ induction; a co-activator of RUNX2 and a co-repressor of PPARγ that promote osteogenic differentiation and suppress adipogenesis, respectively. The association between osteoblast activities and the SIRT1/FOXO1/PGC1α pathway [330] could be explained by the decreased bone volume that accompanies *Pgc1α* conditional deletion.

Prx1-Cre Foxp1$^{fl/fl}$ conditional KO mice display premature skeletal ageing [335, 336]. The premature bone ageing phenotype in *Alpl*$^{+/-}$ and *Prx1-Cre Foxp1*$^{fl/fl}$ animals is characterized by an increase of senescence markers in BMSCs, along with accelerated marrow fat gain and bone loss. In comparison, although that *in vitro* loss of SCARA3 results in reduced osteogenesis and increased adipogenesis in BMSCs [219], this has not been demonstrated *in vivo* and the question of whether mice lacking SCARA3 expression undergo

premature bone ageing remains unanswered. Conversely, the bone of *Scara5*$^{-/-}$ mice appears 'younger', with lower marrow adiposity and an elevated bone volume.

Phenotypic changes in *Scara5*$^{-/-}$ animals included not only altered bone and marrow adiposity but also subcutaneous fat accumulation. Several bone-related factors have been shown to associate with body fat volume, its distribution or adipocyte metabolism [305, 306, 312, 313]. MSC-specific deletion of *Shp1*, a Src homology protein that participates in modulation of mouse embryonic stem cells [337], caused decreased bone mass and increased adipogenesis through suppression of the WNT/β-catenin signalling pathway during MSC differentiation [313]. Moreover, mice lacking *Thy1*, also known as CD90 and a cell marker for MSCs [338], exhibited reduced bone mass and increased marrow adiposity, that was associated with altered WNT signal regulation [312]. Intriguingly both SHP1 or Thy1 deficiency in mice, results in a significantly higher fat mass to body weight ratio and perturbation of WNT pathways [312, 313].

SOST, a WNT antagonist and bone specific cytokine produced by bone matrix-embedded osteocytes, has been shown to contribute to whole-body metabolism and marrow adipogenesis [306, 308]. Studies have

established SOST as a negative regulator of bone acquisition via WNT/β-catenin signalling suppression and induced marrow adipocyte differentiation [308-310]. Indeed, SOST inhibition *in vivo* significantly promoted bone growth and diminished BMAT formation [308]. The anti-sclerostin antibody romosozumab is currently being trialled as a bone anabolic drug [207]. Kim *et al.* demonstrated that *Sost*$^{-/-}$ mice had a reduced fat mass phenotype with smaller adipocyte size [306] due to increased WNT/β-catenin signalling, which resulted in decreased de novo fatty acid synthesis in adipocytes and enhanced fatty acid oxidation [306]. A key co-receptor of WNT/β-catenin pathway, LRP5 has been reported to be a regulator of human body fat accumulation and distribution [305]. Studies also linked LRP5 to altered bone mass and marrow adiposity in humans and mice [181, 201, 307]. Experimental data in this thesis showed that the absence of SCARA5 led to a greater ALP response to WNT3a, suggesting that it may be able to sequester WNT ligands from their cognate signaling receptors and thus reduce bone formation. Further work is needed to confirm this observation.

Histological analysis of bone revealed an unexpected finding of significantly higher vascular density in *Scara5*$^{-/-}$ tibias. Sufficient vascular supply is necessary for efficient gas exchange and nutrient, or waste transport

and for the maintenance of haematopoiesis and the skeleton. Indeed, inadequate blood flow is linked to low bone mass and bone loss disorders [317, 318]. In addition, the increased bone vascularity and elevated bone volume in *Scara5*$^{-/-}$ mice is consistent with the well-established principle of angiogenic-osteogenic coupling [318]. Although the increased number of bone marrow capillaries could be the consequence of adaption to higher energy and nutrient demands because of greater bone formation in the absence of SCARA5, it is also possible that the presence of increased numbers of blood vessels may further promote bone formation.

The coupling of angiogenesis and osteogenesis is essential for bone formation and regeneration [319-321]. Cytokines and molecular signals from perivascular and endothelial cells of the bone vasculature can support osteogenesis and thus bone formation and repair by acting on osteoblasts, chondrocytes, and osteoclasts [319, 320, 326]. Reciprocally, osteolineage cells produce pro-angiogenic factors, including VEGFs, CXCL12, and hypoxia-inducible factor-α at various stages of differentiation [73, 318, 324]. Therefore, the enhanced bone formation in *Scara5*$^{-/-}$ mice could potentially promote greater blood vessel formation than in WT bones via the production of pro-angiogenic factors (Figure 6.3).

Interestingly, SCARA5 overexpression was linked to VEGF-A and VEGF-C downregulation in breast cancer progression [339]. Since VEGFs play an important role in angiogenesis, osteogenesis, and BMSC differentiation [319, 340], it is suspected that SCARA5 depletion promotes VEGF expression and thereby enhances bone and blood vessel formation in *Scara5*$^{-/-}$ animals. Figure 6.3 illustrates an overview on how SCARA5 deficiency may play a role and together with some important factors involved in the coupling of angiogenesis and osteogenesis.

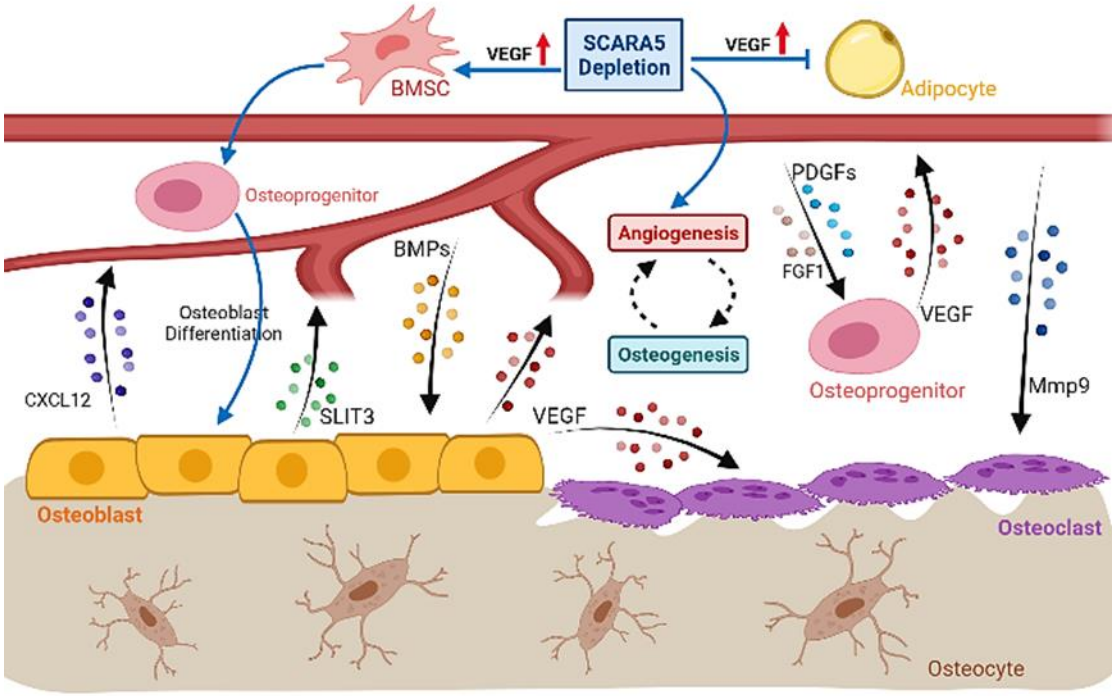

Figure 6.3 Schematic hypothesis of SCARA5's role in the coupling of angiogenesis and osteogenesis. Osteolineage cells produce pro-angiogenic factors to support angiogenesis and blood vessels release angiocrines to promote proliferation, differentiation, and survival of bone lineage cells. Abbreviation: CXCL12, C-X-C motif chemokine 12; FGF1, fibroblast-derived

growth factor 1; Mmp9, matrix metalloproteinase 9; PDGFs, platelet-derived growth factors; SLIT3, slit guidance ligand 3; VEGF, vascular endothelial growth factor; BMPs, bone morphogenetic proteins. Created with Biorender.com.

6.2 Future Directions

The novel role of SCARA5 as an important modulator of osteogenic and adipogenic lineage differentiation raises the opportunity for a number of future research directions. Since SCARA5 deletion *in vivo* increased bone mass and concomitantly reduced white adipose tissue and BMAT volume, accompanied by richer bone vascularity, it is possible that SCARA5 manipulation could be therapeutically valuable, i.e. curbing body fat accumulation, improving bone health, and rejuvenating the bone marrow microenvironment. However, downregulation of *Scara5* has been linked to cancer progression [243, 339], possibly due to effects on cell proliferation and angiogenesis, thus future studies will need to be comprehensively undertaken.

Given the large repertoire of ligands and functional involvement in multiple biological processes, SCARA5 may play different functional roles in respond to distinct ligands and cellular context. Although reports have shown that scavenger receptors were involved in processes such as cell adhesion,

tissue homeostasis, and host immunity [214, 215], understanding of the biological process that SCARA5's ligands may contribute to is currently fairly limited and needs further investigations. Elucidating the mechanism and consequences of SCARA5 interaction with specific ligands by the use of fluorescent-tagged ligands and measuring downstream signalling pathways would aid with cellular localization, trafficking and functional consequences.

All of the works presented in this thesis were in the absence of pathological challenges. Therefore, determining the effects of SCARA5 deficiency on bone diseases, injury, and pharmaceutic challenge, such as estrogen-deficient or age-induced osteoporosis, glucocorticoid treatment, or bone fracture would be of great interest – in the absence of SCARA5 does bone loss occur at the same rate and/or to the same extent?

It would be useful to determine the functional importance and role(s) of different receptor domains of SCARA5 in bone formation using truncation mutants of SCARA5. For example, given that ferritin binds to the cysteine rich domain, would mutation and/or loss of SRCR domain increase or inhibit bone formation?

Lastly, it would be of great interest to investigate effects of SCARA5 deficiency on other tissues, organs, and disorders, such as white and brown

adipose tissues, blood vessels and endothelial cells, or associated vascular disorders like aortic valve stenosis (calcification) and atherosclerosis (plaque formation). The literature in the cancer field is mostly correlative to date and investigating in the *Scara5*$^{-/-}$ mice would be a definitive way to explore the exact role this interesting scavenger receptor plays in disease progression.

Overall, further investigations on SCARA5 are required due to the complex interactions of SCARA5 with ligands and associated signaling pathways and gene regulations under various cellular contexts.

7. References

1. Florencio-Silva, R., et al., *Biology of Bone Tissue: Structure, Function, and Factors That Influence Bone Cells.* Biomed Res Int, 2015. **2015**: p. 421746.
2. Datta, H.K., et al., *The cell biology of bone metabolism.* J Clin Pathol, 2008. **61**(5): p. 577-87.
3. Han, Y., et al., *Paracrine and endocrine actions of bone-the functions of secretory proteins from osteoblasts, osteocytes, and osteoclasts.* Bone Res, 2018. **6**: p. 16.
4. Suchacki, K.J., et al., *Skeletal energy homeostasis: a paradigm of endocrine discovery.* J Endocrinol, 2017. **234**(1): p. R67-R79.
5. Crockett, J.C., et al., *Bone remodelling at a glance.* J Cell Sci, 2011. **124**(Pt 7): p. 991-8.
6. Lian, J.B., et al., *MicroRNA control of bone formation and homeostasis.* Nat Rev Endocrinol, 2012. **8**(4): p. 212-27.
7. Duchamp de Lageneste, O., et al., *Periosteum contains skeletal stem cells with high bone regenerative potential controlled by Periostin.* Nat Commun, 2018. **9**(1): p. 773.
8. Salhotra, A., et al., *Mechanisms of bone development and repair.* Nat Rev Mol Cell Biol, 2020. **21**(11): p. 696-711.
9. Kenkre, J.S. and J. Bassett, *The bone remodelling cycle.* Ann Clin Biochem, 2018. **55**(3): p. 308-327.
10. Hojo, H., S. Ohba, and U.I. Chung, *Signaling pathways regulating the specification and differentiation of the osteoblast lineage.* Regen Ther, 2015. **1**: p. 57-62.
11. Wu, M., G. Chen, and Y.P. Li, *TGF-beta and BMP signaling in osteoblast, skeletal development, and bone formation, homeostasis and disease.* Bone Res, 2016. **4**: p. 16009.
12. Kawane, T., et al., *Runx2 is required for the proliferation of osteoblast progenitors and induces proliferation by regulating Fgfr2 and Fgfr3.* Sci Rep, 2018. **8**(1): p. 13551.
13. Baron, R. and M. Kneissel, *WNT signaling in bone homeostasis and disease: from human mutations to treatments.* Nat Med, 2013. **19**(2): p. 179-92.
14. Houschyar, K.S., et al., *Wnt Pathway in Bone Repair and Regeneration - What Do We Know So Far.* Front Cell Dev Biol, 2018. **6**: p. 170.
15. Maupin, K.A., C.J. Droscha, and B.O. Williams, *A Comprehensive Overview of Skeletal Phenotypes Associated with Alterations in Wnt/beta-catenin Signaling in Humans and Mice.* Bone Res, 2013. **1**(1): p. 27-71.
16. Maeda, K., et al., *The Regulation of Bone Metabolism and Disorders by Wnt Signaling.* Int J Mol Sci, 2019. **20**(22).
17. Hayashi, M., et al., *Weekly intra-articular injections of bone morphogenetic protein-7 inhibits osteoarthritis progression.* Arthritis Res Ther, 2008. **10**(5): p. R118.

18. Shen, J., S. Li, and D. Chen, *TGF-beta signaling and the development of osteoarthritis.* Bone Res, 2014. **2**.
19. Kular, J., et al., *An overview of the regulation of bone remodelling at the cellular level.* Clin Biochem, 2012. **45**(12): p. 863-73.
20. Sharaf-Eldin, W.E., et al., *The Modulatory Effects of Mesenchymal Stem Cells on Osteoclastogenesis.* Stem Cells Int, 2016. **2016**: p. 1908365.
21. Yavropoulou, M.P. and J.G. Yovos, *Osteoclastogenesis--current knowledge and future perspectives.* J Musculoskelet Neuronal Interact, 2008. **8**(3): p. 204-16.
22. Boyce, B.F. and L. Xing, *The RANKL/RANK/OPG pathway.* Curr Osteoporos Rep, 2007. **5**(3): p. 98-104.
23. Bellido, T., *Osteocyte-driven bone remodeling.* Calcif Tissue Int, 2014. **94**(1): p. 25-34.
24. Schaffler, M.B., et al., *Osteocytes: master orchestrators of bone.* Calcif Tissue Int, 2014. **94**(1): p. 5-24.
25. Jiang, J.X., A.J. Siller-Jackson, and S. Burra, *Roles of gap junctions and hemichannels in bone cell functions and in signal transmission of mechanical stress.* Front Biosci, 2007. **12**: p. 1450-62.
26. Rochefort, G.Y., S. Pallu, and C.L. Benhamou, *Osteocyte: the unrecognized side of bone tissue.* Osteoporos Int, 2010. **21**(9): p. 1457-69.
27. van Bezooijen, R.L., et al., *Wnt but not BMP signaling is involved in the inhibitory action of sclerostin on BMP-stimulated bone formation.* J Bone Miner Res, 2007. **22**(1): p. 19-28.
28. Boyce, B.F. and L. Xing, *Functions of RANKL/RANK/OPG in bone modeling and remodeling.* Arch Biochem Biophys, 2008. **473**(2): p. 139-46.
29. Raggatt, L.J. and N.C. Partridge, *Cellular and molecular mechanisms of bone remodeling.* J Biol Chem, 2010. **285**(33): p. 25103-8.
30. Lerner, U.H., E. Kindstedt, and P. Lundberg, *The critical interplay between bone resorbing and bone forming cells.* J Clin Periodontol, 2019. **46 Suppl 21**: p. 33-51.
31. Siddiqui, J.A. and N.C. Partridge, *Physiological Bone Remodeling: Systemic Regulation and Growth Factor Involvement.* Physiology (Bethesda), 2016. **31**(3): p. 233-45.
32. Zaidi, M., et al., *Regulation of Skeletal Homeostasis.* Endocr Rev, 2018. **39**(5): p. 701-718.
33. Nakashima, T., et al., *Evidence for osteocyte regulation of bone homeostasis through RANKL expression.* Nat Med, 2011. **17**(10): p. 1231-4.
34. Heino, T.J., T.A. Hentunen, and H.K. Vaananen, *Osteocytes inhibit osteoclastic bone resorption through transforming growth factor-beta: enhancement by estrogen.* J Cell Biochem, 2002. **85**(1): p. 185-97.
35. Nakamura, T., et al., *Estrogen prevents bone loss via estrogen receptor alpha and*

induction of Fas ligand in osteoclasts. Cell, 2007. **130**(5): p. 811-23.

36. McHugh, K.P., et al., *Mice lacking beta3 integrins are osteosclerotic because of dysfunctional osteoclasts.* J Clin Invest, 2000. **105**(4): p. 433-40.
37. Furuya, M., et al., *Direct cell-cell contact between mature osteoblasts and osteoclasts dynamically controls their functions in vivo.* Nat Commun, 2018. **9**(1): p. 300.
38. Lassen, N.E., et al., *Coupling of Bone Resorption and Formation in Real Time: New Knowledge Gained From Human Haversian BMUs.* J Bone Miner Res, 2017. **32**(7): p. 1395-1405.
39. Sims, N.A. and T.J. Martin, *Coupling the activities of bone formation and resorption: a multitude of signals within the basic multicellular unit.* Bonekey Rep, 2014. **3**: p. 481.
40. Feng, X. and J.M. McDonald, *Disorders of bone remodeling.* Annu Rev Pathol, 2011. **6**: p. 121-45.
41. Cenci, S., et al., *Estrogen deficiency induces bone loss by enhancing T-cell production of TNF-alpha.* J Clin Invest, 2000. **106**(10): p. 1229-37.
42. Riggs, B.L., S. Khosla, and L.J. Melton, 3rd, *Sex steroids and the construction and conservation of the adult skeleton.* Endocr Rev, 2002. **23**(3): p. 279-302.
43. Xie, Y., et al., *Bench-to-bedside strategies for osteoporotic fracture: From osteoimmunology to mechanosensation.* Bone Res, 2019. **7**: p. 25.
44. Singer, F.R., *Paget disease: when to treat and when not to treat.* Nat Rev Rheumatol, 2009. **5**(9): p. 483-9.
45. Stark, Z. and R. Savarirayan, *Osteopetrosis.* Orphanet J Rare Dis, 2009. **4**: p. 5.
46. Driessen, G.J., et al., *Long-term outcome of haematopoietic stem cell transplantation in autosomal recessive osteopetrosis: an EBMT report.* Bone Marrow Transplant, 2003. **32**(7): p. 657-63.
47. Lanske, B. and C. Rosen, *Bone Marrow Adipose Tissue: The First 40 Years.* J Bone Miner Res, 2017. **32**(6): p. 1153-1156.
48. Scheller, E.L., et al., *Region-specific variation in the properties of skeletal adipocytes reveals regulated and constitutive marrow adipose tissues.* Nat Commun, 2015. **6**: p. 7808.
49. Li, Y., Y. Meng, and X. Yu, *The Unique Metabolic Characteristics of Bone Marrow Adipose Tissue.* Front Endocrinol (Lausanne), 2019. **10**: p. 69.
50. Suchacki, K.J., et al., *Bone marrow adipose tissue is a unique adipose subtype with distinct roles in glucose homeostasis.* Nat Commun, 2020. **11**(1): p. 3097.
51. Doucette, C.R., et al., *A High Fat Diet Increases Bone Marrow Adipose Tissue (MAT) But Does Not Alter Trabecular or Cortical Bone Mass in C57BL/6J Mice.* J Cell Physiol, 2015. **230**(9): p. 2032-7.
52. Devlin, M.J., et al., *Caloric restriction leads to high marrow adiposity and low bone mass in growing mice.* J Bone Miner Res, 2010. **25**(9): p. 2078-88.

53. Di Iorgi, N., et al., *Reciprocal relation between marrow adiposity and the amount of bone in the axial and appendicular skeleton of young adults.* J Clin Endocrinol Metab, 2008. **93**(6): p. 2281-6.
54. Hardouin, P., T. Rharass, and S. Lucas, *Bone Marrow Adipose Tissue: To Be or Not To Be a Typical Adipose Tissue?* Front Endocrinol (Lausanne), 2016. **7**: p. 85.
55. Krings, A., et al., *Bone marrow fat has brown adipose tissue characteristics, which are attenuated with aging and diabetes.* Bone, 2012. **50**(2): p. 546-52.
56. Lecka-Czernik, B., *Marrow fat metabolism is linked to the systemic energy metabolism.* Bone, 2012. **50**(2): p. 534-9.
57. Suchacki, K.J. and W.P. Cawthorn, *Molecular Interaction of Bone Marrow Adipose Tissue with Energy Metabolism.* Curr Mol Biol Rep, 2018. **4**(2): p. 41-49.
58. Li, Z., et al., *Development, regulation, metabolism and function of bone marrow adipose tissues.* Bone, 2018. **110**: p. 134-140.
59. Ambrosi, T.H. and T.J. Schulz, *The emerging role of bone marrow adipose tissue in bone health and dysfunction.* J Mol Med (Berl), 2017. **95**(12): p. 1291-1301.
60. Craft, C.S., et al., *Molecular differences between subtypes of bone marrow adipocytes.* Curr Mol Biol Rep, 2018. **4**(1): p. 16-23.
61. Berry, R., et al., *Adipose Tissue Residing Progenitors (Adipocyte Lineage Progenitors and Adipose Derived Stem Cells (ADSC).* Curr Mol Biol Rep, 2015. **1**(3): p. 101-109.
62. Berendsen, A.D. and B.R. Olsen, *Osteoblast-adipocyte lineage plasticity in tissue development, maintenance and pathology.* Cell Mol Life Sci, 2014. **71**(3): p. 493-7.
63. Mizoguchi, T., et al., *Osterix marks distinct waves of primitive and definitive stromal progenitors during bone marrow development.* Dev Cell, 2014. **29**(3): p. 340-9.
64. Ambrosi, T.H., et al., *Adipocyte Accumulation in the Bone Marrow during Obesity and Aging Impairs Stem Cell-Based Hematopoietic and Bone Regeneration.* Cell Stem Cell, 2017. **20**(6): p. 771-784 e6.
65. Seale, P., et al., *PRDM16 controls a brown fat/skeletal muscle switch.* Nature, 2008. **454**(7207): p. 961-7.
66. Lepper, C. and C.M. Fan, *Inducible lineage tracing of Pax7-descendant cells reveals embryonic origin of adult satellite cells.* Genesis, 2010. **48**(7): p. 424-36.
67. Logan, M., et al., *Expression of Cre Recombinase in the developing mouse limb bud driven by a Prxl enhancer.* Genesis, 2002. **33**(2): p. 77-80.
68. Sanchez-Gurmaches, J., W.Y. Hsiao, and D.A. Guertin, *Highly selective in vivo labeling of subcutaneous white adipocyte precursors with Prx1-Cre.* Stem Cell Reports, 2015. **4**(4): p. 541-50.
69. Kawanami, A., et al., *Mice expressing GFP and CreER in osteochondro progenitor cells in the periosteum.* Biochem Biophys Res Commun, 2009. **386**(3): p. 477-82.
70. Chen, J., et al., *Osx-Cre targets multiple cell types besides osteoblast lineage in*

postnatal mice. PLoS One, 2014. **9**(1): p. e85161.

71. Liu, Y., et al., *Osterix-cre labeled progenitor cells contribute to the formation and maintenance of the bone marrow stroma.* PLoS One, 2013. **8**(8): p. e71318.
72. Horowitz, M.C., et al., *Bone marrow adipocytes.* Adipocyte, 2017. **6**(3): p. 193-204.
73. Zhou, B.O., et al., *Leptin-receptor-expressing mesenchymal stromal cells represent the main source of bone formed by adult bone marrow.* Cell Stem Cell, 2014. **15**(2): p. 154-68.
74. Pinho, S., et al., *PDGFRalpha and CD51 mark human nestin+ sphere-forming mesenchymal stem cells capable of hematopoietic progenitor cell expansion.* J Exp Med, 2013. **210**(7): p. 1351-67.
75. Worthley, D.L., et al., *Gremlin 1 identifies a skeletal stem cell with bone, cartilage, and reticular stromal potential.* Cell, 2015. **160**(1-2): p. 269-84.
76. Rendina-Ruedy, E. and C.J. Rosen, *Lipids in the Bone Marrow: An Evolving Perspective.* Cell Metab, 2020. **31**(2): p. 219-231.
77. Scheller, E.L., et al., *Bone marrow adipocytes resist lipolysis and remodeling in response to beta-adrenergic stimulation.* Bone, 2019. **118**: p. 32-41.
78. Tavassoli, M., *Differential response of bone marrow and extramedullary adipose cells to starvation.* Experientia, 1974. **30**(4): p. 424-5.
79. Devlin, M.J., *Why does starvation make bones fat?* Am J Hum Biol, 2011. **23**(5): p. 577-85.
80. Liu, L., J. Aronson, and B. Lecka-Czernik, *Rosiglitazone disrupts endosteal bone formation during distraction osteogenesis by local adipocytic infiltration.* Bone, 2013. **52**(1): p. 247-58.
81. Qiang, G., et al., *Lipodystrophy and severe metabolic dysfunction in mice with adipose tissue-specific insulin receptor ablation.* Mol Metab, 2016. **5**(7): p. 480-490.
82. Frey, J.L., et al., *Wnt-Lrp5 signaling regulates fatty acid metabolism in the osteoblast.* Mol Cell Biol, 2015. **35**(11): p. 1979-91.
83. Lee, W.C., et al., *Energy Metabolism of the Osteoblast: Implications for Osteoporosis.* Endocr Rev, 2017. **38**(3): p. 255-266.
84. Johnson, C.H., J. Ivanisevic, and G. Siuzdak, *Metabolomics: beyond biomarkers and towards mechanisms.* Nat Rev Mol Cell Biol, 2016. **17**(7): p. 451-9.
85. Liu, J., et al., *Comprehensive evaluation of the metabolic effects of porcine CRTC3 overexpression on subcutaneous adipocytes with metabolomic and transcriptomic analyses.* J Anim Sci Biotechnol, 2021. **12**(1): p. 19.
86. Verkouter, I., et al., *The Relation Between Adult Weight Gain, Adipocyte Volume, and the Metabolic Profile at Middle Age.* J Clin Endocrinol Metab, 2021. **106**(11): p. e4438-e4447.
87. Sulston, R.J. and W.P. Cawthorn, *Bone marrow adipose tissue as an endocrine organ:*

close to the bone? Horm Mol Biol Clin Investig, 2016. **28**(1): p. 21-38.

88. Turer, A.T. and P.E. Scherer, *Adiponectin: mechanistic insights and clinical implications.* Diabetologia, 2012. **55**(9): p. 2319-26.
89. Ugarte, F., et al., *Notch signaling enhances osteogenic differentiation while inhibiting adipogenesis in primary human bone marrow stromal cells.* Exp Hematol, 2009. **37**(7): p. 867-875 e1.
90. Xiao, L., et al., *Disruption of the Fgf2 gene activates the adipogenic and suppresses the osteogenic program in mesenchymal marrow stromal stem cells.* Bone, 2010. **47**(2): p. 360-70.
91. Liu, L.F., et al., *Age-related modulation of the effects of obesity on gene expression profiles of mouse bone marrow and epididymal adipocytes.* PLoS One, 2013. **8**(8): p. e72367.
92. Yokota, T., et al., *Paracrine regulation of fat cell formation in bone marrow cultures via adiponectin and prostaglandins.* J Clin Invest, 2002. **109**(10): p. 1303-10.
93. Cawthorn, W.P., et al., *Bone marrow adipose tissue is an endocrine organ that contributes to increased circulating adiponectin during caloric restriction.* Cell Metab, 2014. **20**(2): p. 368-375.
94. Arita, Y., et al., *Paradoxical decrease of an adipose-specific protein, adiponectin, in obesity.* Biochem Biophys Res Commun, 1999. **257**(1): p. 79-83.
95. Delporte, M.L., et al., *Hyperadiponectinaemia in anorexia nervosa.* Clin Endocrinol (Oxf), 2003. **58**(1): p. 22-9.
96. Friedman, J.M. and J.L. Halaas, *Leptin and the regulation of body weight in mammals.* Nature, 1998. **395**(6704): p. 763-70.
97. Laharrague, P., et al., *High expression of leptin by human bone marrow adipocytes in primary culture.* FASEB J, 1998. **12**(9): p. 747-52.
98. Hamrick, M.W., et al., *Leptin treatment induces loss of bone marrow adipocytes and increases bone formation in leptin-deficient ob/ob mice.* J Bone Miner Res, 2005. **20**(6): p. 994-1001.
99. Lindenmaier, L.B., et al., *Hypothalamic Leptin Gene Therapy Reduces Bone Marrow Adiposity in ob/ob Mice Fed Regular and High-Fat Diets.* Front Endocrinol (Lausanne), 2016. **7**: p. 110.
100. Devlin, M.J., et al., *Daily leptin blunts marrow fat but does not impact bone mass in calorie-restricted mice.* J Endocrinol, 2016. **229**(3): p. 295-306.
101. Yue, R., et al., *Leptin Receptor Promotes Adipogenesis and Reduces Osteogenesis by Regulating Mesenchymal Stromal Cells in Adult Bone Marrow.* Cell Stem Cell, 2016. **18**(6): p. 782-96.
102. Gasparrini, M., et al., *Differential expression of cytokines in subcutaneous and marrow fat of aging C57BL/6J mice.* Exp Gerontol, 2009. **44**(9): p. 613-8.

103. Liu, L.F., et al., *Characterization of age-related gene expression profiling in bone marrow and epididymal adipocytes.* BMC Genomics, 2011. **12**: p. 212.
104. Goto, H., et al., *Human bone marrow adipocytes support dexamethasone-induced osteoclast differentiation and function through RANKL expression.* Biomed Res, 2011. **32**(1): p. 37-44.
105. Sebo, Z.L., et al., *Bone Marrow Adiposity: Basic and Clinical Implications.* Endocr Rev, 2019. **40**(5): p. 1187-1206.
106. Devlin, M.J. and C.J. Rosen, *The bone-fat interface: basic and clinical implications of marrow adiposity.* Lancet Diabetes Endocrinol, 2015. **3**(2): p. 141-7.
107. Shen, W., et al., *Relationship between MRI-measured bone marrow adipose tissue and hip and spine bone mineral density in African-American and Caucasian participants: the CARDIA study.* J Clin Endocrinol Metab, 2012. **97**(4): p. 1337-46.
108. Shen, W., et al., *Comparison of the relationship between bone marrow adipose tissue and volumetric bone mineral density in children and adults.* J Clin Densitom, 2014. **17**(1): p. 163-9.
109. A, L.N., et al., *The relationships among total body fat, bone mineral content and bone marrow adipose tissue in early-pubertal girls.* Bonekey Rep, 2013. **2**: p. 315.
110. Li, X., et al., *Unsaturation level decreased in bone marrow fat of postmenopausal women with low bone density using high resolution magic angle spinning (HRMAS) (1)H NMR spectroscopy.* Bone, 2017. **105**: p. 87-92.
111. Patsch, J.M., et al., *Bone marrow fat composition as a novel imaging biomarker in postmenopausal women with prevalent fragility fractures.* J Bone Miner Res, 2013. **28**(8): p. 1721-8.
112. Burkhardt, R., et al., *Changes in trabecular bone, hematopoiesis and bone marrow vessels in aplastic anemia, primary osteoporosis, and old age: a comparative histomorphometric study.* Bone, 1987. **8**(3): p. 157-64.
113. Naveiras, O., et al., *Bone-marrow adipocytes as negative regulators of the haematopoietic microenvironment.* Nature, 2009. **460**(7252): p. 259-63.
114. Zhou, B.O., et al., *Bone marrow adipocytes promote the regeneration of stem cells and haematopoiesis by secreting SCF.* Nat Cell Biol, 2017. **19**(8): p. 891-903.
115. Boyd, A.L., et al., *Acute myeloid leukaemia disrupts endogenous myelo-erythropoiesis by compromising the adipocyte bone marrow niche.* Nat Cell Biol, 2017. **19**(11): p. 1336-1347.
116. Sozen, T., L. Ozisik, and N.C. Basaran, *An overview and management of osteoporosis.* Eur J Rheumatol, 2017. **4**(1): p. 46-56.
117. Verma, S., et al., *Adipocytic proportion of bone marrow is inversely related to bone formation in osteoporosis.* J Clin Pathol, 2002. **55**(9): p. 693-8.
118. Veldhuis-Vlug, A.G. and C.J. Rosen, *Clinical implications of bone marrow adiposity.* J

Intern Med, 2018. **283**(2): p. 121-139.

119. Kawai, M., F.J. de Paula, and C.J. Rosen, *New insights into osteoporosis: the bone-fat connection.* J Intern Med, 2012. **272**(4): p. 317-29.
120. Rodriguez, J.P., et al., *Abnormal osteogenesis in osteoporotic patients is reflected by altered mesenchymal stem cells dynamics.* J Cell Biochem, 1999. **75**(3): p. 414-23.
121. Han, L., et al., *The shift in the balance between osteoblastogenesis and adipogenesis of mesenchymal stem cells mediated by glucocorticoid receptor.* Stem Cell Res Ther, 2019. **10**(1): p. 377.
122. Bredella, M.A., et al., *Marrow fat composition in anorexia nervosa.* Bone, 2014. **66**: p. 199-204.
123. Nehlin, J.O., et al., *Aging and lineage allocation changes of bone marrow skeletal (stromal) stem cells.* Bone, 2019. **123**: p. 265-273.
124. Tencerova, M. and M. Kassem, *The Bone Marrow-Derived Stromal Cells: Commitment and Regulation of Adipogenesis.* Front Endocrinol (Lausanne), 2016. **7**: p. 127.
125. Napoli, N., et al., *Mechanisms of diabetes mellitus-induced bone fragility.* Nat Rev Endocrinol, 2017. **13**(4): p. 208-219.
126. Botolin, S. and L.R. McCabe, *Bone loss and increased bone adiposity in spontaneous and pharmacologically induced diabetic mice.* Endocrinology, 2007. **148**(1): p. 198-205.
127. Botolin, S., et al., *Increased bone adiposity and peroxisomal proliferator-activated receptor-gamma2 expression in type I diabetic mice.* Endocrinology, 2005. **146**(8): p. 3622-31.
128. Slade, J.M., et al., *Human bone marrow adiposity is linked with serum lipid levels not T1-diabetes.* J Diabetes Complications, 2012. **26**(1): p. 1-9.
129. Abdalrahaman, N., et al., *Deficits in Trabecular Bone Microarchitecture in Young Women With Type 1 Diabetes Mellitus.* J Bone Miner Res, 2015. **30**(8): p. 1386-93.
130. Baum, T., et al., *Does vertebral bone marrow fat content correlate with abdominal adipose tissue, lumbar spine bone mineral density, and blood biomarkers in women with type 2 diabetes mellitus?* J Magn Reson Imaging, 2012. **35**(1): p. 117-24.
131. Botolin, S. and L.R. McCabe, *Inhibition of PPARgamma prevents type I diabetic bone marrow adiposity but not bone loss.* J Cell Physiol, 2006. **209**(3): p. 967-76.
132. Iwaniec, U.T. and R.T. Turner, *Failure to generate bone marrow adipocytes does not protect mice from ovariectomy-induced osteopenia.* Bone, 2013. **53**(1): p. 145-53.
133. Bredella, M.A., et al., *Determinants of bone mineral density in obese premenopausal women.* Bone, 2011. **48**(4): p. 748-54.
134. Prieto-Alhambra, D., et al., *The association between fracture and obesity is site-dependent: a population-based study in postmenopausal women.* J Bone Miner Res, 2012. **27**(2): p. 294-300.
135. Premaor, M.O., et al., *The association between fracture site and obesity in men: a*

population-based cohort study. J Bone Miner Res, 2013. **28**(8): p. 1771-7.

136. Bredella, M.A., et al., *Vertebral bone marrow fat is positively associated with visceral fat and inversely associated with IGF-1 in obese women.* Obesity (Silver Spring), 2011. **19**(1): p. 49-53.
137. Bredella, M.A., et al., *Determinants of bone microarchitecture and mechanical properties in obese men.* J Clin Endocrinol Metab, 2012. **97**(11): p. 4115-22.
138. Cohen, A., et al., *Abdominal fat is associated with lower bone formation and inferior bone quality in healthy premenopausal women: a transiliac bone biopsy study.* J Clin Endocrinol Metab, 2013. **98**(6): p. 2562-72.
139. Scheller, E.L., et al., *Changes in Skeletal Integrity and Marrow Adiposity during High-Fat Diet and after Weight Loss.* Front Endocrinol (Lausanne), 2016. **7**: p. 102.
140. Bredella, M.A., et al., *Increased bone marrow fat in anorexia nervosa.* J Clin Endocrinol Metab, 2009. **94**(6): p. 2129-36.
141. Fazeli, P.K., et al., *Marrow fat and preadipocyte factor-1 levels decrease with recovery in women with anorexia nervosa.* J Bone Miner Res, 2012. **27**(9): p. 1864-71.
142. Veldhuis-Vlug, A.G. and C.J. Rosen, *Mechanisms of marrow adiposity and its implications for skeletal health.* Metabolism, 2017. **67**: p. 106-114.
143. Pierce, J.L., et al., *Defining osteoblast and adipocyte lineages in the bone marrow.* Bone, 2019. **118**: p. 2-7.
144. Chan, C.K., et al., *Identification and specification of the mouse skeletal stem cell.* Cell, 2015. **160**(1-2): p. 285-98.
145. Ponzetti, M. and N. Rucci, *Osteoblast Differentiation and Signaling: Established Concepts and Emerging Topics.* Int J Mol Sci, 2021. **22**(13).
146. Chan, C.K.F., et al., *Identification of the Human Skeletal Stem Cell.* Cell, 2018. **175**(1): p. 43-56 e21.
147. Wolock, S.L., et al., *Mapping Distinct Bone Marrow Niche Populations and Their Differentiation Paths.* Cell Rep, 2019. **28**(2): p. 302-311 e5.
148. Chen, Q., et al., *Fate decision of mesenchymal stem cells: adipocytes or osteoblasts?* Cell Death Differ, 2016. **23**(7): p. 1128-39.
149. Sui, B., et al., *Mesenchymal progenitors in osteopenias of diverse pathologies: differential characteristics in the common shift from osteoblastogenesis to adipogenesis.* Sci Rep, 2016. **6**: p. 30186.
150. Zhang, X., et al., *Runx2 overexpression enhances osteoblastic differentiation and mineralization in adipose--derived stem cells in vitro and in vivo.* Calcif Tissue Int, 2006. **79**(3): p. 169-78.
151. Akune, T., et al., *PPARgamma insufficiency enhances osteogenesis through osteoblast formation from bone marrow progenitors.* J Clin Invest, 2004. **113**(6): p. 846-55.
152. Ge, C., et al., *Reciprocal Control of Osteogenic and Adipogenic Differentiation by*

ERK/MAP Kinase Phosphorylation of Runx2 and PPARgamma Transcription Factors. J Cell Physiol, 2016. **231**(3): p. 587-96.

153. Komori, T., *Regulation of Proliferation, Differentiation and Functions of Osteoblasts by Runx2.* Int J Mol Sci, 2019. **20**(7).
154. Pratap, J., et al., *Cell growth regulatory role of Runx2 during proliferative expansion of preosteoblasts.* Cancer Res, 2003. **63**(17): p. 5357-62.
155. Lucero, C.M., et al., *The cancer-related transcription factor Runx2 modulates cell proliferation in human osteosarcoma cell lines.* J Cell Physiol, 2013. **228**(4): p. 714-23.
156. Sinha, K.M. and X. Zhou, *Genetic and molecular control of osterix in skeletal formation.* J Cell Biochem, 2013. **114**(5): p. 975-84.
157. Komori, T., et al., *Targeted disruption of Cbfa1 results in a complete lack of bone formation owing to maturational arrest of osteoblasts.* Cell, 1997. **89**(5): p. 755-64.
158. Nakashima, K., et al., *The novel zinc finger-containing transcription factor osterix is required for osteoblast differentiation and bone formation.* Cell, 2002. **108**(1): p. 17-29.
159. Nishio, Y., et al., *Runx2-mediated regulation of the zinc finger Osterix/Sp7 gene.* Gene, 2006. **372**: p. 62-70.
160. Lee, M.H., et al., *BMP-2-induced Osterix expression is mediated by Dlx5 but is independent of Runx2.* Biochem Biophys Res Commun, 2003. **309**(3): p. 689-94.
161. Celil, A.B. and P.G. Campbell, *BMP-2 and insulin-like growth factor-I mediate Osterix (Osx) expression in human mesenchymal stem cells via the MAPK and protein kinase D signaling pathways.* J Biol Chem, 2005. **280**(36): p. 31353-9.
162. Lefterova, M.I., et al., *PPARgamma and the global map of adipogenesis and beyond.* Trends Endocrinol Metab, 2014. **25**(6): p. 293-302.
163. Imai, T., et al., *Peroxisome proliferator-activated receptor gamma is required in mature white and brown adipocytes for their survival in the mouse.* Proc Natl Acad Sci U S A, 2004. **101**(13): p. 4543-7.
164. Lefterova, M.I., et al., *PPARgamma and C/EBP factors orchestrate adipocyte biology via adjacent binding on a genome-wide scale.* Genes Dev, 2008. **22**(21): p. 2941-52.
165. Barak, Y., et al., *PPAR gamma is required for placental, cardiac, and adipose tissue development.* Mol Cell, 1999. **4**(4): p. 585-95.
166. Wang, F., et al., *Lipoatrophy and severe metabolic disturbance in mice with fat-specific deletion of PPARgamma.* Proc Natl Acad Sci U S A, 2013. **110**(46): p. 18656-61.
167. Tontonoz, P. and B.M. Spiegelman, *Fat and beyond: the diverse biology of PPARgamma.* Annu Rev Biochem, 2008. **77**: p. 289-312.
168. Cao, Z., R.M. Umek, and S.L. McKnight, *Regulated expression of three C/EBP isoforms during adipose conversion of 3T3-L1 cells.* Genes Dev, 1991. **5**(9): p. 1538-52.
169. Mota de Sa, P., et al., *Transcriptional Regulation of Adipogenesis.* Compr Physiol, 2017. **7**(2): p. 635-674.

170. Tanaka, T., et al., *Defective adipocyte differentiation in mice lacking the C/EBPbeta and/or C/EBPdelta gene.* EMBO J, 1997. **16**(24): p. 7432-43.
171. Wang, Q.A., et al., *Distinct regulatory mechanisms governing embryonic versus adult adipocyte maturation.* Nat Cell Biol, 2015. **17**(9): p. 1099-111.
172. Rosen, E.D., et al., *C/EBPalpha induces adipogenesis through PPARgamma: a unified pathway.* Genes Dev, 2002. **16**(1): p. 22-6.
173. Ambele, M.A., et al., *Adipogenesis: A Complex Interplay of Multiple Molecular Determinants and Pathways.* Int J Mol Sci, 2020. **21**(12).
174. Lee, J.E., et al., *Transcriptional and Epigenomic Regulation of Adipogenesis.* Mol Cell Biol, 2019. **39**(11).
175. James, A.W., *Review of Signaling Pathways Governing MSC Osteogenic and Adipogenic Differentiation.* Scientifica (Cairo), 2013. **2013**: p. 684736.
176. Visweswaran, M., et al., *Multi-lineage differentiation of mesenchymal stem cells - To Wnt, or not Wnt.* Int J Biochem Cell Biol, 2015. **68**: p. 139-47.
177. Chen, J. and F. Long, *beta-catenin promotes bone formation and suppresses bone resorption in postnatal growing mice.* J Bone Miner Res, 2013. **28**(5): p. 1160-9.
178. Kim, W., M. Kim, and E.H. Jho, *Wnt/beta-catenin signalling: from plasma membrane to nucleus.* Biochem J, 2013. **450**(1): p. 9-21.
179. Little, R.D., et al., *A mutation in the LDL receptor-related protein 5 gene results in the autosomal dominant high-bone-mass trait.* Am J Hum Genet, 2002. **70**(1): p. 11-9.
180. Boyden, L.M., et al., *High bone density due to a mutation in LDL-receptor-related protein 5.* N Engl J Med, 2002. **346**(20): p. 1513-21.
181. Kato, M., et al., *Cbfa1-independent decrease in osteoblast proliferation, osteopenia, and persistent embryonic eye vascularization in mice deficient in Lrp5, a Wnt coreceptor.* J Cell Biol, 2002. **157**(2): p. 303-14.
182. Sebastian, A., et al., *Wnt co-receptors Lrp5 and Lrp6 differentially mediate Wnt3a signaling in osteoblasts.* PLoS One, 2017. **12**(11): p. e0188264.
183. Li, X., et al., *Wnt3a involved in the mechanical loading on improvement of bone remodeling and angiogenesis in a postmenopausal osteoporosis mouse model.* FASEB J, 2019. **33**(8): p. 8913-8924.
184. Wagner, J.M., et al., *Local Wnt3a treatment restores bone regeneration in large osseous defects after surgical debridement of osteomyelitis.* J Mol Med (Berl), 2020. **98**(6): p. 897-906.
185. Moorer, M.C. and R.C. Riddle, *Regulation of Osteoblast Metabolism by Wnt Signaling.* Endocrinol Metab (Seoul), 2018. **33**(3): p. 318-330.
186. Esen, E., et al., *WNT-LRP5 signaling induces Warburg effect through mTORC2 activation during osteoblast differentiation.* Cell Metab, 2013. **17**(5): p. 745-55.
187. Kida, J., et al., *Interaction of LEF1 with TAZ is necessary for the osteoblastogenic*

activity of Wnt3a. Sci Rep, 2018. **8**(1): p. 10375.

188. Bennett, C.N., et al., *Role of Wnt10b and C/EBPalpha in spontaneous adipogenesis of 243 cells.* Biochem Biophys Res Commun, 2003. **302**(1): p. 12-6.
189. Kawai, M., et al., *Wnt/Lrp/beta-catenin signaling suppresses adipogenesis by inhibiting mutual activation of PPARgamma and C/EBPalpha.* Biochem Biophys Res Commun, 2007. **363**(2): p. 276-82.
190. Laudes, M., *Role of WNT signalling in the determination of human mesenchymal stem cells into preadipocytes.* J Mol Endocrinol, 2011. **46**(2): p. R65-72.
191. Wright, W.S., et al., *Wnt10b inhibits obesity in ob/ob and agouti mice.* Diabetes, 2007. **56**(2): p. 295-303.
192. Lin, G.L. and K.D. Hankenson, *Integration of BMP, Wnt, and notch signaling pathways in osteoblast differentiation.* J Cell Biochem, 2011. **112**(12): p. 3491-501.
193. Itasaki, N. and S. Hoppler, *Crosstalk between Wnt and bone morphogenic protein signaling: a turbulent relationship.* Dev Dyn, 2010. **239**(1): p. 16-33.
194. Tang, N., et al., *BMP-9-induced osteogenic differentiation of mesenchymal progenitors requires functional canonical Wnt/beta-catenin signalling.* J Cell Mol Med, 2009. **13**(8B): p. 2448-2464.
195. Kamiya, N., et al., *BMP signaling negatively regulates bone mass through sclerostin by inhibiting the canonical Wnt pathway.* Development, 2008. **135**(22): p. 3801-11.
196. Chen, Y., et al., *Beta-catenin signaling pathway is crucial for bone morphogenetic protein 2 to induce new bone formation.* J Biol Chem, 2007. **282**(1): p. 526-33.
197. Hata, K., et al., *Differential roles of Smad1 and p38 kinase in regulation of peroxisome proliferator-activating receptor gamma during bone morphogenetic protein 2-induced adipogenesis.* Mol Biol Cell, 2003. **14**(2): p. 545-55.
198. Jin, W., et al., *Schnurri-2 controls BMP-dependent adipogenesis via interaction with Smad proteins.* Dev Cell, 2006. **10**(4): p. 461-71.
199. Bowers, R.R., et al., *Stable stem cell commitment to the adipocyte lineage by inhibition of DNA methylation: role of the BMP-4 gene.* Proc Natl Acad Sci U S A, 2006. **103**(35): p. 13022-7.
200. Bowers, R.R. and M.D. Lane, *A role for bone morphogenetic protein-4 in adipocyte development.* Cell Cycle, 2007. **6**(4): p. 385-9.
201. Fazeli, P.K., et al., *Marrow fat and bone--new perspectives.* J Clin Endocrinol Metab, 2013. **98**(3): p. 935-45.
202. Schwartz, A.V., *Marrow fat and bone: review of clinical findings.* Front Endocrinol (Lausanne), 2015. **6**: p. 40.
203. Grandl, G. and C. Wolfrum, *Adipocytes at the Core of Bone Function.* Cell Stem Cell, 2017. **20**(6): p. 739-740.
204. Fan, Y., et al., *Parathyroid Hormone Directs Bone Marrow Mesenchymal Cell Fate.* Cell

Metab, 2017. **25**(3): p. 661-672.

205. Yu, B., et al., *PGC-1alpha Controls Skeletal Stem Cell Fate and Bone-Fat Balance in Osteoporosis and Skeletal Aging by Inducing TAZ.* Cell Stem Cell, 2018. **23**(4): p. 615-623.
206. Yee, C.S., et al., *Conditional Deletion of Sost in MSC-Derived Lineages Identifies Specific Cell-Type Contributions to Bone Mass and B-Cell Development.* J Bone Miner Res, 2018. **33**(10): p. 1748-1759.
207. Tanaka, S., *Molecular understanding of pharmacological treatment of osteoporosis.* EFORT Open Rev, 2019. **4**(4): p. 158-164.
208. Tu, K.N., et al., *Osteoporosis: A Review of Treatment Options.* P T, 2018. **43**(2): p. 92-104.
209. Nishikawa, K., et al., *Maf promotes osteoblast differentiation in mice by mediating the age-related switch in mesenchymal cell differentiation.* J Clin Invest, 2010. **120**(10): p. 3455-65.
210. Langdahl, B., *Treatment of postmenopausal osteoporosis with bone-forming and antiresorptive treatments: Combined and sequential approaches.* Bone, 2020. **139**: p. 115516.
211. Tam, C.S., et al., *Parathyroid hormone stimulates the bone apposition rate independently of its resorptive action: differential effects of intermittent and continuous administration.* Endocrinology, 1982. **110**(2): p. 506-12.
212. McClung, M.R., et al., *Romosozumab in postmenopausal women with low bone mineral density.* N Engl J Med, 2014. **370**(5): p. 412-20.
213. PrabhuDas, M.R., et al., *A Consensus Definitive Classification of Scavenger Receptors and Their Roles in Health and Disease.* J Immunol, 2017. **198**(10): p. 3775-3789.
214. Canton, J., D. Neculai, and S. Grinstein, *Scavenger receptors in homeostasis and immunity.* Nat Rev Immunol, 2013. **13**(9): p. 621-34.
215. Zani, I.A., et al., *Scavenger receptor structure and function in health and disease.* Cells, 2015. **4**(2): p. 178-201.
216. Lin, Y.L., et al., *The effect of class a scavenger receptor deficiency in bone.* J Biol Chem, 2007. **282**(7): p. 4653-60.
217. Lee, H., et al., *SCARA5 plays a critical role in the commitment of mesenchymal stem cells to adipogenesis.* Sci Rep, 2017. **7**(1): p. 14833.
218. Takemura, K., et al., *Class A scavenger receptor promotes osteoclast differentiation via the enhanced expression of receptor activator of NF-kappaB (RANK).* Biochem Biophys Res Commun, 2010. **391**(4): p. 1675-80.
219. Chen, P., et al., *Scara3 regulates bone marrow mesenchymal stem cell fate switch between osteoblasts and adipocytes by promoting Foxo1.* Cell Prolif, 2021: p. e13095.
220. Kevorkova, O., et al., *Low-bone-mass phenotype of deficient mice for the cluster of*

differentiation 36 (CD36). PLoS One, 2013. **8**(10): p. e77701.

221. Goldstein, J.L., et al., *Binding site on macrophages that mediates uptake and degradation of acetylated low density lipoprotein, producing massive cholesterol deposition.* Proc Natl Acad Sci U S A, 1979. **76**(1): p. 333-7.
222. Kodama, T., et al., *Type I macrophage scavenger receptor contains alpha-helical and collagen-like coiled coils.* Nature, 1990. **343**(6258): p. 531-5.
223. Yu, X., et al., *Scavenger Receptors: Emerging Roles in Cancer Biology and Immunology.* Adv Cancer Res, 2015. **128**: p. 309-64.
224. Zhao, S.J., et al., *Macrophage MSR1 promotes BMSC osteogenic differentiation and M2-like polarization by activating PI3K/AKT/GSK3beta/beta-catenin pathway.* Theranostics, 2020. **10**(1): p. 17-35.
225. Dawodu, D., et al., *oxLDL inhibits differentiation and functional activity of osteoclasts via scavenger receptor-A mediated autophagy and cathepsin K secretion.* Sci Rep, 2018. **8**(1): p. 11604.
226. Guo, S., et al., *Class A Scavenger Receptor Exacerbates Osteoclastogenesis by an Interleukin-6-Mediated Mechanism through ERK and JNK Signaling Pathways.* Int J Biol Sci, 2016. **12**(10): p. 1155-1167.
227. Brodeur, M.R., et al., *Scavenger receptor of class B expressed by osteoblastic cells are implicated in the uptake of cholesteryl ester and estradiol from LDL and HDL3.* J Bone Miner Res, 2008. **23**(3): p. 326-37.
228. Silverstein, R.L. and M. Febbraio, *CD36, a scavenger receptor involved in immunity, metabolism, angiogenesis, and behavior.* Sci Signal, 2009. **2**(72): p. re3.
229. Papachristou, N.I., et al., *High-density lipoprotein (HDL) metabolism and bone mass.* J Endocrinol, 2017. **233**(2): p. R95-R107.
230. Tourkova, I.L., et al., *The high-density lipoprotein receptor Scarb1 is required for normal bone differentiation in vivo and in vitro.* Lab Invest, 2019. **99**(12): p. 1850-1860.
231. Rached, M.T., et al., *FoxO1 is a positive regulator of bone formation by favoring protein synthesis and resistance to oxidative stress in osteoblasts.* Cell Metab, 2010. **11**(2): p. 147-60.
232. Cheng, Z., *The FoxO-Autophagy Axis in Health and Disease.* Trends Endocrinol Metab, 2019. **30**(9): p. 658-671.
233. Jiang, Y., et al., *Identification and characterization of murine SCARA5, a novel class A scavenger receptor that is expressed by populations of epithelial cells.* J Biol Chem, 2006. **281**(17): p. 11834-45.
234. Ojala, J.R., et al., *Progressive reactive lymphoid connective tissue disease and development of autoantibodies in scavenger receptor A5-deficient mice.* Am J Pathol, 2013. **182**(5): p. 1681-95.
235. Mendes-Jorge, L., et al., *L-ferritin binding to scara5: a new iron traffic pathway*

potentially implicated in retinopathy. PLoS One, 2014. **9**(9): p. e106974.

236. Huang, J., et al., *Genetic and epigenetic silencing of SCARA5 may contribute to human hepatocellular carcinoma by activating FAK signaling.* J Clin Invest, 2010. **120**(1): p. 223-41.
237. Wen, X., et al., *Overexpression of SCARA5 inhibits tumor proliferation and invasion in osteosarcoma via suppression of the FAK signaling pathway.* Mol Med Rep, 2016. **13**(3): p. 2885-91.
238. Xu, Z., et al., *Rock2 promotes RCC proliferation by decreasing SCARA5 expression through beta-catenin/TCF4 signaling.* Biochem Biophys Res Commun, 2016. **480**(4): p. 586-593.
239. Levi, S., et al., *Evidence of H- and L-chains have co-operative roles in the iron-uptake mechanism of human ferritin.* Biochem J, 1992. **288 (Pt 2)**: p. 591-6.
240. Arosio, P., R. Ingrassia, and P. Cavadini, *Ferritins: a family of molecules for iron storage, antioxidation and more.* Biochim Biophys Acta, 2009. **1790**(7): p. 589-99.
241. Li, J.Y., et al., *Scara5 is a ferritin receptor mediating non-transferrin iron delivery.* Dev Cell, 2009. **16**(1): p. 35-46.
242. van Nimwegen, M.J. and B. van de Water, *Focal adhesion kinase: a potential target in cancer therapy.* Biochem Pharmacol, 2007. **73**(5): p. 597-609.
243. Yan, N., et al., *Therapeutic upregulation of Class A scavenger receptor member 5 inhibits tumor growth and metastasis.* Cancer Sci, 2012. **103**(9): p. 1631-9.
244. Salasznyk, R.M., et al., *Focal adhesion kinase signaling pathways regulate the osteogenic differentiation of human mesenchymal stem cells.* Exp Cell Res, 2007. **313**(1): p. 22-37.
245. Sun, C., et al., *FAK Promotes Osteoblast Progenitor Cell Proliferation and Differentiation by Enhancing Wnt Signaling.* J Bone Miner Res, 2016. **31**(12): p. 2227-2238.
246. Ersek, A., et al., *Strain dependent differences in glucocorticoid-induced bone loss between C57BL/6J and CD-1 mice.* Sci Rep, 2016. **6**: p. 36513.
247. Dempster, D.W., et al., *Standardized nomenclature, symbols, and units for bone histomorphometry: a 2012 update of the report of the ASBMR Histomorphometry Nomenclature Committee.* J Bone Miner Res, 2013. **28**(1): p. 2-17.
248. Scheller, E.L., et al., *Use of osmium tetroxide staining with microcomputerized tomography to visualize and quantify bone marrow adipose tissue in vivo.* Methods Enzymol, 2014. **537**: p. 123-39.
249. Nicolaidou, V., et al., *Monocytes induce STAT3 activation in human mesenchymal stem cells to promote osteoblast formation.* PLoS One, 2012. **7**(7): p. e39871.
250. Steiner, M., et al., *Comparison between different methods for biomechanical assessment of ex vivo fracture callus stiffness in small animal bone healing studies.*

PLoS One, 2015. **10**(3): p. e0119603.

251. Jepsen, K.J., et al., *Establishing biomechanical mechanisms in mouse models: practical guidelines for systematically evaluating phenotypic changes in the diaphyses of long bones.* J Bone Miner Res, 2015. **30**(6): p. 951-66.
252. Schneider, C.A., W.S. Rasband, and K.W. Eliceiri, *NIH Image to ImageJ: 25 years of image analysis.* Nat Methods, 2012. **9**(7): p. 671-5.
253. Shen, W.J., et al., *Scavenger receptor class B type I (SR-BI): a versatile receptor with multiple functions and actions.* Metabolism, 2014. **63**(7): p. 875-86.
254. Asagiri, M. and H. Takayanagi, *The molecular understanding of osteoclast differentiation.* Bone, 2007. **40**(2): p. 251-64.
255. Greaves, D.R. and S. Gordon, *The macrophage scavenger receptor at 30 years of age: current knowledge and future challenges.* J Lipid Res, 2009. **50 Suppl**: p. S282-6.
256. Jiang, Y., et al., *Identification and characterization of murine SCARA5, a novel class A scavenger receptor that is expressed by populations of epithelial cells.* Journal of Biological Chemistry, 2006. **281**(17): p. 11834-11845.
257. Yu, B., et al., *Interactions of ferritin with scavenger receptor class A members.* J Biol Chem, 2020. **295**(46): p. 15727-15741.
258. Balogh, E., et al., *Iron overload inhibits osteogenic commitment and differentiation of mesenchymal stem cells via the induction of ferritin.* Biochim Biophys Acta, 2016. **1862**(9): p. 1640-9.
259. Guo, D.Y., et al., *Scavenger Receptor SCARA5 Acts as an HMGB1 Recognition Molecule Negatively Involved in HMGB1-Mediated Inflammation in Fish Models.* J Immunol, 2016. **197**(8): p. 3198-3213.
260. Andersson, U. and K.J. Tracey, *HMGB1 is a therapeutic target for sterile inflammation and infection.* Annu Rev Immunol, 2011. **29**: p. 139-62.
261. Antoine, D.J., et al., *A systematic nomenclature for the redox states of high mobility group box (HMGB) proteins.* Mol Med, 2014. **20**: p. 135-7.
262. Venereau, E., et al., *Mutually exclusive redox forms of HMGB1 promote cell recruitment or proinflammatory cytokine release.* J Exp Med, 2012. **209**(9): p. 1519-28.
263. Lee, G., et al., *Fully reduced HMGB1 accelerates the regeneration of multiple tissues by transitioning stem cells to GAlert.* Proc Natl Acad Sci U S A, 2018. **115**(19): p. E4463-E4472.
264. Charoonpatrapong, K., et al., *HMGB1 expression and release by bone cells.* J Cell Physiol, 2006. **207**(2): p. 480-90.
265. Yang, J., et al., *HMGB1 is a bone-active cytokine.* J Cell Physiol, 2008. **214**(3): p. 730-9.
266. Steinhart, Z. and S. Angers, *Wnt signaling in development and tissue homeostasis.* Development, 2018. **145**(11).

267. Mills, K.M., J.L.A. Szczerkowski, and S.J. Habib, *Wnt ligand presentation and reception: from the stem cell niche to tissue engineering.* Open Biol, 2017. **7**(8).
268. Matsushita, Y., et al., *A Wnt-mediated transformation of the bone marrow stromal cell identity orchestrates skeletal regeneration.* Nat Commun, 2020. **11**(1): p. 332.
269. Li, Y., et al., *PPAR-gamma and Wnt Regulate the Differentiation of MSCs into Adipocytes and Osteoblasts Respectively.* Curr Stem Cell Res Ther, 2018. **13**(3): p. 185-192.
270. Banerjee, A., et al., *Targeting Wnt Signaling through Small molecules in Governing Stem Cell Fate and Diseases.* Endocr Metab Immune Disord Drug Targets, 2019. **19**(3): p. 233-246.
271. Takada, I., A.P. Kouzmenko, and S. Kato, *Wnt and PPARgamma signaling in osteoblastogenesis and adipogenesis.* Nat Rev Rheumatol, 2009. **5**(8): p. 442-7.
272. Chen, L., et al., *Structural insight into the mechanisms of Wnt signaling antagonism by Dkk.* J Biol Chem, 2008. **283**(34): p. 23364-70.
273. DeBruine, Z.J., et al., *Wnt5a promotes Frizzled-4 signalosome assembly by stabilizing cysteine-rich domain dimerization.* Genes Dev, 2017. **31**(9): p. 916-926.
274. Yap, N.V., et al., *The Evolution of the Scavenger Receptor Cysteine-Rich Domain of the Class A Scavenger Receptors.* Front Immunol, 2015. **6**: p. 342.
275. Jeney, V., *Clinical Impact and Cellular Mechanisms of Iron Overload-Associated Bone Loss.* Front Pharmacol, 2017. **8**: p. 77.
276. Musumeci, D., G.N. Roviello, and D. Montesarchio, *An overview on HMGB1 inhibitors as potential therapeutic agents in HMGB1-related pathologies.* Pharmacol Ther, 2014. **141**(3): p. 347-57.
277. Minear, S., et al., *Wnt proteins promote bone regeneration.* Sci Transl Med, 2010. **2**(29): p. 29ra30.
278. Niehrs, C., *The complex world of WNT receptor signalling.* Nat Rev Mol Cell Biol, 2012. **13**(12): p. 767-79.
279. Khosla, S., J.J. Westendorf, and M.J. Oursler, *Building bone to reverse osteoporosis and repair fractures.* J Clin Invest, 2008. **118**(2): p. 421-8.
280. Weivoda, M.M., et al., *Wnt Signaling Inhibits Osteoclast Differentiation by Activating Canonical and Noncanonical cAMP/PKA Pathways.* J Bone Miner Res, 2016. **31**(1): p. 65-75.
281. Bao, J., J.J. Zheng, and D. Wu, *The structural basis of DKK-mediated inhibition of Wnt/LRP signaling.* Sci Signal, 2012. **5**(224): p. pe22.
282. Semenov, M., K. Tamai, and X. He, *SOST is a ligand for LRP5/LRP6 and a Wnt signaling inhibitor.* J Biol Chem, 2005. **280**(29): p. 26770-5.
283. MacDonald, B.T. and X. He, *Frizzled and LRP5/6 receptors for Wnt/beta-catenin signaling.* Cold Spring Harb Perspect Biol, 2012. **4**(12).

284. Kim, J., et al., *Sclerostin inhibits Wnt signaling through tandem interaction with two LRP6 ectodomains.* Nat Commun, 2020. **11**(1): p. 5357.
285. Ahn, V.E., et al., *Structural basis of Wnt signaling inhibition by Dickkopf binding to LRP5/6.* Dev Cell, 2011. **21**(5): p. 862-73.
286. Cheng, Z., et al., *Crystal structures of the extracellular domain of LRP6 and its complex with DKK1.* Nat Struct Mol Biol, 2011. **18**(11): p. 1204-10.
287. Kim, J.H., et al., *Wnt signaling in bone formation and its therapeutic potential for bone diseases.* Ther Adv Musculoskelet Dis, 2013. **5**(1): p. 13-31.
288. Baron, R. and G. Rawadi, *Targeting the Wnt/beta-catenin pathway to regulate bone formation in the adult skeleton.* Endocrinology, 2007. **148**(6): p. 2635-43.
289. Balemans, W., et al., *Novel LRP5 missense mutation in a patient with a high bone mass phenotype results in decreased DKK1-mediated inhibition of Wnt signaling.* J Bone Miner Res, 2007. **22**(5): p. 708-16.
290. Li, J., et al., *Dkk1-mediated inhibition of Wnt signaling in bone results in osteopenia.* Bone, 2006. **39**(4): p. 754-66.
291. Balemans, W., et al., *The binding between sclerostin and LRP5 is altered by DKK1 and by high-bone mass LRP5 mutations.* Calcif Tissue Int, 2008. **82**(6): p. 445-53.
292. Semenov, M.V. and X. He, *LRP5 mutations linked to high bone mass diseases cause reduced LRP5 binding and inhibition by SOST.* J Biol Chem, 2006. **281**(50): p. 38276-84.
293. Bovolenta, P., et al., *Beyond Wnt inhibition: new functions of secreted Frizzled-related proteins in development and disease.* J Cell Sci, 2008. **121**(Pt 6): p. 737-46.
294. Xavier, C.P., et al., *Secreted Frizzled-related protein potentiation versus inhibition of Wnt3a/beta-catenin signaling.* Cell Signal, 2014. **26**(1): p. 94-101.
295. Claudel, M., J.Y. Jouzeau, and F. Cailotto, *Secreted Frizzled-related proteins (sFRPs) in osteo-articular diseases: much more than simple antagonists of Wnt signaling?* FEBS J, 2019. **286**(24): p. 4832-4851.
296. Esteve, P. and P. Bovolenta, *The advantages and disadvantages of sfrp1 and sfrp2 expression in pathological events.* Tohoku J Exp Med, 2010. **221**(1): p. 11-7.
297. Bodine, P.V., et al., *The Wnt antagonist secreted frizzled-related protein-1 is a negative regulator of trabecular bone formation in adult mice.* Mol Endocrinol, 2004. **18**(5): p. 1222-37.
298. Wang, F.S., et al., *Secreted frizzled-related protein 1 modulates glucocorticoid attenuation of osteogenic activities and bone mass.* Endocrinology, 2005. **146**(5): p. 2415-23.
299. Yao, W., et al., *Overexpression of secreted frizzled-related protein 1 inhibits bone formation and attenuates parathyroid hormone bone anabolic effects.* J Bone Miner Res, 2010. **25**(2): p. 190-9.

300. Krishnan, V., H.U. Bryant, and O.A. Macdougald, *Regulation of bone mass by Wnt signaling.* J Clin Invest, 2006. **116**(5): p. 1202-9.
301. Kook, S.H., J.S. Heo, and J.C. Lee, *Crucial roles of canonical Runx2-dependent pathway on Wnt1-induced osteoblastic differentiation of human periodontal ligament fibroblasts.* Mol Cell Biochem, 2015. **402**(1-2): p. 213-23.
302. Bennett, C.N., et al., *Wnt10b increases postnatal bone formation by enhancing osteoblast differentiation.* J Bone Miner Res, 2007. **22**(12): p. 1924-32.
303. Boland, G.M., et al., *Wnt 3a promotes proliferation and suppresses osteogenic differentiation of adult human mesenchymal stem cells.* J Cell Biochem, 2004. **93**(6): p. 1210-30.
304. Jing, H., et al., *Epigenetic inhibition of Wnt pathway suppresses osteogenic differentiation of BMSCs during osteoporosis.* Cell Death Dis, 2018. **9**(2): p. 176.
305. Loh, N.Y., et al., *LRP5 regulates human body fat distribution by modulating adipose progenitor biology in a dose- and depot-specific fashion.* Cell Metab, 2015. **21**(2): p. 262-273.
306. Kim, S.P., et al., *Sclerostin influences body composition by regulating catabolic and anabolic metabolism in adipocytes.* Proc Natl Acad Sci U S A, 2017. **114**(52): p. E11238-E11247.
307. Babij, P., et al., *High bone mass in mice expressing a mutant LRP5 gene.* J Bone Miner Res, 2003. **18**(6): p. 960-74.
308. Fairfield, H., et al., *The skeletal cell-derived molecule sclerostin drives bone marrow adipogenesis.* J Cell Physiol, 2018. **233**(2): p. 1156-1167.
309. Moester, M.J., et al., *Sclerostin: current knowledge and future perspectives.* Calcif Tissue Int, 2010. **87**(2): p. 99-107.
310. Burgers, T.A. and B.O. Williams, *Regulation of Wnt/beta-catenin signaling within and from osteocytes.* Bone, 2013. **54**(2): p. 244-9.
311. Yu, B., et al., *PGC-1alpha Controls Skeletal Stem Cell Fate and Bone-Fat Balance in Osteoporosis and Skeletal Aging by Inducing TAZ.* Cell Stem Cell, 2018. **23**(2): p. 193-209 e5.
312. Picke, A.K., et al., *Thy-1 (CD90) promotes bone formation and protects against obesity.* Sci Transl Med, 2018. **10**(453).
313. Jiang, M., et al., *SHP1 Regulates Bone Mass by Directing Mesenchymal Stem Cell Differentiation.* Cell Rep, 2016. **16**(3): p. 769-80.
314. Zhong, L., et al., *Single cell transcriptomics identifies a unique adipose lineage cell population that regulates bone marrow environment.* Elife, 2020. **9**.
315. Baccin, C., et al., *Combined single-cell and spatial transcriptomics reveal the molecular, cellular and spatial bone marrow niche organization.* Nat Cell Biol, 2020. **22**(1): p. 38-48.

316. Tikhonova, A.N., et al., *The bone marrow microenvironment at single-cell resolution.* Nature, 2019. **569**(7755): p. 222-228.
317. Sivaraj, K.K. and R.H. Adams, *Blood vessel formation and function in bone.* Development, 2016. **143**(15): p. 2706-15.
318. Chen, J., et al., *Bone Vasculature and Bone Marrow Vascular Niches in Health and Disease.* J Bone Miner Res, 2020.
319. Grosso, A., et al., *It Takes Two to Tango: Coupling of Angiogenesis and Osteogenesis for Bone Regeneration.* Front Bioeng Biotechnol, 2017. **5**: p. 68.
320. Kusumbe, A.P., S.K. Ramasamy, and R.H. Adams, *Coupling of angiogenesis and osteogenesis by a specific vessel subtype in bone.* Nature, 2014. **507**(7492): p. 323-328.
321. Diomede, F., et al., *Functional Relationship between Osteogenesis and Angiogenesis in Tissue Regeneration.* Int J Mol Sci, 2020. **21**(9).
322. Prisby, R.D., *Mechanical, hormonal and metabolic influences on blood vessels, blood flow and bone.* J Endocrinol, 2017. **235**(3): p. R77-R100.
323. Hendriks, M. and S.K. Ramasamy, *Blood Vessels and Vascular Niches in Bone Development and Physiological Remodeling.* Front Cell Dev Biol, 2020. **8**: p. 602278.
324. Schipani, E., et al., *Regulation of osteogenesis-angiogenesis coupling by HIFs and VEGF.* J Bone Miner Res, 2009. **24**(8): p. 1347-53.
325. Wang, Y., et al., *The hypoxia-inducible factor alpha pathway couples angiogenesis to osteogenesis during skeletal development.* J Clin Invest, 2007. **117**(6): p. 1616-26.
326. Ramasamy, S.K., et al., *Regulation of Hematopoiesis and Osteogenesis by Blood Vessel-Derived Signals.* Annu Rev Cell Dev Biol, 2016. **32**: p. 649-675.
327. Kelley, J.L., et al., *Scavenger receptor-A (CD204): a two-edged sword in health and disease.* Crit Rev Immunol, 2014. **34**(3): p. 241-61.
328. Nakayachi, M., et al., *Lectin-like oxidized low-density lipoprotein receptor-1 abrogation causes resistance to inflammatory bone destruction in mice, despite promoting osteoclastogenesis in the steady state.* Bone, 2015. **75**: p. 170-82.
329. Teixeira, C.C., et al., *Foxo1, a novel regulator of osteoblast differentiation and skeletogenesis.* J Biol Chem, 2010. **285**(40): p. 31055-65.
330. Jing, Z., et al., *Phosphocreatine Promotes Osteoblastic Activities in H2O2-Induced MC3T3-E1 Cells by Regulating SIRT1/FOXO1/PGC-1alpha Signaling Pathway.* Curr Pharm Biotechnol, 2021. **22**(5): p. 609-621.
331. Peng, H., et al., *Identification of SCARA3 with potential roles in metabolic disorders.* Aging (Albany NY), 2020. **13**(2): p. 2149-2167.
332. Boyce, B.F. and L. Xing, *Biology of RANK, RANKL, and osteoprotegerin.* Arthritis Res Ther, 2007. **9 Suppl 1**: p. S1.
333. Kostenuik, P.J., *Osteoprotegerin and RANKL regulate bone resorption, density,*

geometry and strength. Curr Opin Pharmacol, 2005. **5**(6): p. 618-25.

334. Singh, L., et al., *Aging alters bone-fat reciprocity by shifting in vivo mesenchymal precursor cell fate towards an adipogenic lineage.* Bone, 2016. **85**: p. 29-36.
335. Liu, W., et al., *Alpl prevents bone ageing sensitivity by specifically regulating senescence and differentiation in mesenchymal stem cells.* Bone Res, 2018. **6**: p. 27.
336. Li, H., et al., *FOXP1 controls mesenchymal stem cell commitment and senescence during skeletal aging.* J Clin Invest, 2017. **127**(4): p. 1241-1253.
337. Cha, Y., et al., *Zap70 functions to maintain stemness of mouse embryonic stem cells by negatively regulating Jak1/Stat3/c-Myc signaling.* Stem Cells, 2010. **28**(9): p. 1476-86.
338. Saalbach, A. and U. Anderegg, *Thy-1: more than a marker for mesenchymal stromal cells.* FASEB J, 2019. **33**(6): p. 6689-6696.
339. You, K., et al., *SCARA5 plays a critical role in the progression and metastasis of breast cancer by inactivating the ERK1/2, STAT3, and AKT signaling pathways.* Mol Cell Biochem, 2017. **435**(1-2): p. 47-58.
340. Liu, Y. and B.R. Olsen, *Distinct VEGF functions during bone development and homeostasis.* Arch Immunol Ther Exp (Warsz), 2014. **62**(5): p. 363-8.